

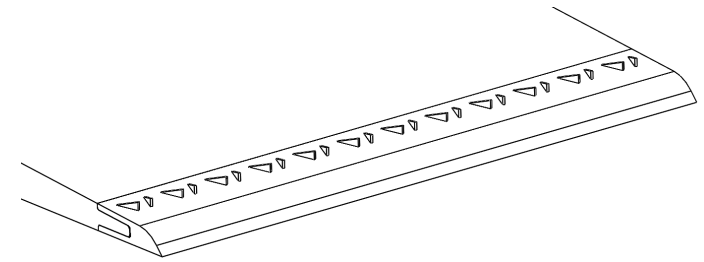
Hasan Besirovic

NTNU
Norwegian University of
Science and Technology
Faculty of Engineering
Department of Energy and Process Engineering

Hasan Besirovic

Vortex generator's effect on trailing edge wake and fluid structure interaction

June 2020





Norwegian University of
Science and Technology

Vortex generator's effect on trailing edge wake and fluid structure interaction

Hasan Besirovic

MTPROD

Submission date: June 2020

Supervisor: Pål-Tore Selbo Storli

Co-supervisor: Kristian Sagmo

Norwegian University of Science and Technology
Department of Energy and Process Engineering

Abstract

Details around vortex generators (VGs) used in hydrodynamic environments and their effects on the mitigation of vortex-induced vibrations (VIVs) have yet to be adequately studied. Hydroelectric power plants are prone to these severe structural vibrations, which can give rise to premature failure of important hydro machinery components, and can benefit from the mitigation of these effects. In order to shed light on this topic, an experimental study has been conducted at the Waterpower laboratory of the Norwegian University of Science and Technology. Effects of VGs attached on the blunt trailing edge of a hydrofoil were studied and compared to a corresponding hydrofoil without VGs, which is shown to experience a state of lock-in due to VIVs. Detailed flow field images of the hydrofoil wake were obtained using particle image velocimetry (PIV) and vibration frequencies were measured using strain gauges situated close to the trailing edge of the hydrofoil. The results indicate that the longitudinal vortices generated by the VGs are able to break up the uniformity of the vortex sheets forming at the trailing edge of the hydrofoil, effectively mitigating the VIVs. Thus it shows that applying VGs at the trailing edge of devices, which tend to experience severe structural vibrations could help mitigate these vibrational effects.

Sammendrag

Detaljer rundt bruk av virvelgeneratorer i hydrodynamiske miljøer og deres effekter på mildning av virvelinduserte vibrasjoner er ennå ikke tilstrekkelig undersøkt i litteraturen. Vannkraftverk som er utsatt for disse strukturelle vibrasjonene, som kan føre til tidlig svikt av komponenter som turbinblader og stagskovler, kan dra nytte av mildningen av disse effektene. For å belyse dette temaet er det utført en eksperimentell studie ved Vannkraftlaboratoriet ved Norges teknisk-naturvitenskapelige universitet. Effekter av virvelgeneratorer festet på den stumpe bakkantlisten av en hydrofoil ble studert og sammenlignet med en tilsvarende hydrofoil uten virvelgeneratorer som hadde blitt vist til å oppleve en tilstand av synkronisering på grunn av virvelinduserte vibrasjoner. Detaljerte bilder av strømfeltet til hydrofoil vaken ble anskaffet ved bruk av "particle image velocimetry" og vibrasjonsfrekvenser ble målt ved bruk av strekkklapper lokalisert nær bakkantlisten av hydrofoilen. Resultatene indikerer at langsgående virvler som er generert av virvelgeneratorene er i stand til å bryte opp den jevne fordelingen av virvelarkene som dannes ved bakkantlisten av hydrofoilen og dermed effektivt dempe de virvelinduserte vibrasjonene. Dermed kan bruken av virvelgeneratorer på enheter som opplever alvorlige strukturelle vibrasjoner bidra til å dempe disse vibrasjonseffektene.

Acknowledgements

This master's thesis is written in collaboration with the Waterpower laboratory at the Norwegian University of Science and Technology (NTNU). It has been a joy writing my project and master's thesis there. The facilities which are provided for us students are of top class and everyone at the laboratory are always eager to help. I do not think I could have asked for a better place to finish my master's degree.

First of all I would like to thank my supervisor Pål-Tore Selbo Storli for guidance during the writing of both this master's thesis and my project thesis. I would also like to thank my co-supervisor Kristian Sagmo for great collaboration around the experimental work in the thesis. He has happily shared of his knowledge about the laboratory, PIV and in fluid mechanics. Without Kristian the execution of the experiments would not have been possible. His help is deeply appreciated and does not go unnoticed. I would also like to show my appreciation to the guys working at the workshop in the waterpower laboratory at NTNU. They have provided assistance in the laboratory in every aspect possible.

Finally I would like to thank my family and friends for all their support during the writing of my thesis. Thank you to Irnis Besirovic and Sondre Tjessem for taking the time to read a draft and give comments on my thesis. I would especially like to thank my student colleague and friend Carsten Cleve Hansen who I have been working closely with during both this master's thesis and my project thesis. We have been working with similar theses and helping each other out. It has been a delight working with him and I truly do not think I could have asked for a better partner.

Hasan Besirovic



Trondheim, June.2020

Table of Contents

Abstract	I
Sammendrag	III
Acknowledgements	V
Table of Contents	IX
List of Tables	XI
List of Figures	XV
Abbreviations	XVI
Nomenclature	XVII
1 Introduction	1
1.1 Objective	1
1.2 Scope and Limitations	2
2 Vortex Generators Theory	3
2.1 Foil Theory	3
2.2 Vortex Shedding	4
2.2.1 Strouhal Number	4
2.2.2 Vortex Induced Vibrations	5
2.3 Vortex Generators	5
2.3.1 Cavitation	6
3 Vortex Generator Literature Review	7
3.1 Vortex Induced Vibrations	7
3.2 Optimisation Studies	7
3.3 Hydrodynamic Applications	9
3.4 Aerodynamical Vortex Generators	10

4	PIV and Data Processing Theory	11
4.1	Particle Image Velocimetry	11
4.1.1	Tracer Particles	11
4.1.2	Interrogation Area	12
4.1.3	Correlation Methods	12
4.1.4	Peak-locking	13
4.2	Signal Processing	14
4.2.1	Sampling	14
4.2.2	Welch's Method	14
4.2.3	Spectral Leakage	14
4.2.4	Window Function	15
5	Experimental Setup	17
5.1	Test Section	17
5.2	Hydrofoil	18
5.3	Vortex Generator Design	18
5.4	Measurement Technique	21
5.4.1	Strain Gauge	21
5.4.2	Particle Image Velocimetry	21
5.5	Overall Measurement Probes	28
5.6	Data Processing	28
6	Results	29
6.1	Hydrofoil with Vortex Generators	30
6.2	Reference Foil	36
7	Discussion	39
8	Conclusion	43
9	Further Work	45
9.1	Computational Fluid Dynamics	45
9.2	Optimisation Study	46
	Bibliography	46
	APPENDICES	50
A	Master Description	51
B	Calibration	53
B.1	Temperature Sensor	53
B.2	Flow-meter	53
B.2.1	Calibration Sheet	55
B.3	Pressure sensors	56
B.3.1	Calibration Sheets	57
C	3D - Printing	59

D Python Scripts	61
E Risk Assessment	85

List of Tables

5.1	Optimal VG parameters as shown in figure 5.3 and figure 5.2 derived from literature	18
5.2	PIV recording parameters for the hydrofoil wake flow measurements with VGs	22
5.3	Measurement probes excluding the strain gauges and PIV	28
B.1	Calibration constant for the flow meter	54
B.2	linear regression line constants c_1 and c_2 respectively being the y-intercept and slope, and uncertainty for some of the pressure sensors available . . .	56

List of Figures

2.1	Pressure field around a foil [5].	3
2.2	Kármán vortex street downstream of a foil.	4
2.3	Vortex generators on an airplane wing [11]	5
3.1	Vortex pairs shown as a function of downstream distance. a) Joined counter-rotating (CoR) VGs. b) Separated CoR VGs [19].	8
3.2	Cavitation on a single triangular vortex generator at 20° incident angle. a) High gauge pressure. b) low gauge pressure [10].	9
3.3	a) CAD drawing of an aerodynamical VG [32]. b) Flow comparison between a regular VG and an aerodynamical VG [33].	10
4.1	Typical PIV set-up [34].	11
4.2	Concept of cross-correlation [35].	13
4.3	The effects of peak locking. a) peak-locking is evident as the displacement is solely determined by a integer number of pixels. b) Smaller degree of peak-locking [36].	13
4.4	Figures illustrating spectral leakage. a) Discontinuities which emerge from repeating a signal with a non-integer number of periods. b) How windowing can help reduce the discontinuities. c) The frequency range of a periodic sine wave without leakage, and a non-periodic sine wave with leakage and with reduced leakage because of windowing [38].	15
4.5	Window functions in the frequency domain with annotations for the main and side lobes [40].	16
5.1	a) Full view of the experimental set-up. b) An enlarged view of the test section with the hydrofoil and VGs.	17
5.2	a) Overall hydrofoil dimensions. b) Attachment mechanism for an interchangeable trailing edge.	18
5.3	Endplate attachment mechanism and VG parameters considered in this thesis	19
5.4	Symmetry-plane and spanwise-plane downstream of the hydrofoil at which PIV measurements were attained.	23
5.5	a) Calibration device with grid used to calibrate camera. b) Laser sheet on calibration device showing uniform thickness of the laser sheet.	24

5.6	Uncertainty in the absolute velocity V . Figures to the left show uncertainty colourmaps at different reference flow velocities and planes. Figures to the right show a histogram plot of the colourmap data to the left with uncertainty non dimensionalized along the x-axis and number of values along the y-axis. a-b) $U_{ref} = 13.1m/s$, symmetry-plane at a arbitrary frame (f:2183/4367). c-d) $U_{ref} = 10.1m/s$, spanwise-plane at a arbitrary frame (f:2183/4367). e-f) $U_{ref} = 10.1m/s$, average across all frames for the symmetry-plane.	25
5.7	Illustration of correlation peaks [48].	26
5.8	Peak ratio from PIV measurements for a reference flow velocity of 10.1m/s for the two planes. Left figures show a colourmap plot of the peak ratio. Right figures show histogram plots of the colourmap data to the right and the number of vectors with peak ratio below respectively two and Three. a- b) Symmetry-plane, arbitrary frame (f:2183/4367). c-d) Spanwise-plane, arbitrary frame (f:2183/4367). e-f) Symmetry-plane, the average across all frames.	27
6.1	Amplitude frequency spectrum obtained by P.D Welchs power spectrum and a Hanning window for the hydrofoil natural frequency measurements. a) Natural frequencies of the reference hydrofoil without VGs from the paper of Sagmo et al. b) Natural frequencies of a hydrofoil with VGs and an interchangeable trailing edge.	29
6.2	Amplitude frequency spektrum for the hydrofoil with VGs using two separate window function sizes in order to smooth out the frequency spectrum. The first and second peaks are annotated. a) $U_{ref} = 6.0\frac{m}{s}$. b) $U_{ref} = 8.0\frac{m}{s}$. c) $U_{ref} = 9.1\frac{m}{s}$. d) $U_{ref} = 9.6\frac{m}{s}$	30
6.3	Power spectrum analysis of PIV data at several reference flow velocities. a) $U_{ref} = 8.0\frac{m}{s}$, b) $U_{ref} = 9.1\frac{m}{s}$, c) $U_{ref} = 9.6\frac{m}{s}$, d) $U_{ref} = 10.1\frac{m}{s}$, e) $U_{ref} = 10.6\frac{m}{s}$, f) $U_{ref} = 11.1\frac{m}{s}$	31
6.4	Vibrational frequencies from strain gauge data and shedding frequencies from PIV data plotted along the right axis with corresponding error bars estimated by the Full Width Half Maximum. Normalised vibrational amplitude of the second peak of the hydrofoil plotted along the left axis. . . .	32
6.5	a) Colormap of average velocity across all frames for $U_{ref} = 10.1\frac{m}{s}$, symmetry plane. b) Average velocity profiles for several reference velocities at $x = 8.3D$. c) Average velocity profiles for several reference velocities at $x = 12.5D$. Errorbars are only plotted for reference velocities $U_{ref} = 9.1\frac{m}{s}$ and $U_{ref} = 13.1\frac{m}{s}$	33
6.6	a) Colormap of average velocity component U_z at $U_{ref} = 10.1\frac{m}{s}$, spanwise plane. b) Average velocity component U_z profiles for several reference flow velocities at $x = 14.6D$. Errorbars are only plotted for a reference flow velocity of $U_{ref} = 10.1\frac{m}{s}$	33
6.7	a) Colormap of average Vorticity at $U_{ref} = 10.1\frac{m}{s}$, spanwise plane. b) Curve fit for the peak vorticity in the vortex core obtained at some points in the wake of the VGs. c) Average vorticity profiles for several reference flow velocities at $x = 10.4D$. d) Average vorticity profiles for several reference flow velocities at $x = 14.6D$	34

6.8	a) Colormap of average Vorticity at $U_{ref} = 10.1 \frac{m}{s}$ for the symmetry plane. b) Curvefit for peak vorticity in the core obtained at some points in the wake of the hydrofoil. c) Average vorticity profiles for several reference velocities at $x = 8.3D$. d) Average vorticity profiles for several reference velocities at $x = 12.5D$	35
6.9	"Amplitude frequency spectra for increasing reference velocities from strain-gauge voltage signal, showing the travelling shedding frequency peak (left peak) approaching the natural (standing) frequency peak of the hydrofoil. (a) $U_{ref} = 9.1 \frac{m}{s}$. (b) $U_{ref} = 9.6 \frac{m}{s}$. (c) $U_{ref} = 10.1 \frac{m}{s}$. (d) $U_{ref} = 10.6 \frac{m}{s}$ " [4].	36
6.10	"Hydrofoil vibration frequencies and shedding frequencies measured by PIV, strain-gauges and LD-Vibrometer. The relative hydrofoil vibrational amplitude is plotted along the right y-axis." [4]	37
6.11	"Time-averaged PIV measured velocity distributions normalised with respect to the mean channel velocity for different downstream positions. Height normalised by trailing edge thickness, with $y = 0$ set at the hydrofoil center line. In (a) and (c) $x = 9.9D$. In (b) and (d) $x = 13.3D$. Uncertainty error bars are only plotted for reference velocities of $9.1 \frac{m}{s}$ and $11.1 \frac{m}{s}$, for clarity." [4]	37
B.1	Linear regression line for flow meter calibration data	54
C.1	Attachment method for a 3D - Printed piece. Piece number three is the 3D - Printed piece and can be attached simply with glue.	59

Abbreviations

NTNU	=	Norwegian University of Science and Technology
VG	=	Vortex generator
VIV	=	Vortex induced vibration
PIV	=	Particle image velocimetry
TE	=	Trailing edge
CFD	=	Computational fluid dynamics
CoR	=	Counter rotating
FOV	=	Field of view
IA	=	Interrogation area
FFT	=	Fast fourier transform
DFT	=	Discrete fourier transform
Hann	=	Hanning
NI	=	National instruments
DAQ's	=	Data acquisition devices
sym.P	=	Symmetry plane
sw.P	=	Spanwise plane
px	=	Pixels
FWHM	=	Full width half maximum

Nomenclature

St	=	Strouhal number
f_s	=	Vortex shedding frequency
L	=	Characteristic length
U_∞	=	Free stream velocity
U	=	Local velocity
d_τ	=	Particle image diameter
z_0	=	Distance between image plane and lens
Z_0	=	Distance between lens and object plane
F	=	F-number of camera lens
d_P	=	Particle diameter
λ	=	Laser wavelength
δ	=	Boundary layer thickness
Re	=	Reynolds number
Re_c	=	Chord based reynolds number
σ	=	Cavitation number
P_∞	=	Ambient pressure
P_V	=	Vapour pressure
ρ	=	Fluid density

Introduction

Every so often there is discussion about the world being in an energy crisis [1], [2]. This crisis usually ties up with the depleting fossil fuel reservoirs around the world and that we will not be able to meet the future energy demands of a growing world population. Thus it becomes more and more important to utilise, produce, and store energy as environmentally friendly and cost-efficient as possible. Both the environmental impact and the cost are important to consider when looking at new energy solutions or ways of improving on preexisting solutions. No matter how environmentally friendly a solution is, it will not be utilised on a global scale if the cost is not comparable to older, more polluting solutions. A common trait amongst energy production is that one type of energy source needs to be converted to utilisable energy through mechanical devices. Such mechanical devices will experience variable and strong forces which can lead to wear and inevitably failure. With the reduction of this wear, it is possible to reduce cost and possibly the environmental impact. Devices which either are utilised for the production of energy or use energy in environments with liquids tend to move large amounts of masses over time and are prone to severe structural vibrations. These vibrations over time can lead to failure of important components. Examples of such devices are rudders in ships, stay vanes in hydroelectric power plants, and wind- and water turbine blades. The hydropower devices are especially important in Norway, where hydroelectric power plants account for 95% of the total power production [3]. New hydroelectric power plants are planned every year, and old plants have to be refurbished due to wear from severe structural vibrations, among other things. This pushes for innovation in the hydropower technology sector regarding the reduction of manufacturing cost while simultaneously maintaining or increasing performance. To give an insight into how simple alterations can help reduce severe structural vibrations in hydroelectric power plants and potentially reduce cost, an experimental study is conducted at the Waterpower laboratory of the Norwegian University of Science and Technology (NTNU).

1.1 Objective

In this master's thesis, it is proposed to introduce vortex generators (VGs) close to the trailing edge of devices in fluids which experience severe structural vibrations due to vortex-induced vibrations (VIVs). The belief is that these VGs will generate strong vortices which might mitigate the effects of these vibrations. A measurement campaign with particle image velocimetry (PIV) and strain gauges is performed on a hydrofoil with a blunt trailing edge, which has been shown to experience these vibrational effects. VGs are attached on the trailing edge of this hydrofoil and compared to the hydrofoil without VGs in order to investigate the effects these devices have on the VIVs.

1.2 Scope and Limitations

The effects a specific design of VGs have on the wake of a simple hydrofoil will be discussed, and experimental results obtained from PIV and strain gauges will be presented. Uncertainties within the PIV measurements are also presented and discussed. The relevant theory concerning VGs, PIV, data attainment and data processing is presented. A relatively short literature review is presented, showing the inspiration for the design of the VGs. An optimal VG design was developed as part of a project thesis in the fall semester of 2019, a short summary of these results is given. The experimental setup is discussed, and methods around data attainment are laid forth. Results of the experiments performed concerning the effects of the VGs are also discussed in great detail. Finally, some keynotes on future work are given.

Experiments with an additional hydrofoil having no VGs called the reference hydrofoil were planned, but due to the situation with Covid-19, these experiments proved to be challenging to complete. Instead, the experimental results obtained for the hydrofoil with VGs are compared to earlier experiments with a corresponding hydrofoil performed by Sagmo et al. [4]. A summary of their results is presented in chapter 6. This is not ideal but deemed to be sufficient for the execution of this master's thesis. Devices like serrated trailing edges and splitter plates are mentioned, but not discussed upon as the focus of the thesis is to quantify the effects of the VGs on the wake behind a hydrofoil and VIVs. Other types of flow control devices are not discussed.

Vortex Generators Theory

2.1 Foil Theory

A foil is a lifting surface meaning an object when placed in a moving fluid generates a force perpendicular to the flow direction several times greater than the resisting, tangential force acting on the object. The perpendicular force is called lift, and the tangential force is called drag. When the acting fluid is water, the object is called a hydrofoil, and the forces are called hydrodynamic forces. A simple explanation of the lifting force can be obtained with Newton's second and third laws. As fluid flows over a foil, the foil exerts a downward force on the fluid, and the fluid will then push back with an equal and opposite force. Fluid is also deflected and accelerated downwards, causing a net force upwards according to Newton's second and third laws. While the mechanisms behind the lifting force can be simply explained by Newton's laws, a more complex and detailed explanation is needed to understand how the air "pushes back" on the foil. This explanation can be found in a paper by Doug Mclean from 2018 [5]. Essentially there exists a pressure field around the foil, which is a result of applied forces from the fluid with reduced and increased relative pressure above and below the foil respectively. This pressure field is illustrated in figure 2.1. In this pressure field, the flow will accelerate in the direction of decreasing pressure forces, according to Newton's second law. This is consistent with the principle of Bernoulli, where the higher velocity flow on the upper surface experiences a lower pressure. It is thus this pressure field along with the accelerating downwards flow, which accounts for the net perpendicular force the foil experiences called lift. The total drag is called parasitic drag and is a combination of skin friction drag and form drag. Skin friction drag is the resistance force caused by the fluid viscosity and surface friction. Form drag is the resistance force which arises from the shape of the body. Flow separation might also occur on such bodies which can lead to vortex shedding. This is told more about in the next section.

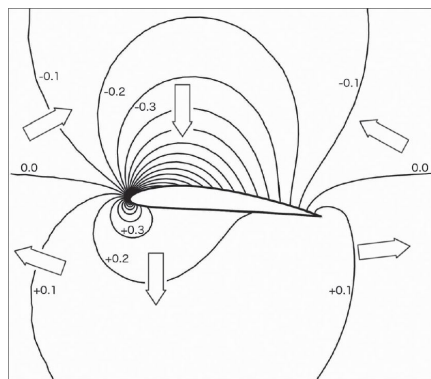


Figure 2.1: Pressure field around a foil [5].

2.2 Vortex Shedding

”Vortex: A local structure in a fluid flow characterised by a concentration of vorticity in a tubular core with circular streamlines around the core axis” [6]. Vortex shedding is a phenomenon that occurs when a fluid flows over a bluff body and is dependent on the fluid velocity and shape of the body. A bluff body is defined as a body where the flow is separated over a portion of its surface. Both Roshko [7] and Gerrard [8] have thoroughly explained the physics and mechanisms of vortex shedding. Their conclusion indicates that as separation occurs a free shear layer forms. Circulation from this shear layer will grow until it is big enough to draw the shear layer on the opposite side, which has a circulation in the opposite direction across. This recirculated flow will detach from the body, causing a single shedding of a vortex. Several of these vortices with alternating circulation will detach every second, producing a pattern called a Kármán vortex street, shown in figure 2.2. In theory, an infinite number of these vortices are shed along the foil width, forming a uniform vortex sheet with the highest pressure in the middle of the vortex. It is the alternating circulation of this vortex sheet which will cause an object to oscillate, something which is told more about later.

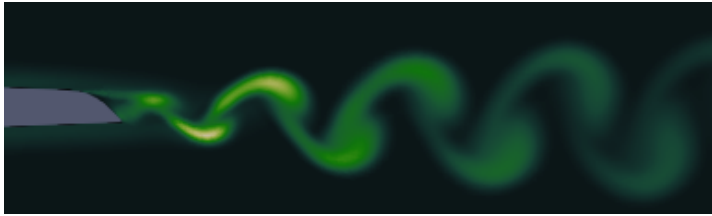


Figure 2.2: Kármán vortex street downstream of a foil.

2.2.1 Strouhal Number

The number that describes the vortex shedding is the Strouhal number (St), which is defined as characteristic flow time divided by the period of oscillation [6] and is given by equation 2.1.

$$St = \frac{f_s L}{U_\infty} \quad (2.1)$$

Where f_s is the vortex shedding frequency, L is the characteristic length and U_∞ is the free stream velocity. Named after the Czech physicist, Vincenc Strouhal who was studying vortex shedding from steel wires. The Strouhal number is approximately constant for a given geometry and flow medium. Rearranging equation 2.1 we get equation 2.2 which can be used to approximate the shedding frequency for a given geometry.

$$f_s = \frac{St U_\infty}{L} \quad (2.2)$$

2.2.2 Vortex Induced Vibrations

As vortices are shed behind a body, the pressure forces around it will no longer be symmetric or in one direction. Alternating lifting forces will act on that body due to the alternating nature of the vortex shedding. A bluff body which is not rigid will oscillate at approximately the same frequency as the vortex shedding frequency [9]. The rate and amplitude of these oscillations will increase as the shedding frequency increases, proportionally to the flow velocity, eventually syncing up with the natural frequency of the system. This will cause resonance, and the system will go into a state called lock-in. Large damages and failure may occur in this state. A solution to these effects can be to introduce longitudinal vortices in the flow that might break up the uniformity of the vortex sheet formed at the trailing edge of a bluff body. Vortex generators (VGs) is an example of devices that could do this and are explained in more detail in the next section.

2.3 Vortex Generators

VGs are passive flow control devices designed to introduce longitudinal vortices in the boundary layer of a system. They are most commonly used on aeroplane wings, as seen in figure 2.3, to control flow separation and increase the stall angle. Therefore they are usually placed on the system surface before the onset of separation. With the introduction of a longitudinal vortex in the boundary layer, it is possible to transfer the higher energy flow above closer down to the surface and transfer the low energy flow away from the surface. A higher kinetic energy flow at the surface will be able to withstand a higher pressure rise, thus delay separation [10]. With this adjustment of the point of separation, it is possible to affect the vortex shedding frequency [4]. The longitudinal vortices generated by VGs could also be used to break up the vortex sheet formed behind a bluff body and thus mitigate the effects of vortex-induced vibrations (VIVs). The use of these devices is not as widespread in liquid flows as for flows with air. A reason for this is that problems with cavitation might arise with the use of these devices in liquid flows.



Figure 2.3: Vortex generators on an airplane wing [11]

2.3.1 Cavitation

As local pressure rapidly drops below the vapour pressure in a liquid, small bubbles or cavities of vapour form within the liquid. These bubbles will move with the flow to regions with higher pressure where they rapidly implode. Bubbles imploding close to the surface can cause substantial damage and erode material from the object's surface. Far from the surface, these bubbles will obstruct the fluid flow forcing it around the cavities. As fluid flows around the VGs, a rapid change in velocity occurs, and in turn, a rapid change in pressure is observed. This can potentially cause cavitation, which can obstruct the flow and make the VGs less efficient or even useless and just a means of drag increase. Therefore it is crucial to design the VGs properly to try to avoid these effects as much as possible, something which is told more about in the next chapters.

Vortex Generator Literature Review

This chapter is devoted to a discussion of previous research done on vortex generators (VGs). Most research has been towards delaying flow separation and thus increasing stall angle of lifting surfaces, like aircraft wings. This again amounts to lower Reynolds number flows than what is the case for the experiments in this master's thesis. Regardless of this, the results from these previous research papers are essential for the end product of this thesis. Some cases where VGs were used to mitigate noise, thus potentially mitigate vortex-induced vibrations (VIVs) are presented in this chapter. Cases, where VGs have been utilised in a hydrodynamic environment are also presented.

VGs were first introduced by Taylor et al. [12] in 1947. They studied the effects of using simple vane-type VGs to control flow separation in diffusers showing that it was possible to avoid flow separation with the introduction of these devices. Devices like these have since been used to delay boundary layer separation [13], increase the performance of aero-plane wings and wind turbine blades [14] and reduce noise [15].

3.1 Vortex Induced Vibrations

In 1972 Kuethe [16] studied the effects of introducing streamwise vortices in the turbulent boundary layer on the wake of flat plates and airfoils. His experiments are showing that vortices generated by VGs have a strong suppression on the formation of the Kármán vortex street. The introduction of VGs at the trailing edge of a flat plate showed a total suppression of the vortex shedding. Maull and Young [17] also studied the effects of longitudinal vortices produced by VGs on the wake of an airfoil. Results are showing in accordance with Kuethe, a decrease in the shedding frequency with the introduction of VGs. Holmes et al. [15] did a study on sub-boundary layer VGs and their effects on interior noise in aeroplanes at high velocities. Their results show that these devices were effectively able to delay separation and break up the Kármán vortex street. Park et al. [18] introduced longitudinal vortices on the trailing edge of a bluff body using devices similar to VGs in order to reduce drag. In addition to reducing the parasitic drag, it was observed that the longitudinal vortices induced a mismatch and reduced the vortical strength in the Kármán vortex street. It was also observed that the Kármán vortex street entirely disappeared right behind the bluff body and occurred at locations further downstream.

3.2 Optimisation Studies

Most research on VGs has been concerned with parametric optimisation of these devices for boundary layer separation control and drag reduction on airfoils. In 2002 Lin [13]

did an extensive review on research performed within the past 15 years on VGs for controlling boundary-layer separation. What he found was a widespread agreement around which type of VGs was the most efficient. VGs with heights smaller than the boundary layer were usually favourable for their separation control efficiency and low device drag. Counter-rotating (CoR) VGs were most effective in controlling 2D flow separation while co-rotating VGs performed better in 3D flow separation. Betterton et al. [19] show that CoR VGs which are spaced at the trailing edge more efficiently control separation than ones joined at the trailing edge. Spaced CoR VGs tend to have lower vortex decay, and vortices are attached to the surface further downstream, this is shown in figure 3.1. Mutual interaction between the vortices generated by the joined VGs causes interference and thus reduces the vortex strength quicker downstream. Results from Godart and Stanislas also show agreement with the findings of Betterton et al. and Lin. They also show a decrease in wall skin friction with the use of VGs, CoR ones contributing to the largest decrease. Mueller-Vahl et al. [20] and Gao et al. [21] performed a parametric study on VGs for wind turbine blades where the chordwise position, VG size and spanwise spacing were studied. Experimental and computational fluid dynamics (CFD) results show that spacing between adjacent VG pairs has a significant impact on the performance of them. Further, the CFD results of Gao et al. show that larger VGs in all dimensions will produce vortices with a higher chance of lifting off from the surface. Li et al. [22], [23] have produced two detailed papers on the effects of the VG height and the orientation angle on the performance of these devices. Their results are showing that height has a significant impact on the drag induced by the VGs. The orientation angle of the VGs has an impact on the diffusion of vortices downstream, with quicker vortex decay for larger angles. Wang and Ghaemi [24] also studied the orientation angle of vane-type VGs with results agreeing with those of Li et al. An experimental study of VGs wake on a flat plate using PIV was conducted by Shim et al. [25] in 2015 where geometrical shape and VG length was examined. It showed that rectangular VGs produced the strongest vortices while triangular VGs produced vortices which stayed closer to the surface downstream.

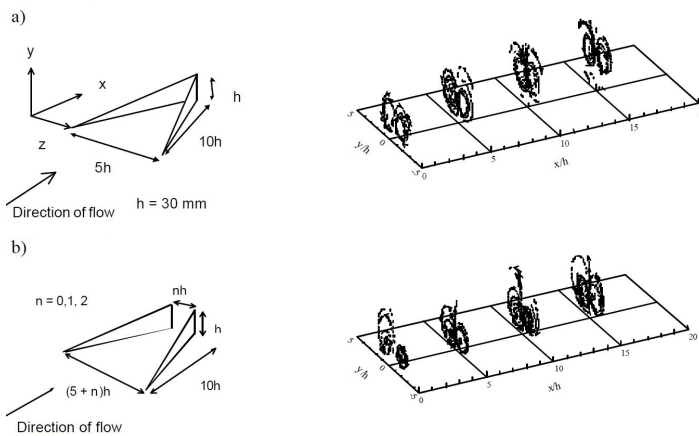


Figure 3.1: Vortex pairs shown as a function of downstream distance. a) Joined counter-rotating (CoR) VGs. b) Separated CoR VGs [19].

3.3 Hydrodynamic Applications

Hydrodynamic applications of VGs are not as widely studied as applications in air, possibly due to the risks of cavitation. Nevertheless, some papers where VGs were applied in hydrodynamic environments were found. A study on the performance and cavitation of a single triangular vortex generator at several incident angles was performed by Brandner and Walker [10]. Their findings are showing promising possibilities of using VGs in hydrodynamic environments. Results are indicating that as long as the gauge pressure is kept high, and the incident angle is smaller than 25° , no disruptive cavitation will occur. While some cavitation could still occur at high gauge pressures, as seen in figure 3.2, it was shown that this had almost no impact on the downstream boundary layer profiles and the lift to drag ratio. Results from Oledal [26] show similar tendencies on triangular VGs used in hydrodynamic environments as Brandner and Walker.

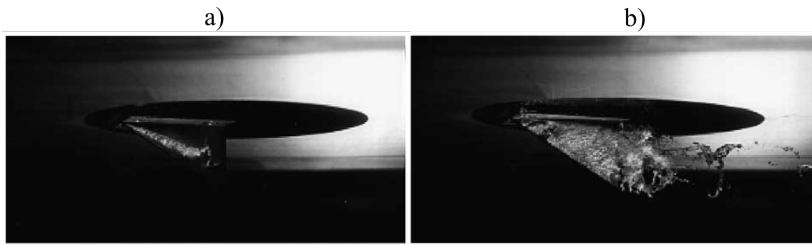


Figure 3.2: Cavitation on a single triangular vortex generator at 20° incident angle. a) High gauge pressure. b) low gauge pressure [10].

Kundu et al. [27] investigated the effects of VGs to improve performance of a hydrofoil commonly used as tidal current turbine blades. CFD simulations with a Reynolds number of $2.4E6$ were performed on several VG configurations. They are concluding with CoR VGs being superior to other types of VGs, like many other researchers. They also see that VGs placed closer to the trailing edge are more efficient when it comes to delaying separation. Velte et al. [28] have done experimental measurements on VGs with the same Reynolds number as Kundu et al. Results are showing agreeance with Kundu et al. when it comes to the VGs effect on delaying separation.

Ahmed et al. [29] researched ship hull resistance reduction by controlling flow separation using simple sub boundary layer VGs. Their results are showing that while the VGs reduce the hull resistance, their addition might lead to a total increase of ship resistance. They also make a point that the addition of VGs may lead to improved flow in the propeller which again would improve efficiency. However, an experimental investigation of this is necessary. Saydam et al. [30] have done studies on wake modification by utilising triangular VGs in order to mitigate propeller-induced vibrations on ships. By placing three VGs on each side of the hull ahead of the ship's propeller, they achieved a significant reduction in vibrations, a delay in separation and a total hull resistance reduction of 3% was observed. This idea of using VGs to create a uniform velocity distribution flow into the propeller and over the rudder of ships was also studied by Matheson [31] with results agreeing with those of Saydam et al. Showing that VGs can be used to improve velocity distribution, thus reduce vibrations and improve ship steering characteristics.

3.4 Aerodynamical Vortex Generators

In recent years more complexly shaped VGs have started to emerge called aerodynamical VGs, shown in figure 3.3. In 2016 Hansen et al. [32] did experiments using aerodynamical VGs to quantify the drag reduction when comparing to standard VGs. From the results, it was evident that the flow around the aerodynamical VGs was less separated, as can be seen in figure 3.3 b). There was a slight improvement in the lift to drag ratio when compared to standard VGs with the same dimensions. However, as the flow was less separated on the aerodynamically shaped VG, it would allow for a higher orientation angle, thus resulting in a significant increase in the lift to drag ratio. Méndez and Gutiérrez [33] performed CFD calculations on the same aerodynamical VGs as Hansen. Results showed agreement with Hansen's result in that there is a small reduction in drag when comparing aerodynamical VGs to regular ones. Another impressive result that was evident from the CFD is that the regular VGs were shown to produce stronger and bigger vortices compared to the aerodynamical ones.

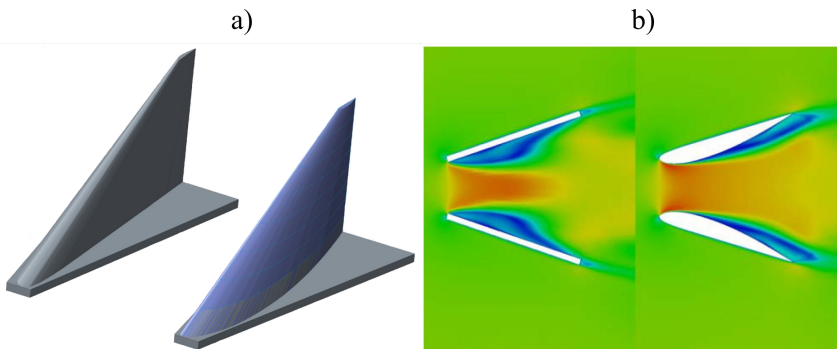


Figure 3.3: a) CAD drawing of an aerodynamical VG [32]. b) Flow comparison between a regular VG and an aerodynamical VG [33].

PIV and Data Processing Theory

4.1 Particle Image Velocimetry

Particle image velocimetry (PIV) is an optical full-field measurement technique with the capability of obtaining a full 2D or 3D plane visualisation of the flow examined. It is a non-intrusive method meaning there is no significant interaction between the flow and the measurement probes. A typical PIV set-up is shown in figure 4.1. Small particles called tracer particles are added to the flow. A thin laser sheet is formed by sending a laser beam through a sheet optic. The laser sheet illuminates the tracer particles which a high-speed camera records. By looking at the particle displacement from one time instant to another, it is possible to obtain a full velocity vector flow field.

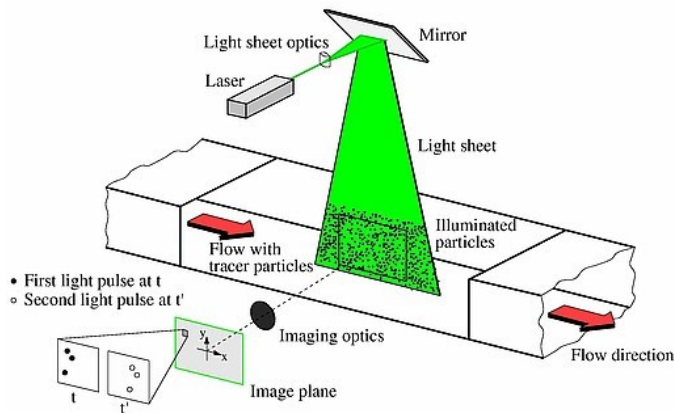


Figure 4.1: Typical PIV set-up [34].

4.1.1 Tracer Particles

The choice of tracer particles is an important one. In order to get accurate measurement results, the particles need to follow the flow perfectly without affecting it nor interacting with other particles. Thus tracer particles have to be neutrally buoyant, having density close to that of the fluid which is examined. The size of the tracer particles is also an important parameter. Too large particles force a larger interrogation area while too small particles can give rise to problems with peak-locking which is told more about in section 4.1.2 and 4.1.4 respectively.

4.1.2 Interrogation Area

The field of view (FOV) is the whole area of the flow which is recorded by the camera. In order to evaluate the flow field by virtue of these recorded images, it is necessary to divide these images into smaller areas, called interrogation areas (IA). An example of this is shown in figure 4.2. Average particle velocity vectors are calculated within these areas using correlation methods, which is told more about in the next section. Several criteria govern the size of the interrogation area. It is important to have a sufficient number of particles within one area, usually set to a minimum of ten particles. This is in order to be able to calculate statistically correct velocity vectors. Another important criterion is for the IA to be able to contain most of the particles from one time instant to another such that particle information is not lost. A way of complying with this criterion is to ensure that the IAs overlap by moving them in the direction which the resultant of particles move. A typical overlapping value is 50% [34].

Multipass Method

When evaluating the vector field obtained from PIV, the highest spatial resolution possible is usually desired. This again amounts to having the smallest possible IA. In order to ensure that vector fields without too many spurious vectors are found when employing a smaller IA, it is possible to use the information of larger IAs to calculate the vector field for the smaller IA. This is the essence of the multipass method. A vector field is first calculated with a sufficiently large IA. The information of this calculation is used to calculate a new vector field which is half the size of the original IA. This loop continues until the desired IA is reached. With this method, it is possible to deter from the rule of at least ten particles within the smallest IAs, but it is still necessary to check that this rule of thumb is complied with for the larger IAs.

4.1.3 Correlation Methods

Correlation methods are one of the most widely used particle tracking algorithms for analysis of PIV images. The most known are autocorrelation and cross-correlation. Autocorrelation is a method where two exposures of the particles are taken in the same picture. This type of correlation is usually used for single-frame recordings where particles are captured at different time instances in the same image. This means there is no way of knowing which direction the particles are moving in. Cross-correlation, on the other hand, uses two images taken with a known time step to calculate the magnitude and direction of the particle velocity vector. It is usually used for recordings in double- or multi-frame and is the method of choice. The concept of cross-correlation is illustrated in figure 4.2.

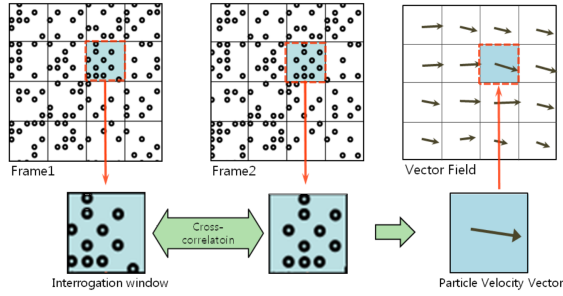


Figure 4.2: Concept of cross-correlation [35].

4.1.4 Peak-locking

Peak-locking is a displacement bias error caused by having too small particle images. Where a particle image is a digital representation of the particle in pixels calculated from the position of the particle and light captured by each pixel. An approximation to the particle image diameter (d_τ) can be calculated using equation 4.1 from the book "Particle Image velocimetry: A practical guide" [34]. Where z_0 is the distance between the image plane and camera lens, Z_0 is the distance between the camera lens and object plane, F is the F-number of the camera lens, d_P is the particle diameter and λ is the laser wavelength. With too small particle images, the software will only be able to track particle displacements of an integer number of pixels which results in particle displacement errors. Figure 4.3 illustrates this. According to Raffel et al. [34] in order to avoid significant errors due to peak-locking particle image diameters of at least two pixels are recommended.

$$d_\tau = \sqrt{\left(\frac{z_0}{Z_0} d_P\right)^2 + (2.44F\left(\frac{z_0}{Z_0} + 1\right)\lambda)^2} \quad (4.1)$$

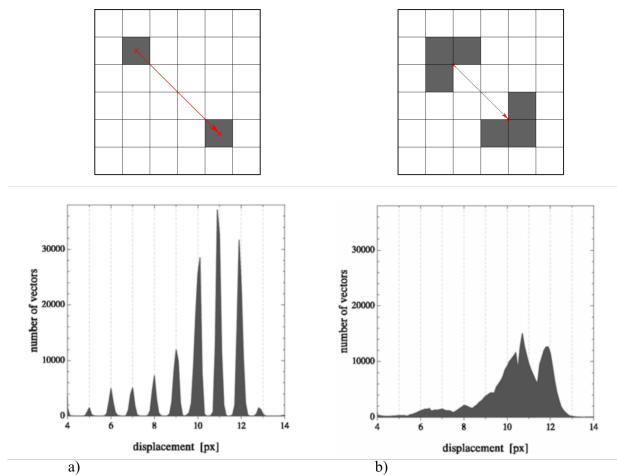


Figure 4.3: The effects of peak locking. a) peak-locking is evident as the displacement is solely determined by an integer number of pixels. b) Smaller degree of peak-locking [36].

4.2 Signal Processing

In order to convert raw voltage data into understandable data, signal post-processing is essential. Several types of post-processing techniques exist depending on what type of data one studies. This section explains the signal post-processing techniques used in this master's thesis.

4.2.1 Sampling

The Nyquist-Shannon theorem states the absolute minimum sampling rate necessary in order to accurately represent the highest frequencies of an analogue signal digitally. It states that everything above two samples per period of the investigated frequencies is sufficient. Not following this criterion aliasing will occur. This is when similar signals become indistinguishable from each other when sampled, something which will give false measurements.

4.2.2 Welch's Method

Welch's method is a way of computing power spectrum density estimations which are used for estimating the power of a signal at different frequencies. A detailed explanation of this method can be found in Welch's paper from 1967 [37]. Summarised the method converts a signal from a time domain into a frequency domain by computing the Discrete Fourier transform (DFT) based on the Fast Fourier Transform (FFT). Where the FFT takes a small part of a signal and repeats it in order to be able to execute a DFT and solve for a frequency spectrum. Using Welch's method, a reduction in noise in the power spectrum density estimation is achieved at the expense of a reduction of the frequency resolution when compared to other methods. This is something which is often desired when analysing raw data with some degree of white noise.

4.2.3 Spectral Leakage

Measured raw signal data is rarely made up of an integer number of periods. As one performs an FFT on this raw signal repeating it for an infinite amount of periods discontinuities emerge in the repeated signal. An example of this effect is shown in figure 4.4 a), where it can be seen that the repeated signal does not match the original signal. This means that values of the signal at the end of each repeated period can leak into the next period making it harder to find the actual frequency of the signal. Something which is illustrated in figure 4.4 c). This is called spectral leakage, and a way of reducing its effect is by enforcing a window over segments of the sampled data with the use of window functions.

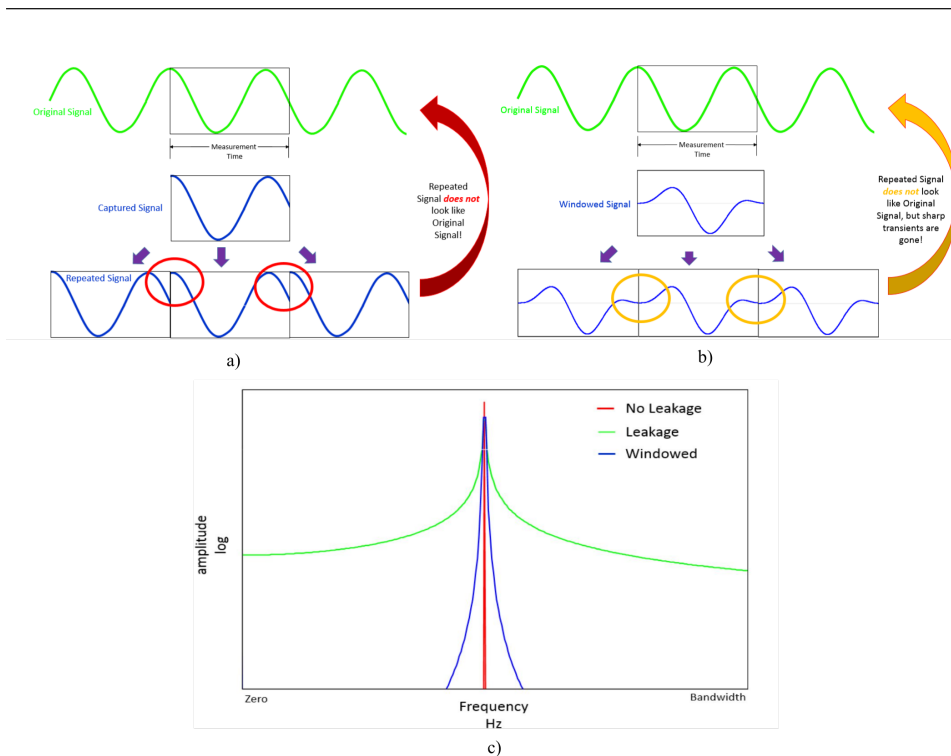


Figure 4.4: Figures illustrating spectral leakage. a) Discontinuities which emerge from repeating a signal with a non-integer number of periods. b) How windowing can help reduce the discontinuities. c) The frequency range of a periodic sine wave without leakage, and a non-periodic sine wave with leakage and with reduced leakage because of windowing [38].

4.2.4 Window Function

Adding a window function to segments of measured raw data can help reduce the discontinuities that cause spectral leakage. A window function reduces the sharp transients in the signal created by performing an FFT on a non-periodic signal, as illustrated in figure 4.4 b). This, in turn, contains the leakage to a smaller frequency range which as is shown in figure 4.4 c). Several types of window functions exist, and depending on what the situation with the raw data is an appropriate window can be found. In choosing the correct window one can look at the main and side lobes of the window function in the frequency domain as illustrated in figure 4.5. There are three parameters to consider when choosing the most appropriate window function. The size of the main lobe, the height of the side lobes and the roll-off rate of the side lobes. A thinner main lobe will in general smear the signal out more and a higher side lobe will cause copying of frequency data which can cause the primary frequency to go unnoticed. Thus ideally one would wish for a thin main lobe and smaller side lobes with a high roll-off rate. This is usually not possible to achieve as the main lobe is dependent on the side lobe and vice versa. Generally one would choose a window with a large main lobe and a large lobe roll-off rate if the signal contains strong interfering frequencies far from the frequency of interest. A signal containing interfering frequencies close to the frequency of interest should apply a window

function with a low maximum side lobe. If two or more frequencies of interest are close to each other, a narrow main lobe might be beneficial. If the amplitude of the frequency is more important than the frequency a window with a wide main lobe should be chosen [39]. Generally, a Hanning (Hann) window is sufficient and used in most cases. Windows are commonly also overlapped from one data segment to another in order to avoid loss of important information.

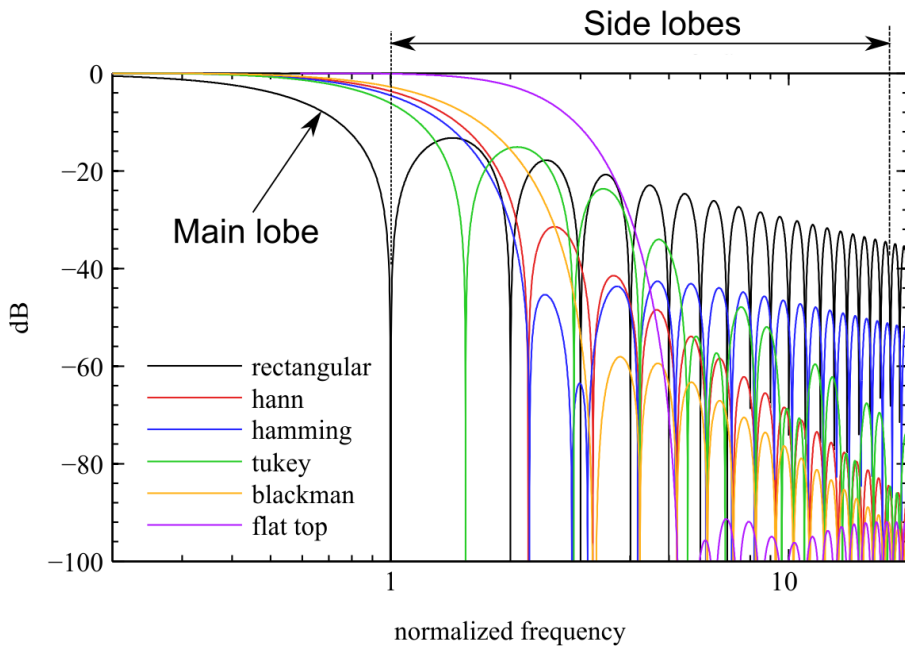


Figure 4.5: Window functions in the frequency domain with annotations for the main and side lobes [40].

Experimental Setup

In order to evaluate the effects longitudinal vortices generated by trailing edge vortex generators (VGs) have on the vortex-induced vibrations (VIVs) an experimental method is utilised. This chapter explains the details around the test section, hydrofoil, measurement technique, calibration and data processing.

5.1 Test Section

The test section is illustrated in figure 5.1. By allowing for a long inlet, the flow is made uniform before the onset of the hydrofoil. The cross-section of the test section is a square measuring 150x150mm and is used to calculate the reference flow velocity. It is equipped with two see-through windows just downstream of the trailing edge (TE) to allow for usage of particle image velocimetry (PIV). The hydrofoil is fully detachable to allow for the ability to have an interchangeable TE which is elaborated on in the next section. The flow meter and temperature sensor are located downstream of the hydrofoil, and a strain gauge is attached on the hydrofoil just upstream of the trailing edge. The highest pressure the test section can sustain is 8bar. This high pressure flow is important in order to avoid cavitation due to the addition of VGs, which is told more about in section 5.3.

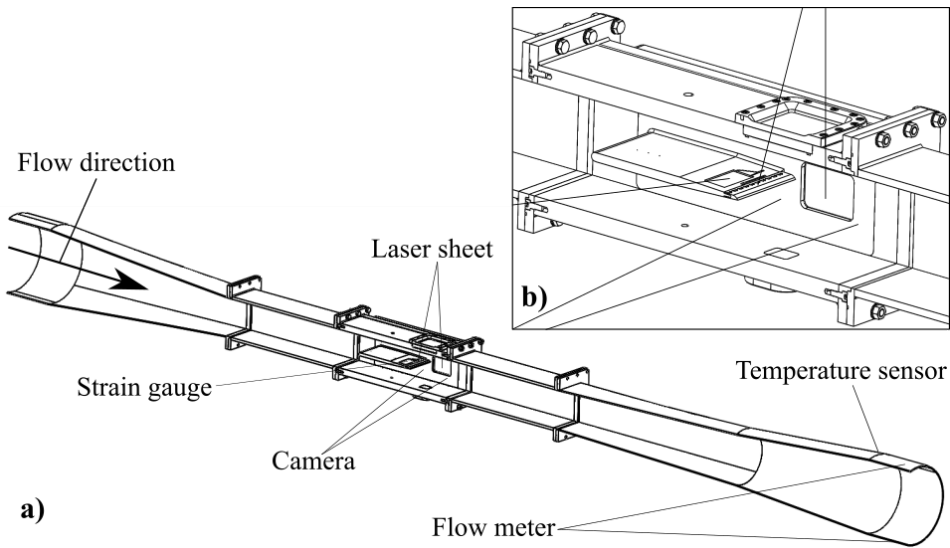


Figure 5.1: a) Full view of the experimental set-up. b) An enlarged view of the test section with the hydrofoil and VGs.

5.2 Hydrofoil

The hydrofoil at which VIVs are studied is illustrated in figure 5.2. Trailing edge thickness at the position where the curve starts is $D = 4.8\text{mm}$ and is used as the characteristic length. The hydrofoil is produced in an aluminium alloy and has an interchangeable trailing edge, as illustrated in figure 5.2 b). This is to make for an easy way of testing several different trailing edges without the means of producing the whole hydrofoil each time a new trailing edge design is to be tested. The trailing edge is glued to the hydrofoil with a strong glue that can expand and "let go" when heated to a temperature of 90 degrees Celsius for relatively easy removal. It is coated in a thin matte black paint in order to reduce laser reflections which can distort the PIV measurements. All measurements are conducted at a static angle of attack of 0° . In the case of this master's thesis, it is planned to execute measurement campaigns on two separate trailing edges, one trailing edge with optimised VGs and one reference trailing edge without VGs. This is in order to be able to compare and quantify the effects VGs have on VIVs. The reference case has been shown to experience a state of lock-in at a velocity range of $11.1\text{m/s} - 12.1\text{m/s}$ by Sagmo et al. [4].

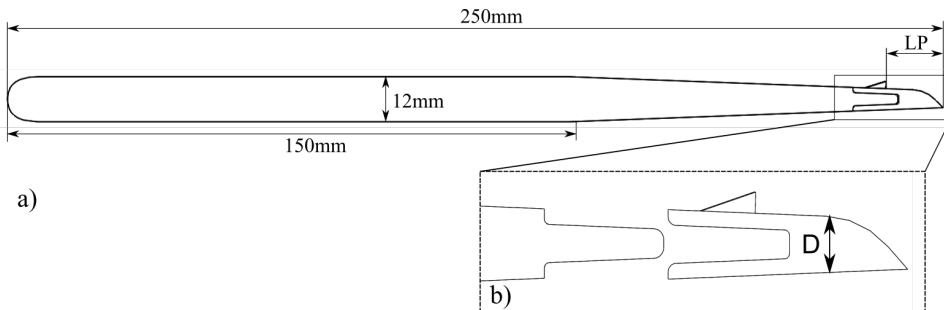


Figure 5.2: a) Overall hydrofoil dimensions. b) Attachment mechanism for an interchangeable trailing edge.

5.3 Vortex Generator Design

Table 5.1: Optimal VG parameters as shown in figure 5.3 and figure 5.2 derived from literature

Configuration	h	L/h	Z/h	S/h	α	LP/h
CoR (counter-rotating)	1.92mm	3	2.5	1.5	20°	5

The VGs used in this master's thesis are designed based on research from the past four decades. Design parameters are chosen such that strong vortices which stay close to the hydrofoil surface are generated without the onset of cavitation. VG parameters are also chosen such that they induce the lowest possible drag without affecting the vortex strength. Design parameters include the configuration, height (h), Length (L), lengthwise position (LP), span (S), the spacing between adjacent VGs (Z) and orientation angle (α). These

parameters are shown in figure 5.2 and 5.3, and discussed upon in this section. A summary of the final parameters is given in table 5.1.

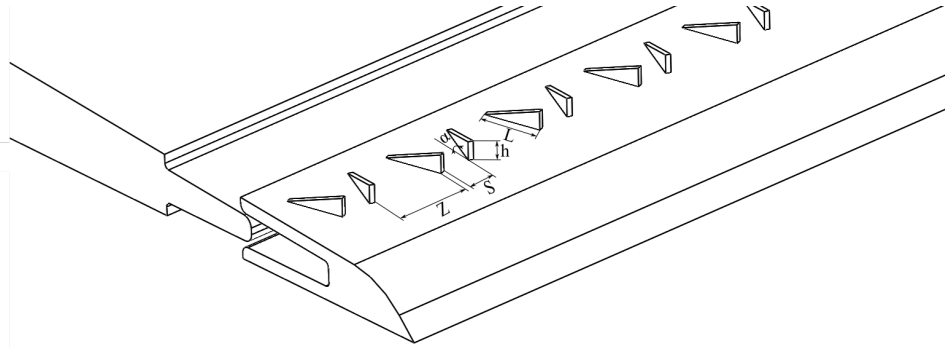


Figure 5.3: Endplate attachment mechanism and VG parameters considered in this thesis

Configuration

The configuration of the VGs consists of the shape of the VGs and how the vortices are generated. For this master's thesis, simple vane-type triangular VGs which generate counter-rotating vortices are chosen. This is because of their superiority in vortex strength generation and lower drag when compared to other configurations [13], [41]. They also tend to produce vortices which stay closer to the surface and diffuse less downstream [25], thus having a higher chance of interacting with the Kármán vortex street and potentially mitigate the VIVs. These types of VGs are illustrated in figure 5.3. Aerodynamical VGs were also considered. This would lower the drag and risk of cavitation, but the idea was omitted due to the complexity of manufacturing when comparing to the benefits it would provide [32].

Height (h)

It has been shown that larger VGs tend to produce stronger vortices [20]. However, since the main objective of the VGs in this master's thesis is to generate vortices which interact with the Kármán vortex street, sub boundary layer VGs would be beneficial. These VGs tend to generate vortices which stay closer to the surface and induce a lower drag [20]. The VG height is usually defined as a fraction of the boundary layer thickness. Approximating the hydrofoil as an infinite flat plate with a fully turbulent boundary layer from the leading edge. Equation 5.1 given by Prandtl in 1921 can then be used to find the boundary layer thickness (δ) [42].

$$\delta = \frac{0.16x}{Re_x^{\frac{1}{2}}} \quad (5.1)$$

An average water temperature was measured to 22° Celsius. The VGs will be situated close to the trailing edge, with this in mind a chord based Reynolds number is calculated. $Re_c = 2.88E6$ is found at a flow velocity of 11m/s and chord length of $c = 250mm$. Using equation 5.1 we find a boundary layer thickness of $\delta = 4.78mm$ at the trailing

edge. VGs with heights from $h = 0.2\delta$ to $h = 0.7\delta$ have been shown to produce the effects desired in this master's thesis [13], [41]. Taking this into account VGs with a height of $h = 0.4\delta \approx 1.92mm$ are manufactured. This is classified as sub boundary layer VGs.

Length (L)

VG length does not have a big impact on the performance of the VGs [41]. It has only been observed that vortices produced by longer VGs diffuse less downstream [25]. However, a significant increase in drag follows with longer VGs [21]. Recommended values range from $L = 2h$ to $L = 4h$. $L = 3h$ is chosen giving a VG length of $L = 5.76mm$. This is believed to be a good approximation when looking at the drag increase longer VGs entail.

Span (S)

Lin et al. [13] has shown that the decay of streamwise vortex strength is an order of magnitude lower for VGs with span when compared to no span. An early liftoff of vortices is also observed with VGs having no span [19]. Recommendations for the span are $1h-2h$, therefore a span of $S = 1.5h = 2.88mm$ was chosen.

Spacing (Z)

A well chosen spacing can have positive effect on the lift to drag ratio of the VGs and on holding the generated vortices close to the surface [21]. Mueller-Vahl et al. [20] found that a value of $Z = 3h$ gives the highest lift to drag ratio. Godard and Stanislas [41] and Betterton et al. [19] found optimal values of $Z = 2h$. With regards to these findings a value of $Z = 2.5h = 4.8mm$ was chosen.

Orientation Angle (α)

This might be the most important parameter when it comes to the performance of VGs in a liquid and for the effects which are desired in this master's thesis. With an optimal orientation angle, strong vortices are induced without the onset of cavitation, which can disrupt the effect of the VGs. Pauley and Eaton [43] found that the vortex strength generated by VGs was increasing linearly up to an orientation angle of 18° . Li et al. [44] showed that a larger orientation angle would lead to higher intensity vortices that diffuse quicker downstream. An angle of 20° was found to be optimal for slow diffusion of vortices. Many other researchers have found similar results for optimal angles [41],[45]. Approximating the hydrofoil as an infinitely thin flat plate, we can use Prandtl's one-seventh power law, equation 5.2 which is in good agreement with turbulent flat plate data to evaluate the velocity (u) at the trailing edge of the VGs. Where a value of $u \approx 10m/s$ is found.

$$\frac{u}{U_\infty} = \left(\frac{y}{\delta}\right)^{\frac{1}{7}} \quad (5.2)$$

Using this velocity, the cavitation number (σ) given by equation 5.3, which is used in the paper of Brandner and Walker [10] can be calculated. Where P_∞ is the ambient pressure, P_V is the vapour pressure, ρ is the fluid density and U is the local flow velocity. With the

ability to have a static pressure of $8bar = 8E5pa$ in the test section, a cavitation number of $\sigma \approx 13$ is found. From the paper of Bradner and walker, it was shown that no cavitation would occur for cavitation numbers above 5 for angles up to 25° . Using the results from Brandner and Walker [10], Li et al. [44] and Pauley and Eaton [43] an angle of 20° was chosen.

$$\sigma = \frac{P_\infty - P_v}{\frac{1}{2}\rho U^2} \quad (5.3)$$

Lengthwise Position (LP)

The best performance is obtained by placing the VGs at a position before the occurrence of separation. Recommendations in the literature range from $5h$ to $10h$ upstream of the point of separation. From visual inspection in the paper of Sagmo et al. [4] the approximate point of flow separation is found at $x \approx 244\text{ mm}$ along the chord of the hydrofoil. The VGs were placed such that the VG trailing edge is positioned $5h = 9.6\text{ mm}$ upstream of the point of separation.

5.4 Measurement Technique

In order to extract data from the test section measurement probes have to be utilised. These are devices which convert forces or images to digital data which can be analysed at a later stage. However, before any measurement campaign can take place calibration of the measurement probes is essential. This is usually done by comparing measurements done with the probe, which is being calibrated to a known standard. By doing this, it ensures that the attained data from these probes are accurate. In this section, the measurement techniques used in this master's thesis are discussed.

5.4.1 Strain Gauge

A strain gauge delivered by Kulite measures the structural vibrations of the hydrofoil. This is a device which converts forces into electrical signals. It is located $\approx 55\text{ mm}$ from the trailing edge, inside the hydrofoil, situated such that the vibrational bending modes of interest are measured. Data attainment is managed by LabVIEW and National Instruments (NI) data acquisition devices (DAQ's). A sampling rate of $\approx 25\text{ kHz}$ is utilised, which gives at least 25 samples per period for the frequencies investigated. This is well within the Nyquist-Shannon sampling theorem and thought to be more than sufficient for the applications in this master's thesis. This sampling rate would also give a significant decrease in the standard deviation when comparing to shorter sampling rates [46].

5.4.2 Particle Image Velocimetry

PIV recordings were performed in two separate planes. One plane which is located on the symmetry line parallel to the hydrofoil chord and normal to the trailing edge of the hy-

Table 5.2: PIV recording parameters for the hydrofoil wake flow measurements with VGs

Symmetry-plane	
Field of view	43.9 mm x 35.1 mm / 1280 px x 1024 px (x,y)
image acquisition rate	2.4 kHz
Spanwise-plane	
Field of view	35.1 mm x 43.9 mm / 1024 px x 1280 px (x,z)
image acquisition rate	0.2 kHz
Both planes	
Recording method & Camera sensor	Double frame/Double exposure & CMOS
Exposure time	250 μ s
Interrogation area	0.55 mm x 0.55 mm / 16 px x 16 px (x,y)
Illumination source	YFL dual cavity laser, 527 nm wavelength
Experimental velocity range	(4 - 16) m/s
Lens F-number	5.4
Observation distance	517 mm
Image processing mode	cross-correlation
Mean tracer particle diameter d_p	13 μ m
Tracer particle density δ_p	1.1g/cm ³

drofoil is used to check the shedding frequency. The second plane, located just above the trailing edge parallel to both the hydrofoil chord and trailing edge, is used to study the longitudinal vortices generated by the VGs. These planes are respectively called symmetry-plane (sym.P) and spanwise-plane (sw.P) and are shown in figure 5.4. A high-speed camera delivered by LaVision GmbH, oriented perpendicular to the plane of interest recorded the flow field. Images of (1280x1024) pixels (px) amounting to a field of view (FOV) of 43.9mm x 35.1mm were acquired. The camera is equipped with a CMOS sensor which has high sensitivity and low noise when compared to other types of sensors. Recordings were performed in a double frame/double exposure with a sampling rate of 2.441kHz for the sym.p and 0.2kHz for the sw.P. Several sampling rates were tested for both planes, and it was evident that sampling over a more extended period was required for sw.P in order to capture the average velocity field accurately. A total number of 4367 image pairs were acquired amounting to a sampling period of ≈ 2 sec and ≈ 22 sec for the sym.P and sw.P respectively. The particles were illuminated using a YFL dual cavity laser providing two laser beams with a wavelength of 527nm. The laser beams were passed through a light sheet optic with a focal length equal to -20 mm provided by LaVision GmbH in order to produce a laser sheet. An observation distance of 51.7cm, Lens F-number of 5.4, and tracer particles with a mean diameter of 13 μ m and density equal to 1.1g/cm³ gave an average particle image diameter of 2.2px. This was deemed sufficient in order to have an acceptable degree of peak locking. The laser pulse separation (dt) was chosen such that particle displacement within each cross-correlation image pair was 4 – 6px. This was in order to ensure that the velocity vectors were calculated correctly with fewer spurious values. Cross-correlation with a multipass method was used to evaluate the vector fields with an initial 64x64px IA stepping down to a 16x16px IA both with 50% overlap. At least ten particle images were observed within an initial IA of 64x64px. Repeatability of measurements was checked showing a suitable range. Data was handled with a software called DaVis 8.4 delivered by LAVision. The PIV parameters are summarised in table 5.2.

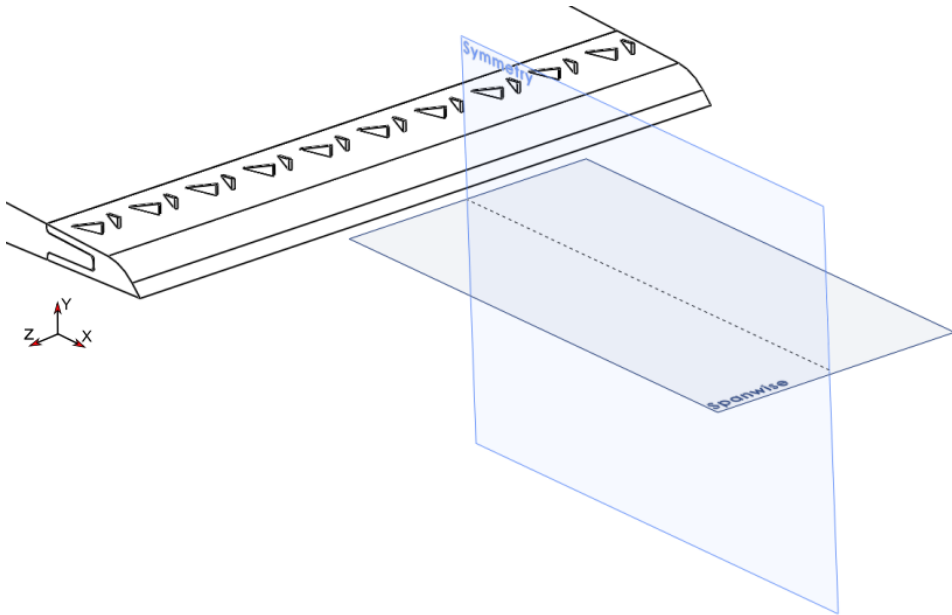


Figure 5.4: Symmetry-plane and spanwise-plane downstream of the hydrofoil at which PIV measurements were attained.

PIV calibration and uncertainty

Calibrating the PIV set up is concerned with checking the laser sheet overlap, adjusting the angle of the laser sheet and calibrating the high-speed camera. First, a laser sheet overlap check was performed of the two laser beams. The overlap was believed to be sufficient with a correlation value of ≈ 0.9 . An adjustment of the laser sheet was then performed by ensuring that the laser sheet hitting the calibration device made a line with consistent thickness, as shown in figure 5.5 b). The camera was then positioned such that the desired field of view was attained and the image was focused. For the calibration of the camera, a calibration grid is attached to the calibration device shown in figure 5.5 a). An image of this grid is taken when the camera is in position. From this image, Davis 8.4 software is used to calibrate the camera. Once the calibration is finished and the calibration device is removed from the test section, it is essential not to move the camera nor the laser. After the measurement campaign, a new calibration is performed to check for movement of components during measurements

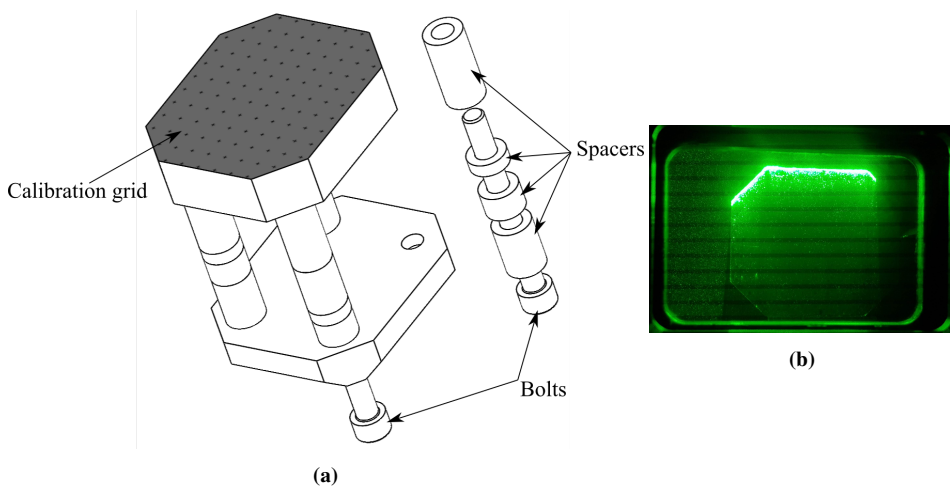


Figure 5.5: a) Calibration device with grid used to calibrate camera. b) Laser sheet on calibration device showing uniform thickness of the laser sheet.

If the PIV is calibrated properly, then most of the uncertainty is based on the recognition and displacement of particles within the software [34]. While the calibration can pose some error due to the calibration device, attachment of the calibration grid and manually checking the perpendicularity of the laser sheet it is close to negligible when compared to the uncertainty due to post-processing of PIV images. Thus, it is the uncertainty of post-processed images where the focus is directed. As the resolution of the camera defines the information in the images, uncertainties arise due to lack of particle information. In the software Davis 8.4 delivered by Lavisio GmbH, the uncertainty of each vector in a vector field is calculated using a method described by Wieneke [47]. The method is based on looking at the difference between particle image intensity in image pairs obtained from correlation. Ideally, the particle image intensities would match perfectly, but in real data, this is not the case. This mismatch is observed by looking at the cross-correlation peaks of these particles. The standard deviation of each particle image intensity is together with the expected asymmetry of the correlation peak used to calculate the uncertainty. Using this method, it was evident that the error in the velocity of vectors was increasing with increasing reference velocity. The normalised error was found to be approximately constant across all velocities and the two planes at which PIV measurements were attained. This is shown in figures 5.6 a-d). A maximum uncertainty of $U/U_{ref} \approx 0.075$ was found where 1.87% and 0.06% of all vectors had uncertainty above $U/U_{ref} \approx 0.045$ for the sym.P and sw.p respectively. The highest uncertainty on average across all frames was found in the wake, as shown in figures 5.6 e-f). A maximum average uncertainty of $U/U_{ref} \approx 0.004$ was found with only 0.12% of vectors having a uncertainty above $U/U_{ref} \approx 0.0035$.

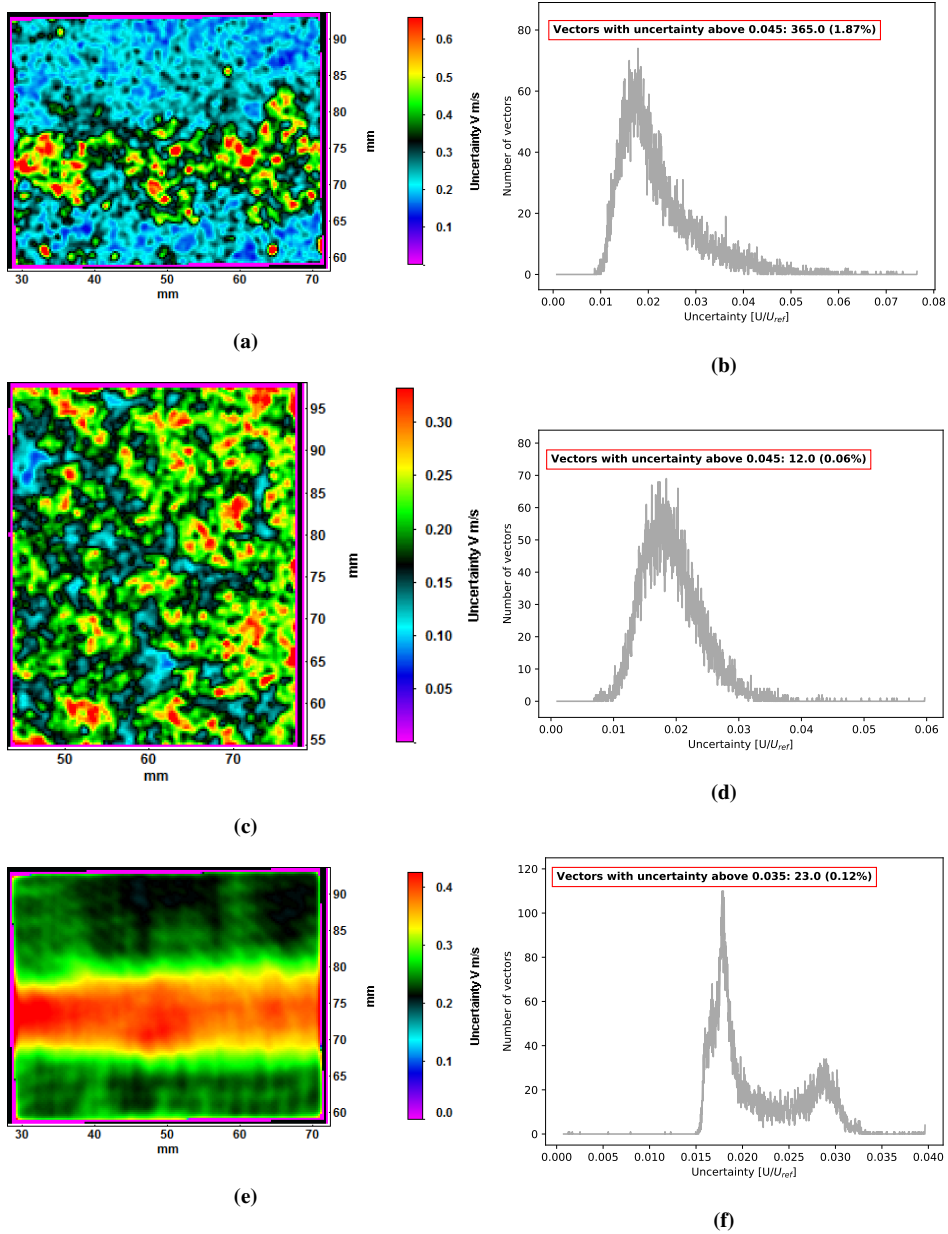


Figure 5.6: Uncertainty in the absolute velocity V . Figures to the left show uncertainty colourmaps at different reference flow velocities and planes. Figures to the right show a histogram plot of the colourmap data to the left with uncertainty non dimensionalized along the x-axis and number of values along the y-axis. a-b) $U_{ref} = 13.1 \text{ m/s}$, symmetry-plane at a arbitrary frame (f:2183/4367). c-d) $U_{ref} = 10.1 \text{ m/s}$, spanwise-plane at a arbitrary frame (f:2183/4367). e-f) $U_{ref} = 10.1 \text{ m/s}$, average across all frames for the symmetry-plane.

Another indication of error and a way of validating PIV is to look at the number of spurious vectors, which are vectors that differ significantly in both direction and length from the surrounding vectors. Vectors like this appear at the edges of almost all PIV images because of particles coming in and leaving the FOV [34]. The spurious vectors which occur around the edges of the FOV are therefore ignored in this analysis. A way of finding these vectors is to look at the peak ratio. This is the ratio between the first and second highest correlation peak of two correlated images [48] as illustrated in figure 5.7 and equation 5.4. Where the highest peak is used to assess the displacement of particles and the other peaks are noise. A peak ratio above two would be sufficient to avoid spurious vectors [49], and according to the LaVision manual [48], a peak ratio of 3–4 is a sign of good PIV data. With a multipass method stepping down from an IA of 64x64 to an IA of 16x16 it was on average across all frames found no or close to no peak ratio below three meaning uncertainty due to spurious vectors was low. This can be seen in figure 5.8 e-f) where an average peak ratio below three is observed only for 11 calculated vectors, 0.06% of all vectors. The peak ratio was observed to be approximately constant across the range of flow velocities tested. For an arbitrary frame, it was found that 6.68% and 1.34% of all vectors for the sym.P and swp.P respectively had a peak ratio below three. These values are further discussed in chapter 7.

$$Peakratio = \frac{P_1 - min}{P_2 - min} \quad (5.4)$$

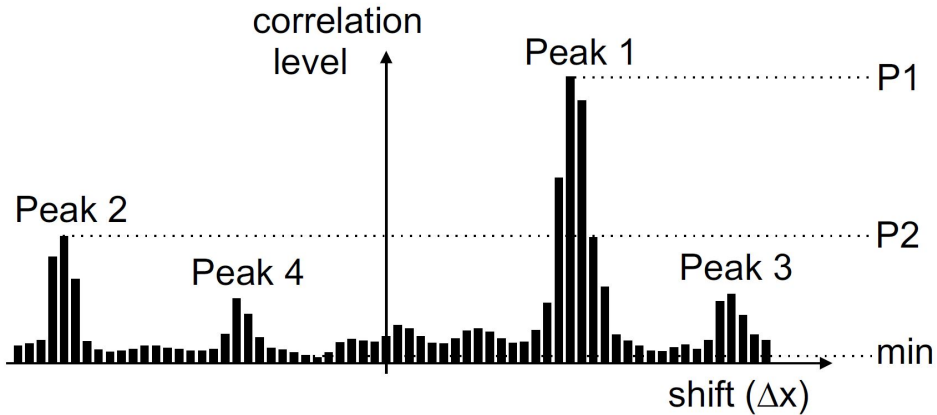


Figure 5.7: Illustration of correlation peaks [48].

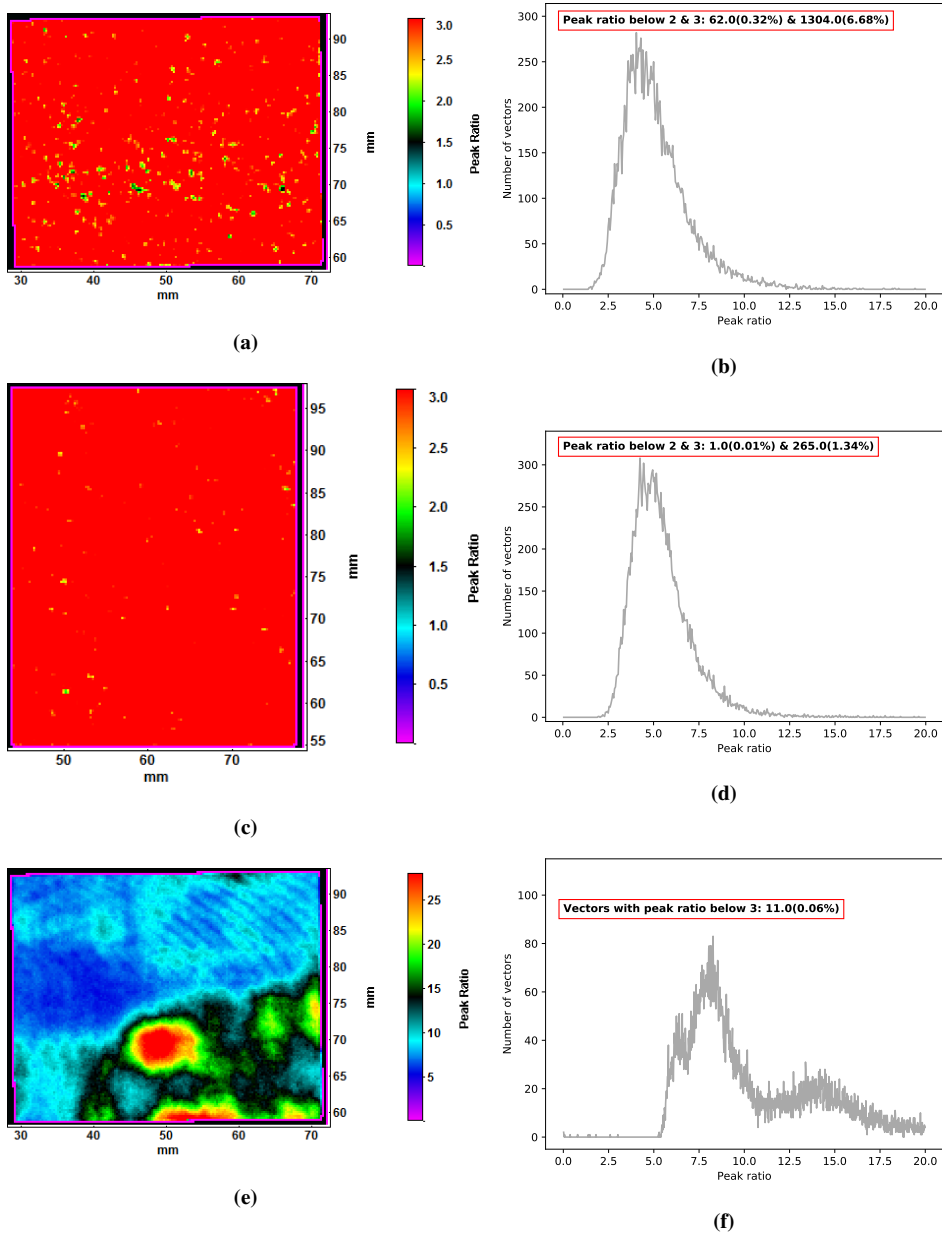


Figure 5.8: Peak ratio from PIV measurements for a reference flow velocity of 10.1m/s for the two planes. Left figures show a colourmap plot of the peak ratio. Right figures show histogram plots of the colourmap data to the right and the number of vectors with peak ratio below respectively two and Three. a-b) Symmetry-plane, arbitrary frame (f:2183/4367). c-d) Spanwise-plane, arbitrary frame (f:2183/4367). e-f) Symmetry-plane, the average across all frames.

5.5 Overall Measurement Probes

Table 5.3: Measurement probes excluding the strain gauges and PIV

Temperature sensors	RTD PT100 thin film, 4-wire
Flow-meter	ABB electromagnetic
Pressure sensors	GE druiK 5000

An overview of other measurement probes utilised in this work is given in table 5.3. An RTD PT 100 thin film, 4-wire temperature sensor, situated downstream of the hydrofoil, was used to measure the water temperature. The 4-wire connection ensures that systematic errors are avoided. An ABB electromagnetic flow-meter situated downstream of the hydrofoil was used to measure the volumetric flow rate of the test section. GE druiK 5000 pressure sensors were used to measure pressures at different positions on both the surface of the hydrofoil and the test section walls. More details about the sensors mentioned above and the calibration process of these sensors can be found in appendix B.

5.6 Data Processing

To obtain the amplitude-frequency spectrum analysis, later presented in the results P.D Welch’s power spectrum method was utilised within the python scripts shown in appendix D. In order to smooth out the frequency spectrum, the raw signal was split into different lengths, and window functions were enforced on these split segments. A Hanning (Hann) window was used as an initial guess and was sufficient for most cases. For signals with strong interfering frequencies close to the frequency of interest a kaiser window, as explained by Harris [50], was enforced on the data. This was evident to be essential for PIV data which contained much noise with strong interfering frequencies. For all window types and lengths, an overlap of 50% was utilised in order for critical frequencies not to end up in between two windows and fall away from the frequency spectrum.

For the post-processing of PIV data, it was first performed a pre-processing of images by removing background noise, which was done by calculating the gaussian average light intensity coming from the PIV images and subtracting it. This makes it easier for the software to distinguish particles from light reflections or noise, giving a lower uncertainty. As explained in section 5.4.2, a multipass method was then utilised to assess the vector fields. Several methods and window sizes for obtaining the vector fields were tested, and it was evident that the method explained in section 5.4.2 was the one which exhibited the lowest uncertainty when limiting the computational time to three hours. From these vector fields, velocity components, vorticity and probability density functions, used for calculating the amplitude-frequency spectrum, were obtained. The vorticity decay functions, later shown in the results, were obtained by tracking the peak vorticity in the vortex core downstream. A regression line, which is the best fit function for a set of data points, was calculated using a curve-fit script in Python. The R-value, which is a measure of the statistical relationship between a fitted function and some data points, was estimated to check the fit of the regression line.

Results

Results obtained from the experimental work are presented in this chapter. First, a comparison between the natural frequencies of a hydrofoil without VGs called the reference foil, and a hydrofoil with VGs attached at an interchangeable trailing edge are presented. Measurements performed on the hydrofoil with VGs during this master's thesis are then given. As the planned experiments with a reference foil with an interchangeable trailing edge were not executed a summary of the most relevant experimental results from a paper by Sagmo et al. [4] are presented in the final section. These results are presented as they are essential for the discussion and used in order to quantify the effects of VGs later in this master's thesis. The only difference between the reference foil studied in the paper, and the one that was planned is an interchangeable trailing edge which would have close to no impact on the measurements and comparisons later discussed.

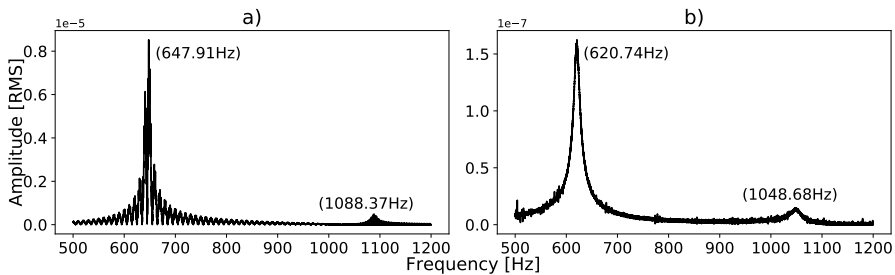


Figure 6.1: Amplitude frequency spectrum obtained by P.D Welch's power spectrum and a Hanning window for the hydrofoil natural frequency measurements. a) Natural frequencies of the reference hydrofoil without VGs from the paper of Sagmo et al. b) Natural frequencies of a hydrofoil with VGs and an interchangeable trailing edge.

Amplitude frequency spectrum for the natural frequency measurements of a reference foil without VGs, and the hydrofoil with VGs and an interchangeable trailing edge is shown in figure 6.1 a) and b) respectively. The first and second peak are identified as the first and third vibrational bending modes, also called the first and third natural frequencies of the hydrofoil as discussed by Ćupr et al. [51]. The natural frequency of interest is given by the first peak. It is $\approx 648 Hz$ for the reference hydrofoil and $\approx 621 Hz$ for the hydrofoil with VGs.

6.1 Hydrofoil with Vortex Generators

Vortex Induced Vibrations

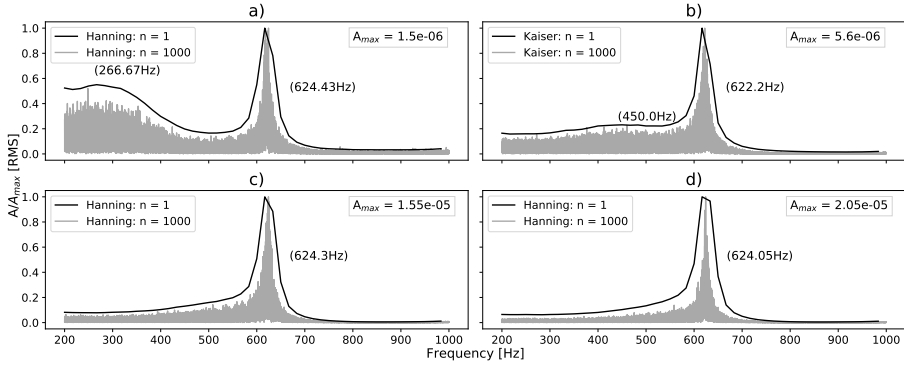


Figure 6.2: Amplitude frequency spectrum for the hydrofoil with VGs using two separate window function sizes in order to smooth out the frequency spectrum. The first and second peaks are annotated. a) $U_{ref} = 6.0 \frac{m}{s}$. b) $U_{ref} = 8.0 \frac{m}{s}$. c) $U_{ref} = 9.1 \frac{m}{s}$. d) $U_{ref} = 9.6 \frac{m}{s}$.

Figure 6.2 presents the amplitude-frequency spectrum at some chosen reference flow velocities. The second peak observed in figures 6.2 a) to d) is identified as the first natural frequency of the hydrofoil. A peak approaching this natural frequency is observed for the lower flow velocities, which is identified as the shedding frequency of the hydrofoil. It is also observed that the amplitude of the first peak is significantly damped as the flow velocity increases. The amplitude-frequency spectrum in figure 6.3 is obtained at $x = 1D$ downstream of the hydrofoil trailing edge from the PIV measurements. The peaks are identified as the shedding frequency of the hydrofoil at different flow velocities and strengthen the statement of the first peak in figure 6.2 being the shedding frequency. As the frequency spectrum for both the strain gauge and PIV data resemble a Gaussian distribution, the full width half maximum (FWHM) of the smoothed out frequency spectrum is used to assess the spread of the maximum frequencies. These extremal values are presented as error bars in figure 6.4. Repeated strain gauge measurements at a reference velocity of $U_{ref} = 9.1 m/s$ were used to assess the uncertainty of the vibrational frequencies. A standard deviation of approximately $1.64 Hz$ at the second peak was calculated.

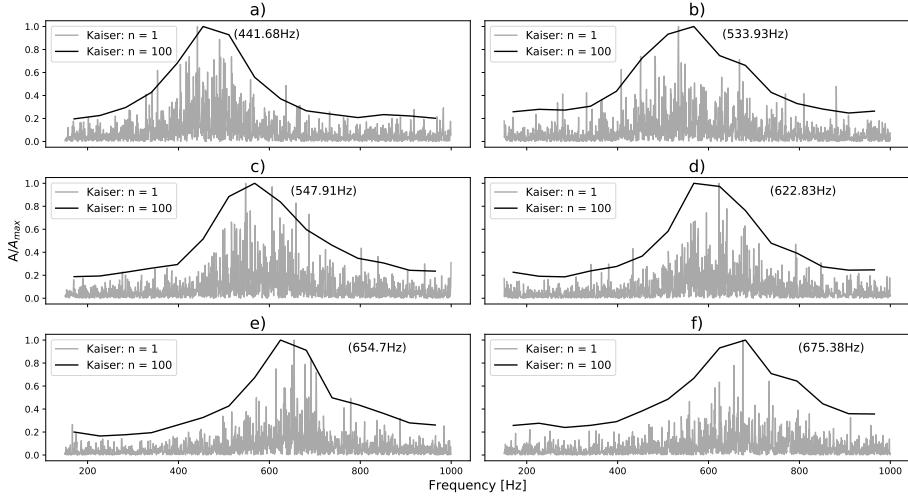


Figure 6.3: Power spectrum analysis of PIV data at several reference flow velocities. a) $U_{ref} = 8.0 \frac{m}{s}$, b) $U_{ref} = 9.1 \frac{m}{s}$, c) $U_{ref} = 9.6 \frac{m}{s}$, d) $U_{ref} = 10.1 \frac{m}{s}$, e) $U_{ref} = 10.6 \frac{m}{s}$, f) $U_{ref} = 11.1 \frac{m}{s}$

The PIV and strain gauge peaks obtained from power spectrum analysis are summarised in figure 6.4. An empirical estimate based on the Strouhal equation with a measured Strouhal number of $St = 0.274$, as found by Sagmo et al. [4], is plotted with a dashed line. Good agreement between the empirical estimate and the shedding frequencies obtained from PIV measurements is observed. A correlation coefficient (R-value) of ≈ 0.95 was calculated, showing a strong positive linear relationship between the PIV data and the empirical estimate. It is also evident from the span of the error bars obtained from FWHM that the shedding frequencies obtained from the PIV measurements are uncertain. Figure 6.4 also shows the relative vibrational amplitude of the second peak. The amplitude is observed to increase gradually from a reference flow velocity of $U_{ref} = 9.1m/s$ to $U_{ref} = 11.1m/s$ before gradually decreasing again and becoming constant. This would be the opposite of what would happen if a state of lock-in was encountered where a sudden rise and drop would be evident for the flow velocities in which lock-in occurs. An overall maximum vibrational amplitude of $A_{max} \approx 3.35E - 5$ for a reference flow velocity of $U_{ref} = 11.1$ was found.

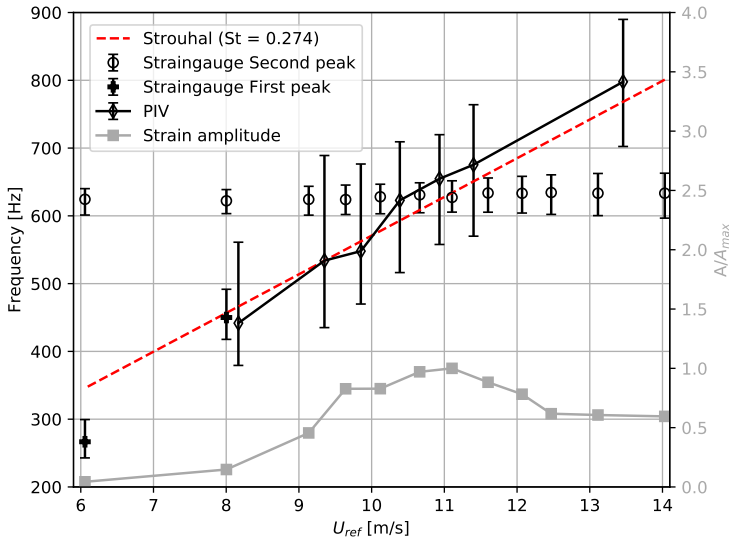


Figure 6.4: Vibrational frequencies from strain gauge data and shedding frequencies from PIV data plotted along the right axis with corresponding error bars estimated by the Full Width Half Maximum. Normalised vibrational amplitude of the second peak of the hydrofoil plotted along the left axis.

Average Velocity

The average wake velocity at a reference flow velocity of $U_{ref} = 10.1\text{m/s}$ and the wake velocity profiles at two positions downstream of the trailing edge are illustrated in figure 6.5 for the symmetry plane. It is observed that there is a considerably higher variation in the velocity profiles at reference flow velocities of $9.1 - 10.1\text{m/s}$ compared to higher and lower velocities. Average velocity component V_z in the spanwise plane at a reference flow velocity of $U_{ref} = 10.1\text{m/s}$ is shown in figure 6.6 along with the V_z velocity profiles at a position of $x = 16.6D$ downstream of the hydrofoil trailing edge. Four alternating positive and negative velocity pairs are observed and identified as the wake from four pairs of vortex generators. It is also observed that the VGs wake is not symmetric across each pair of vortex generators. Velocity uncertainty is plotted as error bars in both figures 6.5 and 6.6 for some reference flow velocities.

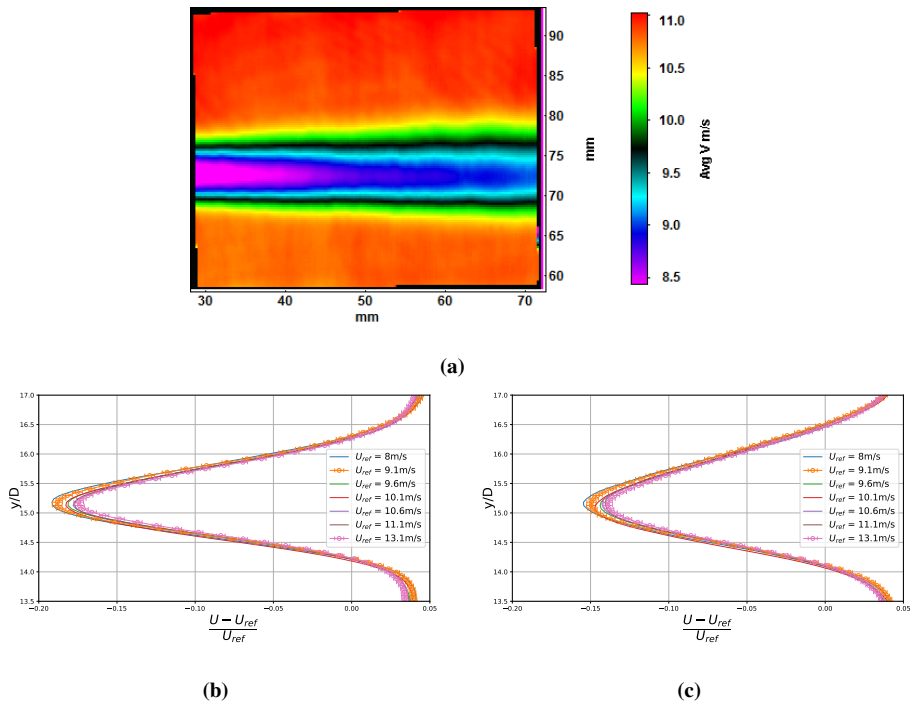


Figure 6.5: a) Colormap of average velocity across all frames for $U_{ref} = 10.1 \frac{m}{s}$, symmetry plane. b) Average velocity profiles for several reference velocities at $x = 8.3D$. c) Average velocity profiles for several reference velocities at $x = 12.5D$. Errorbars are only plotted for reference velocities $U_{ref} = 9.1 \frac{m}{s}$ and $U_{ref} = 13.1 \frac{m}{s}$.

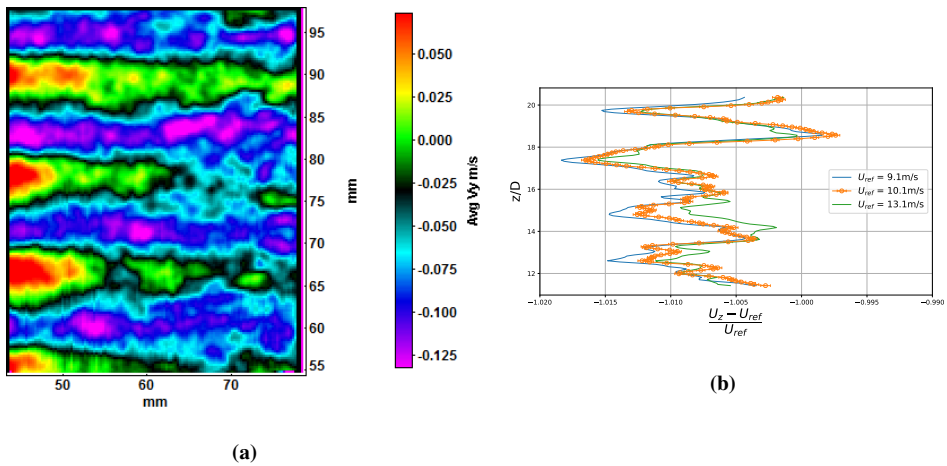


Figure 6.6: a) Colormap of average velocity component U_z at $U_{ref} = 10.1 \frac{m}{s}$, spanwise plane. b) Average velocity component U_z profiles for several reference flow velocities at $x = 14.6D$. Errorbars are only plotted for a reference flow velocity of $U_{ref} = 10.1 \frac{m}{s}$.

Vorticity

Figures 6.7 and 6.8 are showing the negative vorticity normalised by D and U_{ref} in the wake of the hydrofoil, for the sw.P and sym.P respectively, at some reference flow velocities. Figure a) show four alternating vortice pairs which are identified as the wake of four pairs of VGs. A satisfactory symmetry across each pair is noted. A linear relationship between the normalised vorticity and distance x/D downstream was found for the vortices generated by the VGs. It was obtained a Vortex decay gradient of -0.0141 , meaning for each step downstream the normalised vorticity is reduced by that amount. It was also found that an exponential function was a good fit to the data. Where a vortex decay exponent of -0.1109 was found halving the vorticity by two for every $6.25D$ downstream of the VGs.

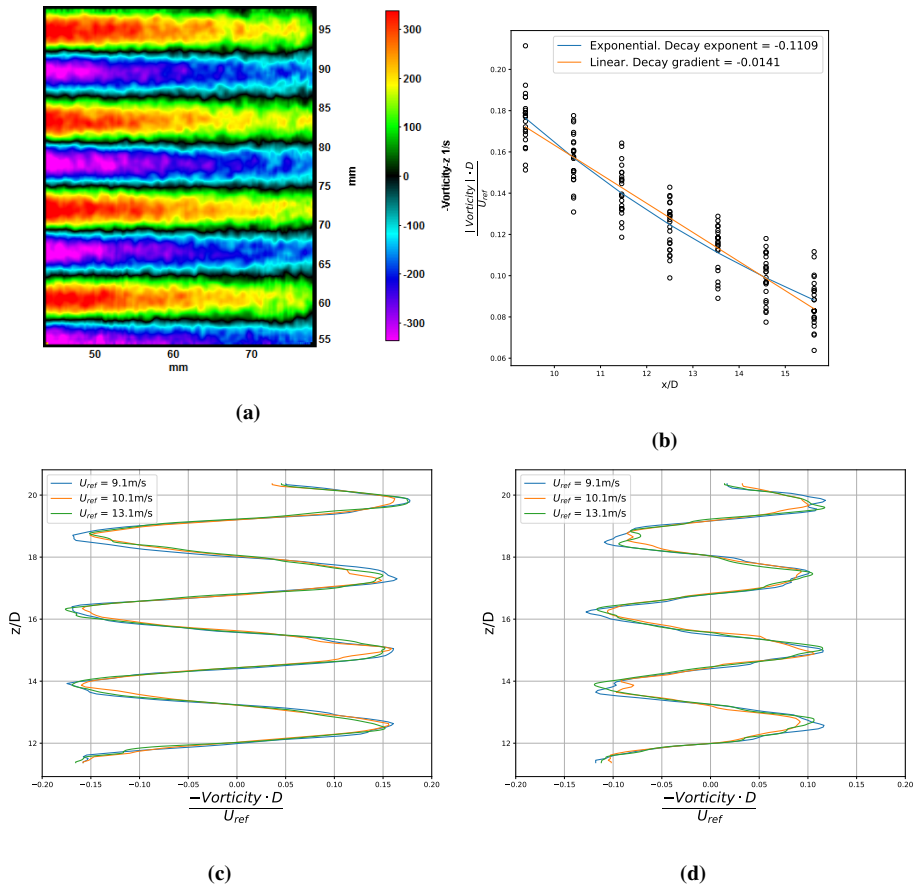


Figure 6.7: a) Colormap of average Vorticity at $U_{ref} = 10.1 \frac{m}{s}$, spanwise plane. b) Curve fit for the peak vorticity in the vortex core obtained at some points in the wake of the VGs. c) Average vorticity profiles for several reference flow velocities at $x = 10.4D$. d) Average vorticity profiles for several reference flow velocities at $x = 14.6D$.

For the symmetry plane, it was observed that the negative vorticity, meaning the upper vortices seem to in general be weaker than the positive lower vortices shed behind the hydrofoil. The rate of decay was similarly calculated as for the vortices coming from the VGs in figure 6.7. It was evident that an exponential regression was best suited for the data obtained with an R-value of ≈ 0.86 giving a good relationship between the model and the data. An exponential decay rate of -0.1234 , meaning the vorticity is halved for approximately every distance $\approx 5.6D$ downstream of the hydrofoil trailing edge, was found.

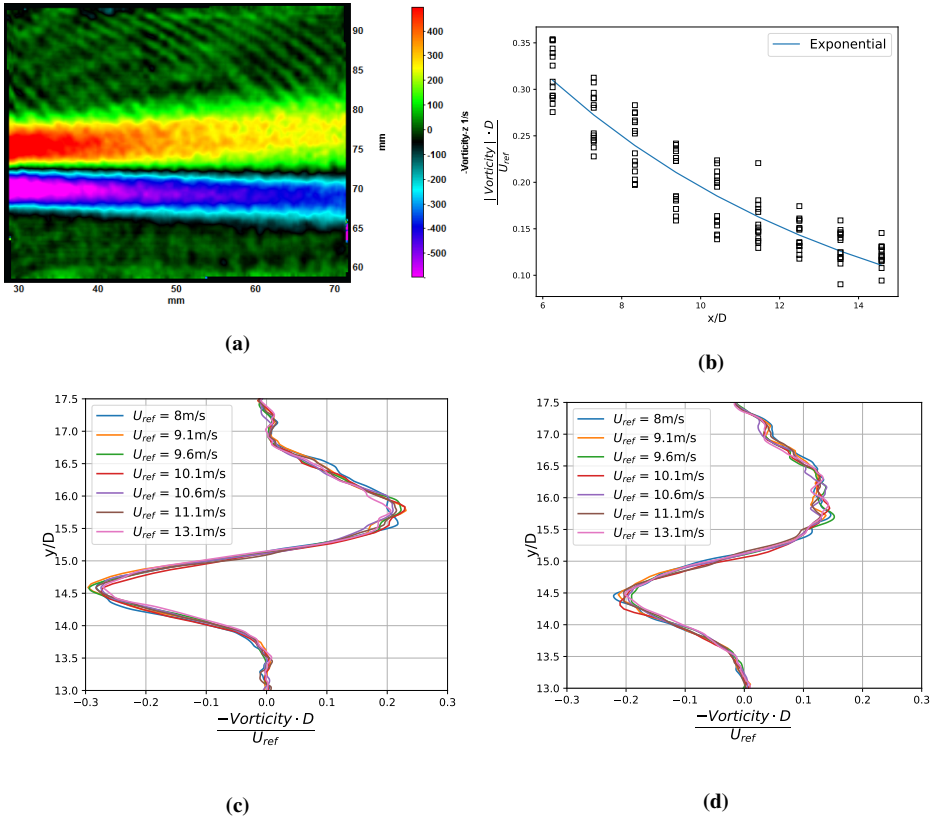


Figure 6.8: a) Colormap of average Vorticity at $U_{ref} = 10.1 \frac{m}{s}$ for the symmetry plane. b) Curvefit for peak vorticity in the core obtained at some points in the wake of the hydrofoil. c) Average vorticity profiles for several reference velocities at $x = 8.3D$. d) Average vorticity profiles for several reference velocities at $x = 12.5D$.

6.2 Reference Foil

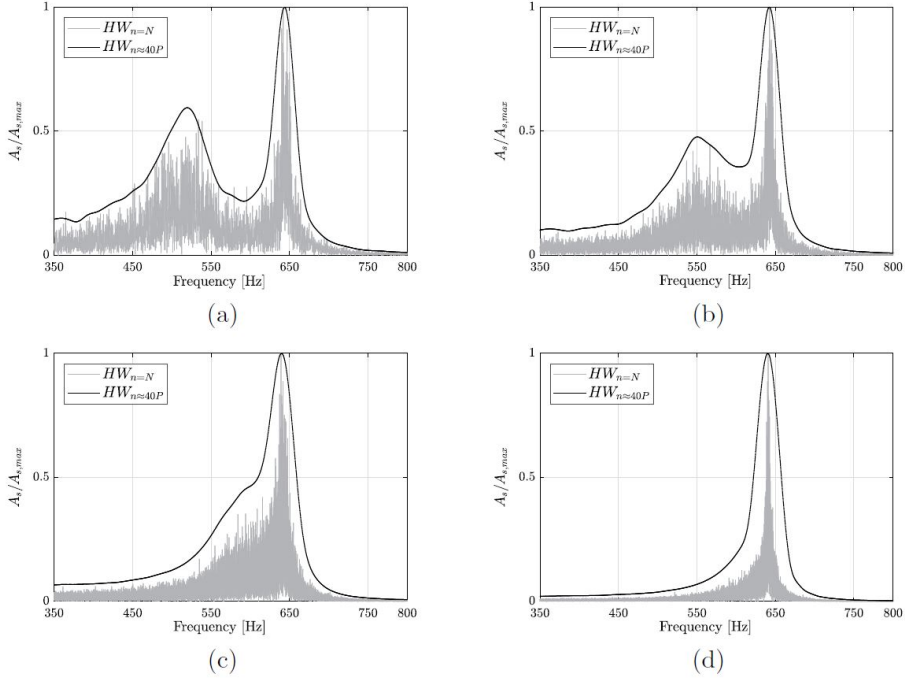


Figure 6.9: "Amplitude frequency spectra for increasing reference velocities from strain-gauge voltage signal, showing the travelling shedding frequency peak (left peak) approaching the natural (standing) frequency peak of the hydrofoil. (a) $U_{ref} = 9.1 \frac{m}{s}$. (b) $U_{ref} = 9.6 \frac{m}{s}$. (c) $U_{ref} = 10.1 \frac{m}{s}$. (d) $U_{ref} = 10.6 \frac{m}{s}$ " [4].

From the experimental work of Sagmo et al. [4] a peak approaching the natural frequency of the hydrofoil as seen in figure 6.9 was observed. As this peak synced up with the natural frequency, a region of lock-in was observed. This was seen at a reference flow velocity of $U_{ref} = 11.1 m/s$, indicated by a sharp rise in the strain amplitude of the first peak and a steady shedding frequency obtained from PIV as seen in figure 6.10. An overall maximum vibrational amplitude of $A_{max} \approx 9.4E - 4$ for a reference flow velocity of $U_{ref} = 11.5 m/s$ was found. Repeated strain gauge peak measurements at a reference velocity of $U_{ref} = 11.1 m/s$ gave a standard deviation of $1.6 Hz$. A measured Strouhal number of $St = 0.274$ was found based on the PIV data at a range of $U_{ref} = 9.1 m/s - U_{ref} = 10.6 m/s$.

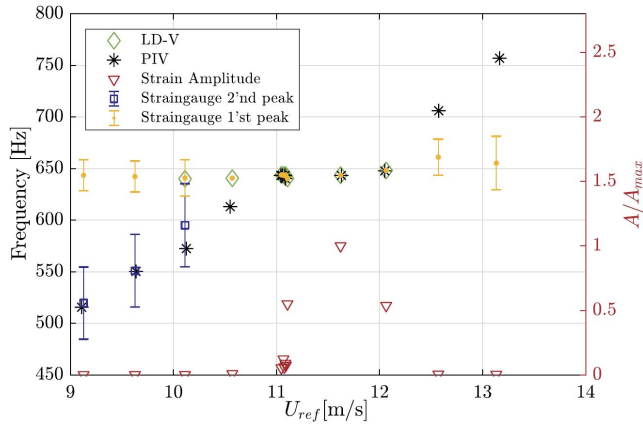


Figure 6.10: "Hydrofoil vibration frequencies and shedding frequencies measured by PIV, strain-gauges and LD-Vibrometer. The relative hydrofoil vibrational amplitude is plotted along the right y-axis." [4]

The wake velocity distribution for the reference foil obtained from PIV is shown in figure 6.11. It was evident that the wake velocity distribution varied quite a lot more for reference flow velocities in lock-in than outside lock-in.

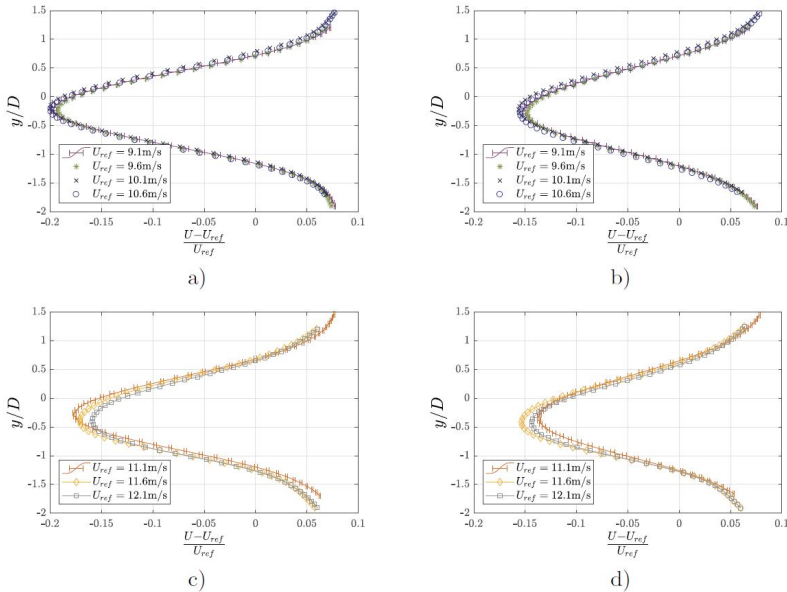


Figure 6.11: "Time-averaged PIV measured velocity distributions normalised with respect to the mean channel velocity for different downstream positions. Height normalised by trailing edge thickness, with $y = 0$ set at the hydrofoil center line. In (a) and (c) $x = 9.9D$. In (b) and (d) $x = 13.3D$. Uncertainty error bars are only plotted for reference velocities of $9.1 \frac{m}{s}$ and $11.1 \frac{m}{s}$, for clarity." [4]

Discussion

From the uncertainty measurements of the vector field given in figure 5.6, the highest uncertainty was observed in the wake of the hydrofoil with increasing uncertainty for increasing reference flow velocities. This is most likely due to the higher turbulence fluctuations in the wake of the hydrofoil. In order to validate the data presented above the focus is directed towards the spurious vectors. Defining the flow as challenging due to the high turbulence fluctuations in the wake of both the hydrofoil and VGs, an indication of high-quality PIV can be set to data with 5% or less spurious vectors [34]. This again depends on how spurious vectors are defined. As illustrated in figure 5.8 only when spurious vectors are defined as vectors with peak ratio below three, an amount of spurious vectors above 5% is found. This was only found in the case of the symmetry plane. Nevertheless, the data is deemed to be of "high-quality" as the average amount of spurious vectors across all frames, defined as vectors with peak ratio below 3 is only 0.06% for the symmetry plane and only 1.34% for an arbitrary frame in the spanwise plane.

It is evident from the natural frequency measurements seen in figure 6.1 that small changes to the trailing edge geometry does not have a significant effect on the natural frequency of the hydrofoil. A change in the natural frequency of $27Hz$ is observed when adding VGs and an interchangeable trailing edge to a blunt trailing edge hydrofoil. As this value is relatively low, it is thought that it will not have a significant impact on the comparisons and measurements of these two hydrofoils. Thus in practice, the only difference in vibrations in the hydrofoil will be due to the addition of VGs and their generation of longitudinal vortices. This makes the reference foil studied in the paper of Sagmo et al. [4] a good candidate for comparison with the hydrofoil with VGs. A smaller difference between the natural frequencies of the reference foil and a hydrofoil with VGs would probably have been observed if both of these foils had an interchangeable trailing edge. Either way, the difference which was accomplished is deemed to be good enough for the comparisons, which are coming up next, performed in this master's thesis.

Comparing these two cases an abrupt change in amplitude and a stationary vortex shedding would indicate a region of lock-in. This is something which is observed for the reference hydrofoil and is absent in the measurements of the hydrofoil with VGs as seen in figures 6.4 and 6.10. Comparing the maximum vibrational amplitudes for the two cases, it can be seen that for the reference foil it is almost thirty times bigger than for the hydrofoil with VGs which would indicate a lot stronger oscillations in the case of the reference foil. Looking at figures 6.4 and 6.10 the peak travelling towards the natural frequency can be observed to be slightly dampened and disappear for the hydrofoil with VGs while for the reference case it merges with the natural frequency. Another factor which is worth considering is the noise coming from the test section. During experiments with the reference foil, a significant increase in noise would have been heard from the test section as the reference flow velocity approached the range of lock-in for the foil. As experiments with the hydrofoil with VGs were performed no significant increase in noise was heard. A slight

increase in the amplitude as is observed for the hydrofoil with VGs could still indicate that a lock-in region with low intensity is present. Ultimately it can be argued that the VGs are able to break up the uniformity of the vortex sheet formed behind the hydrofoil and mitigate the vortex-induced vibrations. A region of lock-in could nevertheless still exist around the velocities that exhibit a gradual increase in the frequency amplitude. An overhaul of these velocities would be necessary to strengthen the statement given above.

The velocity profiles in the wake for the reference case tend to vary substantially more in the region of lock-in than outside. The same trend was found for the hydrofoil with VGs at reference flow velocities of $9.1 - 10.1\text{ m/s}$, which could further indicate that a low-intensity lock-in region are present in this hydrofoil. It was also observed that the Strouhal equation with the measured Strouhal number found in [4] for the reference foil predicted the vortex shedding frequency almost perfectly for the hydrofoil with VGs. This would thus indicate that the addition of VGs does not affect the shedding frequency of the hydrofoil. As it was initially thought that a delayed separation point would indicate an increase in the shedding frequencies there exists two possible answers to why the shedding frequencies of the reference foil and the hydrofoil with VGs are close to identical. The VGs does not affect the point of separation or that the point of separation does not affect the vortex shedding. In order to check these statements, it is necessary to measure the point of separation experimentally for both the reference foil and the hydrofoil with VGs. It is also important to point out the uncertainty of the measured shedding frequencies from PIV as illustrated with error bars in figure 6.4. It could be that the shedding frequency is higher or lower than what is found here, which would make the statements above obsolete.

An asymmetry is evident in the positive and negative vorticity in the symmetry plane where the upper vortex is in direct contact with the longitudinal vortices produced by the VGs. This asymmetry of the vorticity is believed to be because of the interference with longitudinal vortices generated by the VGs and could be one of the driving factors to why the vortex-induced vibrations are mitigated. The asymmetry observed in the vorticity in the symmetry plan could also be due to the asymmetric nature of the hydrofoil trailing edge. An vorticity analysis is also necessary for the reference foil in order to add confidence to the statements above and to indicate why there is a asymmetry. The exponential decay rate of the vortex shedding behind the hydrofoil as illustrated in figure 6.8 is in good agreement with vortex shedding decay theory. It is consistent with the lamb-oseen decaying vortex model as described by Ponta [52] and Hu et al [53] and follows a best fit exponential decay function.

Looking at the vorticity decay of the longitudinal vortices generated by the VGs two functions were found to fit the data. The linear functions is the best fit for the available data, but vortices of this type have been shown to have a vorticity decay in the shape of an exponential function. This is clearly illustrated by several researchers like Shim et al [25], Wendt [54] and Lögberg et al [55]. A point was also made by Lögberg et al. that the decay function for longitudinal vortices generated by VGs was almost linear until far downstream. This would be the reason why the best fit was obtained with a linear function for the data available in this master's thesis. In order to fully check the vorticity decay, it is therefore necessary to check the development of vorticity further downstream. Looking at the average velocity component U_z in figure 6.6 it shows strong asymmetry where it

should be symmetric across each vortex pair. This is also something that could affect the calculated decay of longitudinal vortices. It is evident that a longer sampling period with a higher sampling rate is necessary in order to achieve this and get more accurate readings from the PIV in the spanwise plane.

Conclusion

Vortex generators (VGs) have been studied as a means of an alternation which can be done to new and existing hydropower plant in order to reduce structural vibrations and thus reduce cost while maintaining or increasing performance. An experimental study using PIV and strain gauges have been conducted with VGs attached at the blunt trailing edge of a hydrofoil. Their effects on the wake and vortex-induced vibrations (VIVs) were quantified by comparing to a corresponding hydrofoil without VGs which was shown to experience a region of lock-in at a range of free-stream velocities.

It is observed that the addition of VGs seems to change the range of free-stream velocities at which lock-in occurs and partially mitigate the VIVs. When experiments of a hydrofoil with VGs were compared with experiments of the corresponding hydrofoil without VGs it was evident that the latter hydrofoil experienced thirty times stronger vibrations at maximum. Interference between the longitudinal vortices generated by the VGs and the uniform vortex sheets downstream of the hydrofoil is believed to be the reason for the mitigation of the VIVs that is observed. The longitudinal vortices probably break up the uniformity of the vortex shedding which causes the mitigation. This goes to show that it is possible to use VGs in order to mitigate VIVs in hydrodynamic environments under controlled conditions. Further indicating that these devices can effectively be applied in hydrodynamic environments not only to delay separation as is evident from literature, but also to mitigate VIVs. However, in order to be fully confident when applying these devices to either hydromachinery, rudders in ships or turbine blades it needs to be tested in these environments. More research is therefore necessary, but the results look promising for the potential use of these devices in order to reduce severe structural vibrations.

Further Work

First in the further work would be to finish the experiment that was planned with the reference hydrofoil and compare the results in order to obtain a better quantification of the effects of VGs. With regards to this some advice is given for when performing the experiments;

- The importance of planning enough time in order to perform the experiments is stressed. Unexpected situations will occur, which will prolong the time it takes to finish the experiments.
- When performing the natural frequency measurements, it is important to turn off the fan in the camera as it will cause vibrations in the hydrofoil which will amount to erroneous natural frequency measurements. These vibrations will not affect any other measurements than the natural frequency measurements.
- It is important to check for leakage around the pressure sensors throughout the experiments as leakage will give rise to erroneous pressure measurements

In order to get better and more accurate data from the PIV in the spanwise plane and to properly capture the U_z component, it would be necessary to upgrade the hardware. This is in order to be able to capture the flow for a longer period (more images) with a sufficiently high sampling rate. As of now, it is possible to capture 4367 images before the internal memory of the camera is full and it would be great to have the possibility to capture more images. It would also be interesting to check the flow field further downstream of the hydrofoil in order to fully solve for the decay function of the vorticity of the longitudinal vortices.

9.1 Computational Fluid Dynamics

The natural extension of the experimental work done in this thesis would be to develop a good computational fluid dynamics (CFD) model. There are two ways one could go about in developing this model. Mesh the whole 3D test section with refinements around the VGs and in the wake of the hydrofoil to capture the 3D effects of the vortices. This would include 10 – 20 million cells and have a substantial computational cost. Another option is to develop a model that describes the longitudinal vortices formed downstream of the VGs. A model like this would significantly lower the computational cost. However, on the other hand, the results would be dependent on making a good model which could prove to be complicated. Once a CFD model is developed using one of the two ways mentioned above and validate through previous experiments, it can be used to test out other types of trailing edges. It can also be used to perform a parametric study on the VGs and try to optimise them.

9.2 Optimisation Study

An optimisation study of the VGs is also possible in order to check if a better design which induces stronger vortices can be found. It could be performed both experimentally and using CFD. Parameters which would be interesting to focus on are the orientation angle (α) of the VGs and the configuration because from the literature it was evident that changing these parameters had the most significant effect on the performance of the VGs. If the optimisation study is to be performed experimentally, 3D - printing is a great option where changing both of these parameters and making several iterations is relatively easy. An example of how one could go about using such 3D - Printed VGs is shown in appendix C.

Bibliography

- [1] Steven Iona. Albert A. Bartlett. *The Physics Teacher*, 20(5):298–303, May 1982.
- [2] Jean-Marie Chevalier. The New Energy Crisis. In Jean-Marie Chevalier, editor, *The New Energy Crisis: Climate, Economics and Geopolitics*, pages 6–59. Palgrave Macmillan UK, London, 2009.
- [3] International hydropower association. 2017 hydropower status report. 2017.
- [4] K F Sagmo, E O Tengs, C W Bergan, and P T Storli. PIV measurements and CFD simulations of a hydrofoil at lock-in. *IOP Conference Series: Earth and Environmental Science*, 240:062006, March 2019.
- [5] Doug McLean. Aerodynamic Lift, Part 1: The Science. *The Physics Teacher*, 56(8):516–520, November 2018.
- [6] John M.Cimbala Yunus A.Cengel. *Fluid mechanics: Fundamentals and Applications*. McGraw Hill, 2014.
- [7] Anatol Roshko. ON THE DRAG AND SHEDDING FREQUENCY OF TWO-DIMENSIONAL BLUFF BODIES. page 30, 1954.
- [8] J. H. Gerrard. The mechanics of the formation region of vortices behind bluff bodies. *Journal of Fluid Mechanics*, 25(2):401–413, June 1966.
- [9] T. Sarpkaya. A critical review of the intrinsic nature of vortex-induced vibrations. *Journal of Fluids and Structures*, 19(4):389–447, May 2004.
- [10] P.A Brandner and G.J Walker. Hydrodynamic performance of a vortex generator. *Experimental Thermal and Fluid Science*, 27(5):573–582, May 2003.
- [11] Lisa Zyga. Scientists discover second purpose for vortex generators. 2012.
- [12] Harold D Taylor. The elimination of diffuser separation by vortex generators. *United Aircraft Corporation, East Hartford, CT, Technical Report No*, 4012:3, 1947.
- [13] John C Lin. Review of research on low-profile vortex generators to control boundary-layer separation. *Progress in Aerospace Sciences*, 38(4-5):389–420, May 2002.
- [14] Pranav Manjunath. Computational Study of the Dynamics of the Flow-Field Induced by Vortex Generators. page 104.

-
- [15] ALVIN HOLMES, PAUL HICKEY, WILLIAM MURPHY, and DAVID HILTON. The application of sub-boundary layer vortex generators to reduce canopy' mach rumble'interior noise on the gulfstream iii. In *25th AIAA Aerospace Sciences Meeting*, page 84, 1987.
- [16] A. M. Kuethe. Effect of streamwise vortices on wake properties associated with sound generation. *Journal of Aircraft*, 9(10):715–719, October 1972.
- [17] D. J. Maull and R. A. Young. Vortex shedding from bluff bodies in a shear flow. *Journal of Fluid Mechanics*, 60(2):401–409, September 1973.
- [18] Hyungmin Park, Dongkon Lee, Woo-Pyung Jeon, Seonghyeon Hahn, Jeonglae Kim, Jungwoo Kim, Jin Choi, and Haecheon Choi. Drag reduction in flow over a two-dimensional bluff body with a blunt trailing edge using a new passive device. *Journal of Fluid Mechanics*, 563:389, September 2006.
- [19] J G Betterton, K C Hackett, P R Ashill, M J Wilson, I J Woodcock, C P Tilman, and K J Langan. Laser Doppler Anemometry Investigation on Sub Boundary Layer Vortex Generators for flow control. page 13.
- [20] Hanns Mueller-Vahl, Georgios Pechlivanoglou, C. N. Nayeri, and C. O. Paschereit. Vortex Generators for Wind Turbine Blades: A Combined Wind Tunnel and Wind Turbine Parametric Study. In *Volume 6: Oil and Gas Applications; Concentrating Solar Power Plants; Steam Turbines; Wind Energy*, pages 899–914, Copenhagen, Denmark, June 2012. American Society of Mechanical Engineers.
- [21] Linyue Gao, Hui Zhang, Yongqian Liu, and Shuang Han. Effects of vortex generators on a blunt trailing-edge airfoil for wind turbines. *Renewable Energy*, 76:303–311, April 2015.
- [22] Xinkai Li, Ke Yang, and Xiaodong Wang. Experimental and Numerical Analysis of the Effect of Vortex Generator Height on Vortex Characteristics and Airfoil Aerodynamic Performance. *Energies*, 12(5):959, March 2019.
- [23] Xin-Kai Li, Wei Liu, Ting-Jun Zhang, Pei-Ming Wang, and Xiao-Dong Wang. Experimental and Numerical Analysis of the Effect of Vortex Generator Installation Angle on Flow Separation Control. *Energies*, 12(23):4583, December 2019.
- [24] Sen Wang and Sina Ghaemi. Effect of vane sweep angle on vortex generator wake. *Experiments in Fluids*, 60(1):24, January 2019.
- [25] Ho-Joon Shim, Ki-Jung Kwon, and Seung-O Park. Experimental Study on the Wake Characteristics of Vane-Type Vortex Generators in a Flat Plate Turbulent Boundary Layer. page 9.
- [26] M Oledal. Application of vortex generators in ship propulsion system design. *WIT Transactions on The Built Environment*, 27, 1970.
- [27] Parikshit Kundu, Arunjyoti Sarkar, and Vishwanath Nagarajan. Improvement of performance of S1210 hydrofoil with vortex generators and modified trailing edge. *Renewable Energy*, 142:643–657, November 2019.

-
- [28] Clara Marika Velte, Martin Otto Lavér Hansen, Knud Erik Meyer, Peter Fuglsang, and LM Glasfiber. Evaluation of the Performance of Vortex Generators on the DU 91-W2-250 Profile using Stereoscopic PIV. page 6.
- [29] Yasser M Ahmed, A H Elbatran, and H M Shabara. Study of the Effect of Low Profile Vortex Generators on Ship Viscous Resistance. page 7, 2014.
- [30] Ahmet Ziya Saydam, Serhan Gokcay, and Mustafa Insel. CFD based vortex generator design and full-scale testing for wake non-uniformity reduction. *Ocean Engineering*, 153:282–296, April 2018.
- [31] N Matheson et al. Experimental studies to modify the velocity in the wake of ships' hulls. In *7th Australasian Conference on Hydraulics and Fluid Mechanics 1980: Preprints of Papers*, page 557. Institution of Engineers, Australia, 1980.
- [32] M. O. L. Hansen, C. M. Velte, S. Øye, R. Hansen, N. N. Sørensen, J. Madsen, and R. Mikkelsen. Aerodynamically shaped vortex generators: Vortex generators, boundary layer control. *Wind Energy*, 19(3):563–567, March 2016.
- [33] B. Méndez and R. Gutiérrez. Non-conventional vortex generators calculated with CFD. *Journal of Physics: Conference Series*, 1037:022029, June 2018.
- [34] Markus Raffel, Christian E Willert, Fulvio Scarano, Christian J Kähler, Steve T Wereley, and Jürgen Kompenhans. *Particle image velocimetry: a practical guide*. Springer, 2018.
- [35] Sung Min Choi, Wi Han Kim, Daniel Côté, Cheol-Woo Park, and Ho Lee. Blood cell assisted in vivo Particle Image Velocimetry using the confocal laser scanning microscope. *Optics Express*, 19(5):4357, February 2011.
- [36] Dana Dabiri. Cross-Correlation Digital Particle Image Velocimetry – A Review. page 54.
- [37] P. Welch. The use of fast Fourier transform for the estimation of power spectra: A method based on time averaging over short, modified periodograms. *IEEE Transactions on Audio and Electroacoustics*, 15(2):70–73, June 1967.
- [38] Tim Mila (Siemens). Windows and Spectral Leakage. Aug 2019.
- [39] National Instruments. Understanding ffts and windowing. *Instrument Fundamentals: Complete Guide*.
- [40] Window function. *Wikipedia*, March 2020. Page Version ID: 943357029.
- [41] G. Godard and M. Stanislas. Control of a decelerating boundary layer. Part 1: Optimization of passive vortex generators. *Aerospace Science and Technology*, 10(3):181–191, April 2006.
- [42] Frank N. White. *Viscous Fluid Flow: Third Edition*. McGraw Hill, 2006.
- [43] Wayne R. Pauley and John K. Eaton. Experimental study of the development of longitudinal vortex pairs embedded in a turbulent boundary layer. *AIAA Journal*, 26(7):816–823, July 1988.
-

-
- [44] Xin-Kai Li, Wei Liu, Ting-Jun Zhang, Pei-Ming Wang, and Xiao-Dong Wang. Experimental and Numerical Analysis of the Effect of Vortex Generator Installation Angle on Flow Separation Control. *Energies*, 12(23):4583, December 2019.
- [45] Kerri A. Raykowski. Optimization of a Vortex Generator Configuration for a 1/4-Scale Piper Cherokee Wing. 1999.
- [46] LeCroy Corporation. LAB 429 - How Fast Must I Sample? page 2.
- [47] Bernhard Wieneke. PIV uncertainty quantification from correlation statistics. *Measurement Science and Technology*, 26(7):074002, July 2015.
- [48] LaVision GmbH. T1003005 flowmaster d84. LaVision GmbH, 2017.
- [49] R. Hain and C. J. Kähler. Fundamentals of multiframe particle image velocimetry (PIV). *Experiments in Fluids*, 42(4):575–587, March 2007.
- [50] Fredric Harris, J. On the Use of Windows for Harmonic Analysis with the Discrete Fourier Transform. *IEEE*, page 33.
- [51] P Čupr, D Štefan, V Habán, and P Rudolf. Fsi analysis of francis-99 hydrofoil employing sbes model to adequately predict vortex shedding. In *Journal of Physics: Conference Series*, volume 1296, page 012002. IOP Publishing, 2019.
- [52] Fernando L. Ponta. Vortex decay in the Kármán eddy street. *Physics of Fluids*, 22(9):093601, September 2010.
- [53] Yili Hu, Bin Yang, Xiang Chen, Xiaolin Wang, and Jingquan Liu. Modeling and experimental study of a piezoelectric energy harvester from vortex shedding-induced vibration. *Energy Conversion and Management*, 162:145–158, April 2018.
- [54] B. Wendt. Initial peak vorticity behavior for vortices shed from airfoil vortex generators. In *36th AIAA Aerospace Sciences Meeting and Exhibit*, Reno, NV, U.S.A., January 1998. American Institute of Aeronautics and Astronautics.
- [55] Ola Lögdberg, Jens H. M. Fransson, and P. Henrik Alfredsson. Streamwise evolution of longitudinal vortices in a turbulent boundary layer. *Journal of Fluid Mechanics*, 623:27–58, March 2009.

Master Description

Norwegian University of
Science and Technology

Faculty of Engineering
Department of Energy and Process Engineering

EPT-M-2020



MASTER WORK

for
student Hasan Besirovic

Spring 2020

*“Vortex generator’s effect on trailing edge wake and fluid structure interaction”
“Effekten av virvel-generatorer på avløpskantens vake og fluid struktur interaksjon”*

Background and objective

By energizing the boundary layer, vortex generators (VG’s) can effectively delay separation and stall in fluid machinery. It is interesting to see if the introduction of stream wise vortices by VGs can also be used to mitigate vortex-induced vibrations (VIVs) in hydrofoils. Such VIVs can be observed in several components in hydropower plants, and effective ways to mitigate VIVs of such components are interesting from an industrial perspective.

Work has been performed to prepare a test rig at the Waterpower laboratory for experimental investigations of the effect of vortex generators. The work of the candidate is to finalize this work and to execute a measurement campaign including particle image velocimetry (PIV) measurement technique to quantify the effect of VGs.

If for some reason the experimental investigation can’t be performed, CFD investigation of the setup should be performed if time allows.

The following tasks are to be considered:

1. A literature review of passive flow controllers for mitigation of vortex induced vibrations with focus on vortex generators.
2. Decide on a measurement campaign on the test rig vortex generators at the waterpower laboratory
3. Complete the installation, instrumentation and calibration needed to perform the measurement campaign
4. Execute the measurement campaign
5. If the student will go to Nepal for an excursion, earlier and further work will be presented as a publication and presented at the conference; 10th *International symposium on Current Research in Hydropower Technologies (CRHT-IX)* at Kathmandu University

-- “ --

Address
N-7034 Trondheim
Norway

Location
K. Hejes vei 1b

Tel. +47 73 59 38 60
Fax +47 73 59 35 80
Org. no. NO 974 767 880

Page 1 of 2

The master work comprises 30 ECTS credits.

The work shall be edited as a scientific report, including a table of contents, a summary in Norwegian, conclusion, an index of literature etc. When writing the report, the candidate must emphasise a clearly arranged and well-written text. To facilitate the reading of the report, it is important that references for corresponding text, tables and figures are clearly stated both places.

By the evaluation of the work the following will be greatly emphasised: The results should be thoroughly treated, presented in clearly arranged tables and/or graphics and discussed in detail.

The candidate is responsible for keeping contact with the subject teacher and teaching supervisors.

Risk assessment of the candidate's work shall be carried out according to the department's procedures. The risk assessment must be documented and included as part of the final report. Events related to the candidate's work adversely affecting the health, safety or security, must be documented and included as part of the final report. If the documentation on risk assessment represents a large number of pages, the full version is to be submitted electronically to the supervisor and an excerpt is included in the report.

According to "Utfyllende regler til studieforskriften for teknologistudiet/sivilingeniørstudiet ved NTNU" § 20, the Department of Energy and Process Engineering reserves all rights to use the results and data for lectures, research and future publications.

Submission deadline: To be found in Inpera.

- Work to be done in lab (Water power lab, Fluids engineering lab, Thermal engineering lab)
 Field work

Department for Energy and Process Engineering 4/1 2020



Pål-Tore Storli
Supervisor

Co-Supervisor(s): Kristian Sagmo

Calibration

B.1 Temperature Sensor

Measurements from a RTD PT 100 thin film temperature sensor is based on the resistance properties of a material at given temperatures. The resistance which is what is measured increases proportionally to the temperature. These type of sensors are also quite resistant to vibrations. The PT 100 sensor is a platinum device with a resistance of 100Ω at a temperature of $0^\circ C$ and increase in resistance of $0.385\Omega/C^\circ$. Calibrating the temperature sensor was done by making two measurements at two known temperatures and fitting a linear function to these points. Something similar to that which was done for the calibration of the flow meter explained in the next section. This was because two reference temperatures were easy to obtain quite accurately while temperatures in between these were harder to obtain as accurate. These temperatures were 0° Celsius and 100° Celsius which were obtained by respectively adding ice to water and boiling water. With the assumption that of a linear dependence between these measurement points a calibration line was obtained giving quite accurate temperatures between these two endpoints. Thus a final calibrated temperature range of 0° celsius to 100° celsius which is considered sufficient for the applications in the experiments conducted in this master's thesis was obtained with a good accuracy.

B.2 Flow-meter

As the output signal from this flow-meter is in volt a calibration is necessary in order to accurately convert the voltage signal to volumetric flow rate. Calibration was performed using a weighing tank system and the equations B.1-B.4 below. The tank was filled for a given time period and the weight was manually observed before and after the filling. A weight correction was done using equation B.1 where a , b , c , d and e are weighing tank correction constants given in table B.1 and W_m is the manually observed weight. The water and air densities were found respectively from equations B.2 and B.3. Where a_1 and a_2 are constants given in table B.1, P_{atm} is the atmospheric pressure and T_w and T_{air} are respectively the water and air temperature. The volumetric flow rate was then calculated using the weight increase during the given filling time period and equation B.4. The final flow calibration sheet can be found in appendix B.2.1.

$$W = a * \frac{W_m^5}{5} + b * \frac{W_m^4}{4} + c * \frac{W_m^3}{3} + d * \frac{W_m^2}{2} + e * W_m \quad (B.1)$$

$$\rho_w = \frac{1000}{(1 - a_1 P_{atm}) + 8E - 6(T_w - 4 + a_2 P_{atm})^2 - 6E - 8(T_w - 4 + a_2 P_{atm})^3} \quad (B.2)$$

$$\rho_a = \frac{P_{atm}}{287 * (273,15 + T_{air})} \quad (B.3)$$

$$Q = \frac{\Delta W}{t * (\rho_w - \rho_a)} \quad (B.4)$$

Table B.1: Calibration constant for the flow meter

a	$2.27E - 22$
b	$-3.09E - 17$
c	$1.417E - 12$
d	$-3.44E - 8$
e	$9.99E - 1$
a_1	$4.6699E - 10$
a_1	$2.1318913E - 7$
C_0	-0.165376967
C_1	0.083528531
Standard deviation	0.000182

The flow rate was calculated at several points, twice at the same point to check for repeatability and the flow-meter voltage was observed at each point. These points were plotted in excel with the flow rate signal in volt along the x axis and the calculated volumetric flow rate along the y axis. A linear regression line was fitted to these data points as shown in figure B.1. The slope and y-intercept was found for this line and respectively called calibration constants C_0 and C_1 which are shown in table B.1. The flow-meter was calibrated for a final flow rate range of $0.052m^3/s$ to $0.414m^3/s$ or a test section velocity range of $2.3m/s$ to $18.4m/s$. A standard deviation based on the difference between the calculated flow rate and the estimated flow rate based on the linear regression line was found to be 0.000182 .

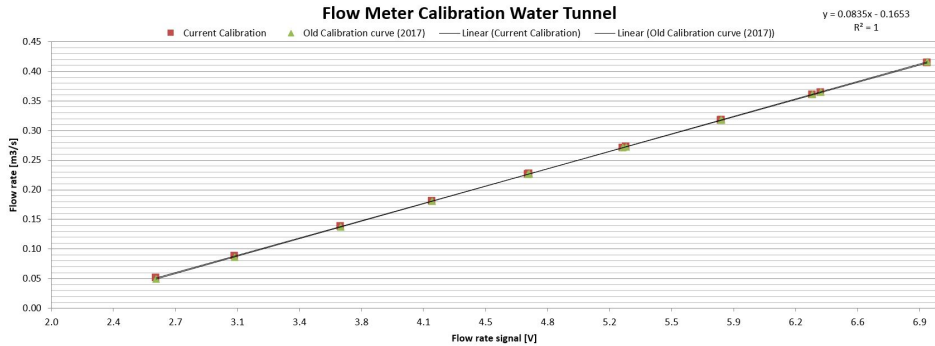


Figure B.1: Linear regression line for flow meter calibration data

B.2.1 Calibration Sheet



WATERPOWER LABORATORY

Calibration Sheet

Calibration of flow meter

Date: 19/02/2020

Operator: Kristian Sagmo, Heian B. Carsten C.

Calibrator: Weighing tank system
Comment: Timerecordings are considered accurate to pm 0.01 s, due to error in logging the time-intervals

Calibration constants for weighing tank correction	Value
a_1	2.27E-22
a_2	-3.48E-17
a_3	1.41E-10
a_4	-3.44E-26
a_5	9.99E-01

Corrected weight is calculated from formula where parameters a_1 to a_5 and e is achieved through substitution calibration.

$$W = m \cdot \left(\frac{m}{m_0} \right)^{a_1} \cdot \left(\frac{m}{m_0} \right)^{a_2} \cdot \left(\frac{m}{m_0} \right)^{a_3} \cdot \left(\frac{m}{m_0} \right)^{a_4} \cdot \left(\frac{m}{m_0} \right)^{a_5} + e$$

Density of water is calculated from formula

$$\rho = \frac{1000}{1 + 0.000173 \cdot (t - 4)^2 - 0.0000000214 \cdot (t - 4)^4}$$

Density of air is calculated from formula

$$\rho_a = \frac{1.293 \cdot (1 - 1.78 \cdot 10^{-5} \cdot t)}{1 + 0.00348 \cdot t - 9 \cdot 10^{-6} \cdot t^2}$$

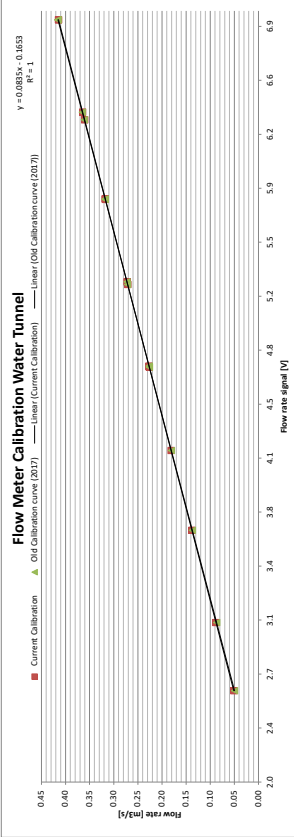
Parameters	Value
ρ_{water}	0.00119
ρ_{air}	0.00119

Discharge is found from formula

$$Q = \frac{V}{t} \cdot \left(\frac{V}{V_0} \right)^{a_1} \cdot \left(\frac{V}{V_0} \right)^{a_2} \cdot \left(\frac{V}{V_0} \right)^{a_3} \cdot \left(\frac{V}{V_0} \right)^{a_4} \cdot \left(\frac{V}{V_0} \right)^{a_5} + e$$

Manual Observation before	Manual Observation after	Manual Weight	Manual Voltage	Manual Observation	Time	Ambient pressure P_{amb}	Water temp T_w	Air temp T_a	Calculated value before	Calculated value after	Differential weight	Density of water ρ	Density of air ρ_a	Differential volume	Calculated Flow Rate	Estimate	Deviation	Outlier detection	Old Calibration Flow Rate	
17912.14	17911.17	17911.17	3.033762	65.10	16.20	99.766	14.81	19.22	12188.2	17895.8	5727.6	999.2142	1.1896	5.73890	0.081552	0.08503	-0.14338	0.00013	-0.44128	0.04336
17912.21	17911.29	17911.29	3.032777	40.10	99.763	14.87	19.16	17894.9	23430.4	5535.5	999.2952	1.1898	5.54693	0.138175	0.13802	-0.21432	0.00030	0.00030	1.67423	0.13701
26868.33	26867.35	26867.35	3.030566	30.10	99.827	14.78	19.11	17897.8	35671.7	35671.7	999.1890	1.1903	6.31368	0.263862	0.26338	0.00478	-0.00001	-0.68775	0.26212	
35792.39	35793.03	35793.03	3.0103624	30.10	99.804	14.93	19.08	18008	35671.3	48699.8	6188.5	999.1857	1.1906	8.20516	0.2725866	0.27262	0.00681	-0.00002	-0.09699	0.27275
31192.39	31188.95	31188.95	3.011796	30.10	99.865	15.15	19.05	18008	48699.8	48699.8	999.1857	1.1907	0.25033	0.2444101	0.34475	-0.00511	0.00002	0.13472	0.34276	
31192.39	31188.95	31188.95	3.011796	30.10	99.865	15.15	19.05	18008	48699.8	48699.8	999.1857	1.1907	0.25033	0.2444101	0.34475	-0.00511	0.00002	0.13472	0.34276	
38059.90	38059.90	38059.90	3.0103624	30.10	99.813	15.83	18.82	36774.5	48223.0	12448.5	999.0264	1.1918	12.47597	0.4445774	0.44448	-0.02492	-0.00010	-0.55094	0.44591	
45994.84	45994.84	45994.84	3.0103624	30.10	99.829	15.77	18.81	45949.4	47499.4	7499.4	999.0266	1.1918	12.47597	0.4445774	0.44448	-0.02492	-0.00010	-0.55094	0.44591	
50653.74	50653.74	50653.74	3.0103624	30.10	99.813	15.83	18.82	50600.9	60449.4	60449.4	999.0266	1.1911	9.56020	0.3791337	0.37951	-0.12832	0.00040	-2.46292	0.37803	
42592.95	42593.54	42593.54	3.0103624	30.10	99.837	15.75	19.02	42590.8	50687.0	6136.3	999.0359	1.1912	8.15383	0.2706915	0.27117	0.10370	-0.00028	-1.48911	0.27129	
46772.795	47101.85	47101.85	3.0103624	30.10	99.833	15.78	19.08	46532.7	47653.9	8523.2	999.0359	1.1909	6.53307	0.2771082	0.27719	-0.04182	0.00010	0.25241	0.26975	
36691.73	42123.13	42123.13	3.022753	40.10	99.853	15.73	19.02	36656.2	42381.5	54281.5	999.0381	1.1915	5.43871	0.1585787	0.15556	-0.01558	0.00002	0.10988	0.15462	
39040.88	41897.26	41897.26	3.020319	65.10	99.865	15.96	19.11	39006.4	41826.0	5819.5	999.0408	1.1912	5.83003	0.0895858	0.08941	-0.18471	0.00017	0.62909	0.09798	
41897.26	48133.05	48133.05	2.866594	743.10	99.869	15.72	19.20	41826.0	48119.9	62943.9	999.0408	1.1909	6.26948	0.0822023	0.08234	0.27055	-0.00014	-0.17483	0.08260	

Calibration constants	Old calibration (D)	Current calibration (D)
C_1	-0.165376887	-0.168842000
C_2	0.083328531	0.084422000



B.3 Pressure sensors

The pressure sensors were calibrated at a range of 0 – 10 bar. They were calibrated using a water dead weight tester. This device functions by allowing for a piston to spin almost frictionless when weights amounting to a specific pressure are put on the device pressurising the whole system. The importance of having an airtight system is stressed as air will be substantially compressed when pressurised compared to water and give rise to erroneous results. The water dead weight tester has a measurement uncertainty of 0.008%. Measurements are then performed at different pressures, meaning at different weights and plotted. A linear regression is then performed on this data giving a linear function which is used for calculating the pressure in the range of which the sensor was calibrated. The measurement data sheets for two of such measurements are shown in section B.3.1. The total uncertainty for some of the pressure sensors are summarised in table B.2.

Table B.2: linear regression line constants c_1 and c_2 respectively being the y-intercept and slope, and uncertainty for some of the pressure sensors available

Sensor	c_1	c_2	Max uncertainty [Pa]
Reference sensor	$509.81E - 3$	79.95	9.638
Absolute Pressure sensors	-249.80	124.98	0.025019

CALIBRATION REPORT

CALIBRATION PROPERTIES

Calibrated by: Kristian Sagnio
 Type/Producer: GE Druck PMP Unk 5000
 SN: 5453978
 Range: 0-3 bar
 Unit: Kpa

CALIBRATION SOURCE PROPERTIES

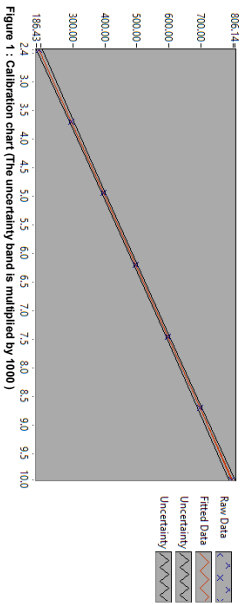
Type/Producer: Pressurments deadweight tester P3223-1
 SN: 66256
 Uncertainty [%]: 0.008

POLY FIT EQUATION:

$$Y = + 509.80516779E-3X^0 + 79.94623289E-0X^1$$

CALIBRATION SUMMARY:

Max Uncertainty : 0.004731 [%]
 Max Uncertainty : 0.008539 [KPa]
 RSD : 1.000000
 Calibration points : 28



Kristian Sagnio

CALIBRATION VALUES

Value [KPa]	Voltage [V]	Best Poly Fit [KPa]	Deviation [KPa]	Uncertainty [%]	Uncertainty [KPa]
195.756854	2.442216	195.755745	0.000909	0.004725	0.008250
295.867726	3.694643	295.862628	0.005097	0.002454	0.007280
396.028796	4.947576	396.049831	-0.021035	0.001538	0.006089
496.189867	6.200319	496.201951	-0.012084	0.001049	0.005203
596.340938	7.452942	596.344458	-0.003521	0.000927	0.005825
696.472009	8.705689	696.467647	0.0025638	0.001060	0.007385
796.623080	9.958922	796.630571	-0.007492	0.001175	0.008368
796.623080	9.957874	796.604324	0.018756	0.001197	0.008539
696.662009	8.705303	696.665950	-0.003941	0.001050	0.007311
596.300938	7.452480	596.307530	-0.006592	0.000988	0.005789
496.159867	6.199698	496.152285	0.007582	0.001043	0.005175
396.008796	4.946934	396.098524	0.010272	0.001456	0.005765
295.857725	3.693970	296.828820	0.028905	0.002456	0.007288
195.676854	2.441474	195.696450	-0.019796	0.004731	0.009258
295.837725	3.693908	195.688937	-0.010283	0.004729	0.009254
395.978796	4.946883	295.823870	0.013855	0.002456	0.007285
496.139867	6.199424	395.970489	0.008297	0.001461	0.005787
596.290938	7.452201	496.130409	0.009458	0.001050	0.005207
696.442009	8.705143	596.285204	0.005733	0.000966	0.005761
796.593080	9.957466	696.453171	-0.011162	0.001050	0.007311
796.603080	9.967682	796.571701	0.021378	0.001172	0.008334
696.452009	8.705239	796.587383	0.015716	0.001167	0.008294
596.300938	7.452515	696.460887	-0.008858	0.001052	0.007327
496.149867	6.199843	596.310282	-0.009344	0.000965	0.005753
396.008796	4.947057	496.163907	-0.014040	0.001038	0.005152
295.857725	3.694379	396.008343	0.000452	0.001466	0.005807
195.716854	2.441587	295.861508	-0.003783	0.002453	0.007289
		195.705496	0.011158	0.004725	0.009248

COMMENTS:
 Reference sensor for 16 pressure channel pressure rack.

The accuracy is indicated with 95% confidence. The uncertainty includes the performance in the calibrated instrument during the calibration, standard uncertainty in the instrument or property which the calibration points to a known calibration equation. The calculated uncertainty can be used as the total systematic uncertainty of the measured instrument when the given instrument equation.

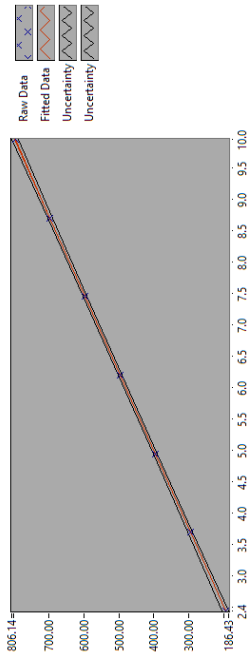
CALIBRATION REPORT

CALIBRATION PROPERTIES
 Calibrated by: Kristian Sagmo
 Type/Producer: GE Druck PMP Unik 5000
 SN: 5453978
 Range: 0-8 bar
 Unit: kPa

CALIBRATION SOURCE PROPERTIES
 Type/Producer: Pressurements deadweight tester P3223-1
 SN: 66256
 Uncertainty [%]: 0.008

POLYFIT EQUATION:
 $Y = 509.805161779E-3X^0 + 79.94623299E+0X^1$

CALIBRATION SUMMARY:
 Max Uncertainty : 0.004731 [%]
 Max Uncertainty : 0.009539 [kPa]
 RSQ : 1.000000
 Calibration points : 28



Kristian Sagmo

CALIBRATION VALUES

Value [kPa]	Voltage [V]	Best Poly Fit [kPa]	Deviation [kPa]	Uncertainty [%]	Uncertainty [kPa]
195.756654	2.442216	195.755745	0.000909	0.004725	0.009250
295.887725	3.694643	295.882628	0.005097	0.002454	0.007260
396.028796	4.947576	396.049831	-0.021035	0.001538	0.006089
496.189867	6.200319	496.201951	-0.012084	0.001049	0.005203
596.340938	7.452942	596.344458	-0.003521	0.000977	0.005825
696.472009	8.705689	696.497647	-0.025638	0.001060	0.007385
796.623080	9.958202	796.630571	-0.007492	0.001175	0.009363
896.763080	9.957874	796.604324	0.118756	0.001197	0.009539
996.462009	8.705303	696.465950	-0.003941	0.001050	0.007311
596.300938	7.452480	596.307530	-0.006592	0.000968	0.005769
496.159867	6.199698	496.152285	0.007582	0.001043	0.005175
396.008796	4.946934	395.998624	0.010272	0.001456	0.005765
295.857725	3.693970	295.828820	0.028905	0.002456	0.007268
195.676654	2.441474	195.696450	-0.019796	0.004731	0.009258
295.837725	2.441355	195.686937	-0.010283	0.004729	0.009254
395.978796	3.693908	295.823870	0.013855	0.002456	0.007265
496.138867	4.946583	395.970499	0.008297	0.001461	0.005787
596.290938	6.199424	496.130409	0.009458	0.001050	0.005207
696.442009	7.452201	596.285204	0.005733	0.000966	0.005761
796.593080	8.705143	696.453171	-0.011162	0.001050	0.007311
796.603080	9.957466	796.571701	0.021378	0.001172	0.009334
696.452009	9.957662	796.587363	0.015716	0.001167	0.009294
596.300938	8.705239	696.460867	-0.008858	0.001052	0.007327
496.149867	7.452515	596.310282	-0.009344	0.000965	0.005753
396.008796	6.199843	496.163907	-0.014040	0.001038	0.005152
295.857725	4.947057	396.008343	0.000452	0.001466	0.005807
195.716654	3.694379	295.861508	-0.003783	0.002453	0.007259
	2.441587	195.705496	0.011158	0.004725	0.009248

COMMENTS:
 Reference sensor for 16 pressure channel pressure rack.

The uncertainty is calculated with 95% confidence. The uncertainty includes the randomness in the calibrated instrument during the calibration, systematic uncertainty in the reference or property which the instrument under calibration is compared with (dead weight manometer, calibrated weights etc.) and due to the limited resolution of the calibration equipment. The calculated uncertainty can be used as the total systematic uncertainty of the calibrated instrument with the given calibration equation.

3D - Printing

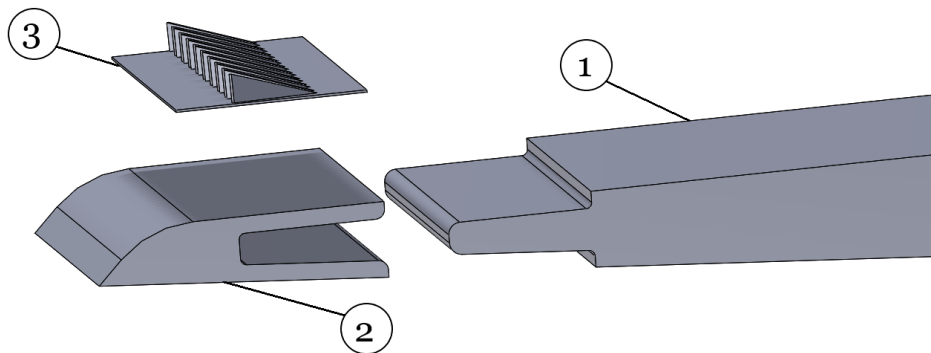


Figure C.1: Attachment method for a 3D - Printed piece. Piece number three is the 3D - Printed piece and can be attached simply with glue.

Python Scripts

```

1  "Created by Hasan Besirovic"
2  "Functions to extract data and do frequency analysis"
3
4  from nptdms import TdmsFile
5  import numpy as np
6  import scipy.signal as sps
7
8  """
9  Function that extracts values of the desired channel and group of data from a Tdms file.
10 """
11 def data_you_want(Tdms_file, name_of_dataGroup, name_of_dataChannel):
12     tdms_file = TdmsFile(Tdms_file)
13     for group in tdms_file.groups():
14         if group == name_of_dataGroup:
15             for channel in tdms_file.group_channels(group):
16                 C_Name = channel.properties["NI_ChannelName"]
17                 if C_Name == name_of_dataChannel:
18                     data = channel.data
19                     time = channel.time_track()
20                     dt = channel.properties["wf_increment"]
21                     break
22             break
23     return data, dt, time
24
25 "Welch on the data that was collected"
26 """Difference between this and the next function is that this one take some specific datagroups and find and plots the
27 power spectrum while the other takes all the groups and finds the peaks."""
28 def Welch_func(Tdms_file, Datagroups, overlap_None, nperseg_N, Min_plot_freq, Max_plot_freq, Natural_1_or_not_0):
29     k = 0
30     Pspektrum = []
31     f = []
32     Pspektrum_max = []
33     f_max = []
34     Pspektrum_secondMax = []
35     f_secondMax = []
36     Velocity = []
37     Windowtype = []
38
39     for file in Tdms_file:
40         for i in range(len(Datagroups) / len(Tdms_file)):
41             data = data_you_want(file, Datagroups[i+k], "Strain")
42
43             if nperseg_N == "N":
44                 nperseg_N_lokke = data[0].size
45             else:
46                 nperseg_N_lokke = data[0].size/nperseg_N
47
48             dt = data[1]
49
50             if Datagroups[i+k] == "8ms":
51                 f_lokke, Pxx = sps.welch(data[0], 1 / dt, window=('kaiser', 2), nperseg=nperseg_N_lokke,
52                                     noverlap=overlap_None, scaling="spectrum")
53                 Windowtype.append('Kaiser')
54             else:
55                 f_lokke, Pxx = sps.welch(data[0], 1 / dt, window='hann', nperseg=nperseg_N_lokke,
56                                     noverlap=overlap_None, scaling="spectrum")
57                 Windowtype.append('Hanning')
58
59             "Limit the frequency spectrum and add them for plotting"
60             Pspektrum_lokke = np.sqrt(Pxx)[maxmin_freq(f_lokke, Min_plot_freq):maxmin_freq(f_lokke, Max_plot_freq)]
61             f_lokke = f_lokke[maxmin_freq(f_lokke, Min_plot_freq):maxmin_freq(f_lokke, Max_plot_freq)]
62             f.append(f_lokke)
63             Pspektrum.append(Pspektrum_lokke)
64
65             "Finding the spectrum peak with corresponding frequency"
66             Pspektrum_max.append(max(Pspektrum_lokke))
67             f_max.append(f_lokke[np.where(Pspektrum_lokke==max(Pspektrum_lokke))])
68
69             "Finding the second max for the Natural Frequency sweep and flow velocity for the power"
70             "spectrum plot from the calibrated constants"
71             if Natural_1_or_not_0 == 1:
72                 peaks_ = sps.find_peaks(Pspektrum_lokke, distance=len(Pspektrum_lokke)/4)
73                 if len(peaks_) > 1:
74                     Pspektrum_secondMax.append(sorted(Pspektrum_lokke[peaks_])[-2])
75                     f_secondMax.append(f_lokke[np.where(Pspektrum_lokke==sorted(Pspektrum_lokke[peaks_])[-2])])
76             else:
77                 Flow = 0.083528531 * round(np.mean(data_you_want(file, Datagroups[i+k], "Flow")[0]),5) - 0.165376967
78                 Velocity.append(Flow / 0.15 ** 2)
79

```

```

80     k = k + len(Datagroups) / len(Tdms_file)
81     return Psppektrum, f, Psppektrum_max, f_max, Psppektrum_secondMax, f_secondMax, Velocity, Windowtype
82
83     """
84     Function for taking all the groups from a Tdms file and calculating the FFT of a given channel.
85     Then finding the peak of this frequency analysis. It also extracts the flow speed in the cross section at the foil.
86     First peak will move while second will be still at almost a constant place corresponding to the eigenfrequency.
87     """
88     def Welch_and_Max_of_data(Tdms_file, name_of_dataChannel, max_freq, min_freq, SamplesPerWindow):
89         MAX_Amplitude = []
90         Velocities_Measured = []
91         Second_Peak_frequency = []
92         First_Peak_frequency = []
93         Velocities_Measured_First_Peak = []
94         Errorbars_SecPeak = []
95         Errorbars_FirstPeak = []
96
97     for file in Tdms_file:
98         tdms_file = TdmsFile(file)
99         for group in tdms_file.groups():
100
101             "Skipping certain files"
102             if file == "" and group != "9_1ms":
103                 continue
104             elif group == "10_6ms" or group == "4ms" or group == "15ms" or group == "16ms":
105                 continue
106
107             for channel in tdms_file.group_channels(group):
108                 C_Name = channel.properties["NI_ChannelName"]
109                 if C_Name == name_of_dataChannel:
110                     "Finding the second peak"
111                     N = len(channel.data)
112                     dt = channel.properties["wf_increment"]
113
114                     "Choosing which groups to have another type of window on"
115                     if group == "8ms":
116                         f_lokke, Psppektrum_lokke = sps.welch(channel.data, 1 / dt, window=('kaiser',2),
117                                                             nperseg=N, noverlap=None, scaling="spectrum")
118                     else:
119                         f_lokke, Psppektrum_lokke = sps.welch(channel.data, 1 / dt, window='hann',
120                                                             nperseg=N, noverlap=None, scaling="spectrum")
121
122                     "Finding the limits and limiting data"
123                     Max_freq = maxmin_freq(f_lokke, max_freq)
124                     Min_freq = maxmin_freq(f_lokke, min_freq)
125                     Psppektrum = np.sqrt(Psppektrum_lokke)[Min_freq:Max_freq]
126                     f = f_lokke[Min_freq:Max_freq]
127
128                     "Finding the second peak"
129                     Max_peak = max(Psppektrum)
130                     MAX_Amplitude.append(Max_peak)
131                     Second_Peak_frequency.append([np.where(Psppektrum == Max_peak)])
132
133                     "Finding the first peak, Using a larger window to find the peak"
134                     if group == "8ms":
135                         f_hanning, Psppektrum_hanning = sps.welch(channel.data, 1 / dt, window=('kaiser',3),
136                                                                 nperseg=N/SamplesPerWindow, noverlap=None, scaling="spectrum")
137                     else:
138                         f_hanning, Psppektrum_hanning = sps.welch(channel.data, 1 / dt, window='hann',
139                                                                 nperseg=N/SamplesPerWindow, noverlap=None, scaling="spectrum")
140
141                     Max_freq_H = maxmin_freq(f_hanning, max_freq)
142                     Min_freq_H = maxmin_freq(f_hanning, min_freq)
143                     Psppektrum_hanning_first_peak = np.sqrt(Psppektrum_hanning)[Min_freq_H:Max_freq_H]
144                     f_hanning_first_peak = f_hanning[Min_freq_H:Max_freq_H]
145
146                     "In order to find the Full Width Half Max (FWHM) of the first and second peaks"
147                     peaks, _ = sps.find_peaks(Psppektrum_hanning_first_peak, distance=len(Psppektrum_hanning_first_peak)/6
148                                             , height=max(Psppektrum_hanning_first_peak)*0.15)
149                     FWHM = sps.peak_widths(Psppektrum_hanning_first_peak, peaks, rel_height=0.5)
150
151                     "For interpolation to find FWHM in frequency [Hz]"
152                     LowLimit = sorted(FWHM[2])
153                     HighLimit = sorted(FWHM[3])
154
155                     LowLimFreq = f_hanning_first_peak[int(LowLimit[-1])] + (LowLimit[-1] - int(LowLimit[-1])) * \
156                                     (f_hanning_first_peak[int(LowLimit[-1]+1)] - f_hanning_first_peak[int(LowLimit[-1])])
157                     HighLimFreq = f_hanning_first_peak[int(HighLimit[-1])] + (HighLimit[-1] - int(HighLimit[-1])) * \
158                                     (f_hanning_first_peak[int(HighLimit[-1]+1)] - f_hanning_first_peak[int(HighLimit[-1])])

```

```

159
160     Errorbars_SecPeak.append([float(f[np.where(Pspektrum == Max_peak)]-LowLimFreq),
161                             float(HighLimFreq-f[np.where(Pspektrum == Max_peak)])])
162
163     "Finding the errorbars of the first peak frequency"
164     if len(peaks) > 1:
165         First_Peak_frequency.append(f_hanning_first_peak[np.where(Pspektrum_hanning_first_peak
166                             == sorted(Pspektrum_hanning_first_peak[peaks])[-2])[0]])
167
168         LowLimFreq = f_hanning_first_peak[int(LowLimit[-2])] + (LowLimit[-2] - int(LowLimit[-2])) * \
169             (f_hanning_first_peak[int(LowLimit[-2]+1)] - f_hanning_first_peak[int(LowLimit[-2])])
170         HighLimFreq = f_hanning_first_peak[int(HighLimit[-2])] + (HighLimit[-2] - int(HighLimit[-2])) * \
171             (f_hanning_first_peak[int(HighLimit[-2]+1)] - f_hanning_first_peak[int(HighLimit[-2])])
172
173         Errorbars_FirstPeak.append([float(f_hanning_first_peak[np.where(Pspektrum_hanning_first_peak
174                             == sorted(Pspektrum_hanning_first_peak[peaks])[-2])[0]] - LowLimFreq),
175                                     float(HighLimFreq - f_hanning_first_peak[np.where(Pspektrum_hanning_first_peak
176                                             == sorted(Pspektrum_hanning_first_peak[peaks])[-2])[0]])])
177
178     "Finding the flow velocity"
179     elif C_Name == "Flow":
180         Flow = 0.083528531 * round(np.mean(channel.data), 5) - 0.165376967
181         Velocities_Measured.append(Flow/0.15**2)
182     if len(peaks) > 1:
183         Velocities_Measured_First_Peak.append(Flow/0.15**2)
184     continue
185 return MAX_Amplitude, Velocities_Measured, Second_Peak_frequency, First_Peak_frequency, \
186        Velocities_Measured_First_Peak, Errorbars_SecPeak, Errorbars_FirstPeak
187
188 "The same thing as the above just for the PIV data"
189 def Welch_func_PIV(Velocities, overlap_None, npersege_N, Min_plot_freq, Max_plot_freq):
190     Pspektrum = []
191     f = []
192     Pspektrum_max = []
193     f_max = []
194     Windowtype = []
195     Flow_Velocity = []
196     Errorbars_PIV = []
197
198     "Finding the positions of the files"
199
200     Files = []
201     Velo_Files = []
202     for Str in Velocities:
203         if Str == '11_1' or Str == '13_1':
204             Files.append("PIV/PD(40,82)/" + Str + "ms_PD_Pos(40,82)/B00002.dat")
205         elif Str == 'Some velocity':
206             Files.append("PIV/PD(10,82)/" + Str + "ms_PD_Pos(10,82)/B00002.dat")
207         else:
208             Files.append("PIV/PD(5,82)/" + Str + "ms_PD_Pos(5,82)/B00002.dat")
209
210     Velo_Files.append("PIV/AvgV/" + Str + "ms_AvgV_40mm/B00001.dat")
211
212     "Main of the function"
213     for i in range(len(Files)):
214         Value = xy_plotting(Files[i])
215         Strength = Value[2]
216
217         if npersege_N == "N":
218             npersege_N_lokke = len(Strength)
219         else:
220             npersege_N_lokke = len(Strength)/npersege_N
221             N = len(Strength)
222
223         if Velocities[i] == "Some velocity":
224             f_lokke, Pspektrum_lokke = sps.welch(Strength, 2441, window='hann', npersege=npersege_N_lokke,
225                 overlap=overlap_None, scaling='spectrum')
226             f_lokke_N, Pspektrum_lokke_N = sps.welch(Strength, 2441, window='hann', npersege=len(Strength),
227                 overlap=overlap_None, scaling='spectrum')
228             Windowtype.append("Hanning")
229         else:
230             f_lokke, Pspektrum_lokke = sps.welch(Strength, 2441, window=('kaiser', 2), npersege=npersege_N_lokke,
231                 overlap=overlap_None, scaling='spectrum')
232             f_lokke_N, Pspektrum_lokke_N = sps.welch(Strength, 2441, window=('kaiser', 2), npersege=len(Strength),
233                 overlap=overlap_None, scaling='spectrum')
234             Windowtype.append("Kaiser")
235
236     "Limit the frequency spectrum and add them for plotting"
237     #Always have one with the smallest possible window size

```

```

238     Pspektrum_lokke_N = Pspektrum_lokke_N[maxmin_freq(f_lokke_N, Min_plot_freq):maxmin_freq(f_lokke_N,
Max_plot_freq)]
239     f_lokke_N = f_lokke_N[maxmin_freq(f_lokke_N, Min_plot_freq):maxmin_freq(f_lokke_N, Max_plot_freq)]
240
241     Pspektrum_lokke = Pspektrum_lokke[maxmin_freq(f_lokke, Min_plot_freq):maxmin_freq(f_lokke, Max_plot_freq)]
242     f_lokke = f_lokke[maxmin_freq(f_lokke, Min_plot_freq):maxmin_freq(f_lokke, Max_plot_freq)]
243     f.append(f_lokke)
244     Pspektrum.append(Pspektrum_lokke)
245
246     "Finding the spectrum peak with corresponding frequency. Only one frequency for the PIV data"
247     Pspektrum_max.append(max(Pspektrum_lokke))
248     f_max.append(f_lokke[np.where(Pspektrum_lokke==max(Pspektrum_lokke))])
249
250     "Finding the Full Width Half Max from a smaller window type"
251     peaks,_ = sps.find_peaks(Pspektrum_lokke,height=max(Pspektrum_lokke))
252     FWHM = sps.peak_widths(Pspektrum_lokke,peaks,rel_height=0.5)
253     LowLimit = sorted(FWHM[2])
254     HighLimit = sorted(FWHM[3])
255     LowLimFreq = f_lokke[int(LowLimit[-1])] + (LowLimit[-1] - int(LowLimit[-1])) * \
256         (f_lokke[int(LowLimit[-1] + 1)] - f_lokke[int(LowLimit[-1])])
257     HighLimFreq = f_lokke[int(HighLimit[-1])] + (HighLimit[-1] - int(HighLimit[-1])) * \
258         (f_lokke[int(HighLimit[-1] + 1)] - f_lokke[int(HighLimit[-1])])
259
260     "Finding the errorbar limits with the original peak (With N windows) as zeropoint"
261     Errorbars_PIV.append([float(f_lokke_N[np.where(Pspektrum_lokke_N == max(Pspektrum_lokke_N))] - LowLimFreq),
262         float(HighLimFreq - f_lokke_N[np.where(Pspektrum_lokke_N == max(Pspektrum_lokke_N))])])
263
264     "Finding the flow velocity from PIV data"
265     Velo_value = xy_plotting(Velo_Files[i])
266     Flow_Velocity.append(np.mean(Velo_value[1]))
267
268     return Pspektrum, f, Pspektrum_max, f_max, Windowtype, Flow_Velocity, Errorbars_PIV
269
270     """
271     Function for finding the position of the max and min frequencies for plotting
272     """
273     def maxmin_freq(x,maxmin_value):
274         for i in range(len(x)):
275             if x[i] <= maxmin_value:
276                 continue
277             else:
278                 MAX_MIN = i
279                 break
280         return MAX_MIN
281
282     "Function that finds out if string is only made out of numbers or has letters in i too"
283     def is_float(string):
284         """ True if given string is float else False """
285         try:
286             return float(string)
287         except ValueError:
288             return False
289
290     "Function that splits the file gotten from PIV post processing so that it is possible to extract data"
291     def xy_plotting(file_location):
292
293         data = open(file_location, "r")
294
295         Value_1 = []
296         Value_2 = []
297         Value_3 = []
298         Value_4 = []
299
300         for lines in data.readlines():
301             "Splits for each space between numbers"
302             Value = lines.split(" ")
303
304             if is_float(Value[0]) and is_float(Value[1]) or is_float(Value[0]) and len(Value) > 2 :
305                 Value_1.append(float(Value[0]))
306                 Value_2.append(float(Value[1]))
307                 if len(Value) > 2:
308                     Value_3.append(float(Value[2]))
309                     Value_4.append(float(Value[3]))
310
311         return Value_1, Value_2, Value_3, Value_4

```

```

1 "Created by Hasan Besirovic"
2 "Script which calculates the the uncertainty from for each vector from a histogram plot"
3
4 import matplotlib.pyplot as plt
5 import Simple_Functions as SF
6 import numpy as np
7
8 "Choosing the file"
9 File_Velo = "13_1"
10 AVG_or_NO = "AVG " # "AVG " or " "
11 SWP_or_NO = "" # "SWP or ""
12 File = "PIV/Uncertainty/V_Uncertainty" + AVG_or_NO + File_Velo + ".ms" + SWP_or_NO + "B00001.dat"
13 File_AvgVelo = "PIV/AvgV/" + File_Velo + "ms_AvgV_40mm/B00001.dat"
14
15 "Defining the range for plotting"
16 Min_peak_ratio = 0.01
17
18 "Getting the data"
19 #Uncertainty data
20 xy = SF.xy_plotting(File)
21 Number_all = xy[2]
22 Uncertainty = xy[0]
23 #AVG velocity data for reference velocity
24 U_ref = np.mean(SF.xy_plotting(File_AvgVelo)[1])
25
26 "Making the velocity uncertainty dimensionless"
27 Uncertainty_dimless = []
28 for k in Uncertainty:
29     Uncertainty_dimless.append(k/U_ref)
30
31 "Finding the plotting range positions"
32 Min_range = SF.maxmin_freq(Uncertainty, Min_peak_ratio)
33 Min_range_dimless = SF.maxmin_freq(Uncertainty_dimless, Min_peak_ratio)
34
35 "Limiting the functions for plotting"
36 Number = Number_all[Min_range:]
37 Uncertainty = Uncertainty[Min_range:]
38 Uncertainty_dimless = Uncertainty_dimless[Min_range:]
39
40 "Finding the number of vectors with uncertainty above a certain value"
41 summing = 0
42 Uncertainty_limit = 0.035
43 for i in range(len(Number)):
44     if Uncertainty_dimless[i] >= Uncertainty_limit:
45         summing = summing + Number[i]
46
47 "Plotting"
48 plt.figure(figsize=(6,4.5))
49 plt.plot(Uncertainty_dimless, Number, color='darkgray')
50 plt.ylim(-5, max(Number)+15)
51 plt.xlabel("Uncertainty [U/$U_{ref}$]", fontsize = 12)
52 plt.ylabel("Number of vectors", fontsize = 12)
53
54 plt.text(0, max(Number)+5, "Vectors with uncertainty above " + str(Uncertainty_limit) + ": " + str(summing) +
55         " (" + str(round(summing/sum(Number_all)*100,2)) + "%)", weight = 'bold',
56         bbox=dict(facecolor='none', edgecolor='red'))
57
58 plt.tight_layout()
59 plt.savefig("PICS/GraphsToUse/Uncertainty_V_Histogram_13_1_AVG.pdf")
60 plt.show()
61

```

```

1  "Created by Hasan Besirovic"
2  "Script which get Peak ratio histogram data and plots this. Also finds values under a specific value"
3
4  import matplotlib.pyplot as plt
5  import Simple_Functions as SF
6
7
8  File = "PIV/Peak_ratio/Peak_ratio_10_1ms/B00001.dat"
9  "Defining the range for plotting"
10 Max_peak_ratio = 20
11 Min_peak_ratio = 0.01
12
13 "Getting the data"
14 xy = SF.xy_plotting(File)
15 Number_all = xy[2]
16 Peak_ratio = xy[0]
17
18 "Finding the plotting range positions"
19 Max_range = SF.maxmin_freq(Peak_ratio,Max_peak_ratio)
20 Min_range = SF.maxmin_freq(Peak_ratio,Min_peak_ratio)
21
22 "Limiting the functions for plotting"
23 Number = Number_all[Min_range:Max_range]
24 Peak_ratio = Peak_ratio[Min_range:Max_range]
25
26 "Finding the sum of vectors with peak ratio below either one or two values"
27 summing = 0
28 summing_3 = 0
29 for i in range(len(Number)):
30     if Peak_ratio[i] <= 2:
31         summing = summing+Number[i]
32     if Peak_ratio[i] <= 3:
33         summing_3 = summing_3+Number[i]
34
35 "Plotting"
36 plt.figure(figsize=(6,4.5))
37 plt.plot(Peak_ratio,Number,color='darkgray')
38 plt.ylim(-5,max(Number)+32)
39 plt.xlabel("Peak ratio", fontsize = 12)
40 plt.ylabel('Number of vectors', fontsize = 12)
41
42 plt.text(0,max(Number)+10,"Vectors with peak ratio below 3: "+str(summing_3)+
43         "("+str(round(summing_3/sum(Number_all)*100,2))+"%)",weight = 'bold',
44         bbox=dict(facecolor='none', edgecolor='red'))
45
46 plt.tight_layout()
47 plt.savefig("PICS\GraphsToUse\PeakRatio_Histogram_10_1ms.pdf")
48 plt.show()
49

```

```

1  "Written by Hasan Besriovic - Spring 2020"
2  "A script to extract frequency data for a hydrofoil"
3
4  import Simple_Functions as SF
5  import matplotlib.pyplot as plt
6
7  "Gets data that is wanted"
8  Datagroups = ["Sweep2-100-1000Hz4Hzincrements@0,3sEach_0", "NewRun"]
9  Tdms_files = ["STRAIN_GAUGE/Ref_Foil/NaturalFrequency/ReferenceFoilFreqSweepClosedWater.tdms",
10               "STRAIN_GAUGE/VG_Foil/NaturalFrequency/NaturalFrequencyPreMeasurements.tdms"]
11  Titles = ["VG foil", "Reference foil"]
12  Max_plot_freq = 1200
13  Min_plot_freq = 500
14
15  "Welch with a Hanning window with 50% overlap"
16  data = SF.Welch_func(Tdms_files, Datagroups, None, 'N', Min_plot_freq, Max_plot_freq, 1)
17  Pspektrum = data[0]
18  f = data[1]
19  Pspektrum_max = data[2]
20  f_max = data[3]
21  Pspektrum_secondMax = data[4]
22  f_secondMax = data[5]
23
24  "Plotting"
25  Numbering = ["a", "b", "c", "d", "e", "f", "g", "h", "i", "k", "l", "m", "n", "o", "p"]
26  k = 0
27  if len(Tdms_files)/len(Datagroups) == 1:
28      fig, axs = plt.subplots(len(Datagroups) / len(Tdms_files), len(Tdms_files), figsize=(12, 4))
29  else:
30      fig, axs = plt.subplots(len(Tdms_files), len(Datagroups) / len(Tdms_files), figsize=(15, 10))
31
32  for i in range(len(Tdms_files)):
33      for j in range(len(Datagroups) / len(Tdms_files)):
34          "For one sweep (1-Figure)"
35          if len(Datagroups) == 1:
36              plt.plot(f[j+k], Pspektrum[j+k], color="k")
37              plt.ticklabel_format(axis='y', style='sci', scilimits=(-2, 2))
38              plt.title(Datagroups[j+k])
39              plt.annotate("(" + str(round(f_max[j+k], 2)) + " Hz)", xy=(f_max[j+k]*1.02, Pspektrum_max[j+k]*0.9),
40                          fontsize = 12)
41              plt.annotate("(" + str(round(f_secondMax[j+k], 2)) + ")", xy=(f_secondMax[j+k],
42                                  Pspektrum_secondMax[j+k]*1.20), fontsize = 12)
43          "For one sweep-file, with several sweeps (1-Row)"
44          elif len(Tdms_files) < 2:
45              axs[j].plot(f[j+k], Pspektrum[j+k], color="k")
46              axs[j].ticklabel_format(axis='y', style='sci', scilimits=(-2, 2))
47              axs[j].set_title(Datagroups[j+k])
48              axs[j].annotate("(" + str(round(f_max[j+k], 2)) + ")", xy=(f_max[j+k]*1.02, Pspektrum_max[j+k]*0.9),
49                          fontsize = 12)
50              axs[j].annotate("(" + str(round(f_secondMax[j+k], 2)) + ")", xy=(f_secondMax[j+k],
51                                  Pspektrum_secondMax[j+k]*1.20), fontsize = 12)
52          "For several sweep-files, with several sweeps (len(Tdms_file)-Rows & len(Datagroups)-Columns)"
53          elif len(Tdms_files)/len(Datagroups) == 1:
54              axs[i].plot(f[j+k], Pspektrum[j+k], color="k")
55              axs[i].ticklabel_format(axis='y', style='sci', scilimits=(-2, 2))
56              axs[i].set_title(Numbering[j+k], fontsize = 18)
57              axs[i].annotate("(" + str(round(f_max[j+k], 2)) + " Hz)", xy=(f_max[j+k]*1.02, Pspektrum_max[j+k]*0.9),
58                          fontsize = 14)
59              axs[i].annotate("(" + str(round(f_secondMax[j+k], 2)) + " Hz)", xy=(f_secondMax[j+k]*0.90,
60                                  Pspektrum_secondMax[j+k]*1.50), fontsize = 14)
61              axs[i].tick_params(labelsize=14)
62          else:
63              axs[i,j].plot(f[j+k], Pspektrum[j+k], color="k")
64              axs[i,j].ticklabel_format(axis='y', style='sci', scilimits=(-2, 2))
65              axs[i,j].set_title(Datagroups[j+k])
66              axs[i,j].annotate("(" + str(round(f_max[j+k], 2)) + ")", xy=(f_max[j+k]*1.02, Pspektrum_max[j+k]*0.9),
67                          fontsize = 12)
68              axs[i,j].annotate("(" + str(round(f_secondMax[j+k], 2)) + ")", xy=(f_secondMax[j+k]*0.98,
69                                  Pspektrum_secondMax[j+k]*1.50), fontsize = 12)
70
71      k = k + len(Datagroups) / len(Tdms_files)
72
73  """"""
74  Labels to compare tdms files internally
75  if len(Datagroups) > 1:
76
77      Label = ["Pre Measurements", "Post Measurements", "Post Retake Measurements"]
78      if len(Tdms_files) > 2:
79          for i in range(len(Tdms_files)):

```

```
80         axs[i,0].set(ylabel = Label[i])
81     elif len(Tdms_files)>1:
82         for i in range(len(Tdms_files)):
83             axs[i].set(ylabel = Label[i])
84     """
85     "To add a common x and y label"
86     fig.add_subplot(111, frameon=False)
87     plt.tick_params(labelcolor='none', top=False, bottom=False, left=False, right=False)
88     plt.xlabel("Frequency [Hz]", fontsize=16)
89     plt.ylabel("Amplitude [RMS]", fontsize=16)
90
91     plt.tight_layout()
92     plt.savefig("PICS/GraphsToUse/NaturalFrequencyCompare.pdf")
93     plt.show()
```

```

1  "Created by Hasan Besirovic"
2  "Script which plots and calculates a frequency comparison plot"
3
4  import Simple_Functions as SF
5  import matplotlib.pyplot as plt
6  import numpy as np
7  "limiting the data"
8  max_freq = 1000
9  min_freq = 150
10 "Importing the data"
11 Files = ["STRAIN_GAUGE/VG_Foil/SymPlaneMeasurements/RampDown.tdms"]
12
13 #Strain Gauge data
14 SamplesPerWindow = 1000
15 data = SF.Welch_and_Max_of_data(Files,"Strain", max_freq,min_freq,SamplesPerWindow)
16 Error_SecPeak = np.transpose(data[5])
17 Error_FirstPeak = np.transpose(data[6])
18
19 #PIV DATA
20 Velocity_files_PIV = ["8","9_1","9_6","10_1","10_6","11_1","13_1"]
21
22 data_PIV = SF.Welch_func_PIV(Velocity_files_PIV,None,'N',min_freq,max_freq)
23 P_max = data_PIV[2]
24 f_max = data_PIV[3]
25 Velo = data_PIV[5]
26 "To plot the errorbars of PIV data found from FWHM (Full Width Half Maximum)"
27 SamplesPerWindow = 100
28 data_PIV_2 = SF.Welch_func_PIV(Velocity_files_PIV,None,SamplesPerWindow,min_freq,max_freq)
29 Error_PIV = np.transpose(data_PIV_2[6])
30
31 "Experimental Strouhal number"
32 St = 0.274
33
34 "To find the R value of the PIV points to the strouhal graph"
35 Strouhal_Linefit = [i*St*1000/4.8 for i in Velo]
36 Horisont = [sum(f_max)/len(f_max)]*len(Velo)
37
38 Differences_Strouhal = [Strouhal_Linefit[i]-f_max[i] for i in range(len(f_max))]
39 Linesum_Strouhal = 0
40 for i in Differences_Strouhal:
41     Linesum_Strouhal = Linesum_Strouhal+i*i
42
43 Differences_Horisont = [Horisont[i]-f_max[i] for i in range(len(f_max))]
44 Linesum_Horisont = 0
45 for i in Differences_Horisont:
46     Linesum_Horisont = Linesum_Horisont + i*i
47
48 R = (Linesum_Horisont-Linesum_Strouhal)/Linesum_Horisont
49 print R
50
51 "Plotting"
52 fig, ax1 = plt.subplots()
53
54 ax1.errorbar(data[1], data[2],yerr=Error_SecPeak,capsize=3,
55             label = "Straingauge Second peak",marker='o',markerfacecolor = "None",color='k',ls='none')
56 ax1.errorbar(data[4],data[3],yerr=Error_FirstPeak,capsize=3,marker="P",color='k',
57             label = "Straingauge First peak",ls='none')
58 ax1.errorbar(Velo,f_max,yerr=Error_PIV,marker="d",color='k', label = "PIV",capsize=3,markerfacecolor = 'None')
59 ax1.plot(data[1],[i*St*1000/4.8 for i in data[1]],'--',color = "r",label = "Strouhal (St = 0.274)")
60 ax1.set_xlabel("St_{ref} [m/s]")
61 ax1.set_ylabel("Frequency [Hz]")
62 ax1.set_ylim(200,900)
63 ax1.set_xlim(5.9,14.1)
64 plt.grid()
65
66 "Dividing the axis such that the right axis is amplitude"
67 ax2 = ax1.twinx()
68 ax2.plot(data[1], data[0]/max(data[0]),"s-",color="darkgray", label = "Strain amplitude")
69 ax2.set_xlabel("St_{ref} [m/s]")
70 ax2.set_ylabel("A/A_{max} [RMS]",color="darkgray")
71 ax2.tick_params(axis='y', labelcolor = "darkgray")
72 ax2.set_ylim(0,4)
73
74 fig.tight_layout()
75 fig.legend(bbox_to_anchor=(0.5,0.95))
76 plt.savefig("PICS/GraphsToUse/Vibration_Frequencies.pdf")
77 plt.show()

```

```

1  "Created by Hasan Besirovic"
2  "Script which calculates the WelchPowerSpectrum for a set of strain gauge data"
3
4  import Simple_Functions as SF
5  import matplotlib.pyplot as plt
6  import numpy as np
7  import matplotlib.lines as lin
8  import scipy.signal as sps
9
10 "Gets data that is wanted"
11 Datagroups = ["6ms", "8ms", "9_1ms", "9_6ms"]
12 Tdms_file = ["STRAIN_GAUGE/VG_Foil/SymPlaneMeasurements/RampDown.tdms",
13             "STRAIN_GAUGE/VG_Foil/SymPlaneMeasurements/RampDown.tdms"]
14 "Limits the data to these frequencies"
15 Max_plot_freq = 1000
16 Min_plot_freq = 200
17
18 "Welch with a chosen window with 50% overlap"
19 data = SF.Welch_func(Tdms_file, Datagroups, None, "N", Min_plot_freq, Max_plot_freq, 0)
20 Psppektrum = data[0]
21 f = data[1]
22 Psppektrum_max = data[2]
23 f_max = data[3]
24 Velocity = data[6]
25 Windowtype = data[7]
26 "Welch with a bigger window"
27 SamplesPerWindow = 1000
28 data = SF.Welch_func(Tdms_file, Datagroups, None, SamplesPerWindow, Min_plot_freq, Max_plot_freq, 0)
29 Psppektrum_N = data[0]
30 f_N = data[1]
31 Psppektrum_max_N = data[2]
32 f_max_N = data[3]
33
34 "Plotting"
35 Numbering = ["a", "b", "c", "d", "e", "f", "g", "h", "i", "j", "k", "l", "m", "n", "o", "p"]
36 k = 0
37 fig, axs = plt.subplots(len(Tdms_file), len(Datagroups) / len(Tdms_file), sharex = True, sharey = True, figsize=(14,4,6))
38 for i in range(len(Tdms_file)):
39     for j in range(len(Datagroups)/len(Tdms_file)):
40
41
42         "For one spectrum (1-Figure)"
43         if len(Datagroups) == 1:
44             peaks, _ = sps.find_peaks(Psppektrum_N[j+k], distance=len(Psppektrum_N[j+k])/6,
45                                     height=Psppektrum_max_N[j+k]*0.1)
46             "First Peak from the one with bigger hanning window"
47             if len(peaks)>1:
48                 FirstPeak = f_N[j+k][np.where(Psppektrum_N[j+k]==sorted(Psppektrum_N[j+k][peaks])[-2])[0]]
49                 plt.annotate("(" + str(round(FirstPeak,2)) + " Hz)",
50                             xy=(FirstPeak,sorted(Psppektrum_N[j+k][peaks])[-2]/Psppektrum_max_N[j+k]*1.15),fontsize=12)
51
52             plt.plot(f[j+k],np.abs(Psppektrum[j+k])/Psppektrum_max[j+k], color="darkgray")
53             plt.plot(f_N[j+k],np.abs(Psppektrum_N[j+k])/Psppektrum_max_N[j+k], color="k")
54             plt.annotate("(" + str(round(f_max[j+k], 2)) + " Hz)",
55                         xy=(f_max[j+k]+10, Psppektrum_max[j+k]/(2*Psppektrum_max[j+k])),fontsize=12)
56             #plt.title(Numbering[j+k])
57             plt.title(str(round(Velocity[j+k],2)) + r" $\frac{m}{s}$ ")
58             lines = [lin.Line2D([0], [0], color="k"), lin.Line2D([0], [0], color="darkgray")]
59             plt.legend((lines), (Windowtype[j+k]+": n = 1", Windowtype[j+k]+
60                          ": n = " + str(SamplesPerWindow)),loc = "upper left",fontsize=12)
61
62
63         "For one file with several velocities"
64         elif len(Tdms_file) < 2:
65             peaks, _ = sps.find_peaks(Psppektrum_N[j+k], distance=len(Psppektrum_N[j+k])/6,
66                                     height=Psppektrum_max_N[j+k]*0.1)
67             "First Peak from the one with bigger hanning window"
68             if len(peaks)>1:
69                 FirstPeak = f_N[j+k][np.where(Psppektrum_N[j+k]==sorted(Psppektrum_N[j+k][peaks])[-2])[0]]
70                 axs[j].annotate("(" + str(round(FirstPeak,2)) + " Hz)",
71                                xy=(FirstPeak,sorted(Psppektrum_N[j+k][peaks])[-2]/Psppektrum_max_N[j+k]*1.15),fontsize=12)
72
73             axs[j].plot(f[j+k],np.abs(Psppektrum[j+k])/Psppektrum_max[j+k], color="darkgray")
74             axs[j].plot(f_N[j+k],np.abs(Psppektrum_N[j+k])/Psppektrum_max_N[j+k], color="k")
75             axs[j].annotate("(" + str(round(f_max[j+k], 2)) + " Hz)",
76                            xy=(f_max[j+k]+1.07,Psppektrum_max[j+k]/(2*Psppektrum_max[j+k])),fontsize=12)
77             #axs[j].set_title(Numbering[j+k])
78             axs[j].set_title(str(round(Velocity[j+k],2)) + r" $\frac{m}{s}$ ")
79             lines = [lin.Line2D([0], [0], color="k"), lin.Line2D([0], [0], color="darkgray")]

```

```

80     axs[j].legend((lines), (Windowtype[j+k]+"'": n = 1", Windowtype[j+k]+
81         "'": n = " + str(SamplesPerWindow)),loc = "upper left",fontsize=12)
82
83
84     "For several files with several velocities"
85 else:
86     peaks, _ = sps.find_peaks(Pspektrum_N[j+k], distance= len(Pspektrum_N[j+k])/6,
87         height=Pspektrum_max_N[j+k]*0.1)
88     "First Peak from the one with bigger hanning window"
89     if len(peaks)>1:
90         FirstPeak = f_N[j+k][np.where(Pspektrum_N[j+k]==sorted(Pspektrum_N[j+k][peaks])[-2])[0]]
91         axs[i,j].annotate("(" + str(round(FirstPeak,2)) + "Hz)",
92             xy=(FirstPeak*0.98,sorted(Pspektrum_N[j+k][peaks])[-2]/Pspektrum_max_N[j+k]*1.15),fontsize=13)
93         print sorted(Pspektrum_N[j+k][peaks])[-2]
94
95     axs[i, j].plot(f[j + k], np.abs(Pspektrum[j + k])/Pspektrum_max[j + k], color="darkgray")
96     axs[i, j].plot(f_N[j + k], np.abs(Pspektrum_N[j + k])/Pspektrum_max_N[j + k], color="k")
97
98     axs[i,j].annotate("(" + str(round(f_max[j + k], 2)) + "Hz)",
99         xy=(f_max[j + k]*1.07,Pspektrum_max[j + k]/(2*Pspektrum_max[j+k])),fontsize=13)
100    axs[i,j].set_title(Numbering[j+k],fontsize=18)
101    #axs[i,j].set_title(str(round(Velocity[j+k],2)) + r" $\frac{m}{s}$ ")
102    lines = [lin.Line2D([0], [0], color="k"), lin.Line2D([0], [0], color="darkgray")]
103    axs[i,j].legend((lines), (Windowtype[j+k]+"'": n = 1", Windowtype[j+k]+
104        "'": n = " + str(SamplesPerWindow)),loc = "upper left",fontsize=12)
105    axs[i,j].tick_params(labelsize=12)
106
107
108    k = k + len(Datagroups) / len(Tdms_file)
109
110 print Velocity
111
112 "To add common y and x labels"
113 fig.add_subplot(111, frameon=False)
114 plt.tick_params(labelcolor='none', top=False, bottom=False, left=False, right=False)
115 plt.xlabel("Frequency [Hz]",fontsize=14)
116 plt.ylabel("A/$A_{max}$ [RMS]",fontsize=14)
117 fig.tight_layout()
118
119 plt.savefig("PICS/GraphsToUse/Welch_PowerSpektrum_SymPlane.pdf")
120 plt.show()
121
122

```

```

1  "Created by Hasan Besirovic"
2  "Script which calculates the Welch Power spectrum for a set of PIV data"
3
4  import matplotlib.pyplot as plt
5  import Simple_Functions as SF
6  import matplotlib.lines as lin
7
8  "Choosing velocities and limiting the frequencies for which data is plotted"
9  Velocities = ["8", "9_1", "9_6", "10_1", "10_6", "11_1"]
10 Min_plot_freq = 150
11 Max_plot_freq = 1000
12
13 "Full Welch method with smallest window possible, one window for each sample"
14 data = SF.Welch_func_PIV(Velocities, None, "N", Min_plot_freq, Max_plot_freq)
15 Pspektrum = data[0]
16 f = data[1]
17 Pspektrum_max = data[2]
18 f_max = data[3]
19 Windowtype = data[4]
20 "Welch's method with a larger window, one window for each SamplesPerWindow"
21 SamplesPerWindow = 100
22 data = SF.Welch_func_PIV(Velocities, None, SamplesPerWindow, Min_plot_freq, Max_plot_freq)
23 Pspektrum_N = data[0]
24 f_N = data[1]
25 Pspektrum_max_N = data[2]
26 f_max_N = data[3]
27
28 "Plotting"
29 Numbering = ["a", "b", "c", "d", "e", "f", "g", "h", "i", "k", "l", "m", "n", "o", "p"]
30 fig, axs = plt.subplots(len(Velocities)/2, 2, sharex=True, sharey=True, figsize=(14.4, 8))
31 k=0
32 for i in range(len(Velocities)/2):
33     for j in range(2):
34         axs[i, j].plot(f[j+k], Pspektrum[j+k]/Pspektrum_max[j+k], color="darkgray")
35         axs[i, j].plot(f_N[j+k], Pspektrum_N[j+k]/Pspektrum_max_N[j+k], color="k")
36         axs[i, j].set_title(Numbering[j+k], fontsize=18)
37         #axs[i, j].set_title(Velocities[j+k]+" m/s")
38         axs[i, j].annotate(""+str(round(f_max[j+k], 2)) + " Hz",
39                          xy=(f_max[j+k]*1.18, Pspektrum_max[j+k]/(Pspektrum_max[j+k]*0.9)), fontsize=13)
40         "Creating the legend"
41         lines = [lin.Line2D([0], [0], color="darkgray"), lin.Line2D([0], [0], color="k")]
42         axs[i, j].legend((lines), (Windowtype[j+k]+": n = 1", Windowtype[j+k]+": n = " + str(SamplesPerWindow)),
43                        loc = "upper left", fontsize=12)
44         k = k+2
45
46 "To add common y and x labels"
47 fig.add_subplot(111, frameon=False)
48 plt.tick_params(labelcolor="none", top=False, bottom=False, left=False, right=False)
49 plt.xlabel("Frequency [Hz]", fontsize=14)
50 plt.ylabel("A/$A_{max}$", fontsize=14)
51
52 fig.tight_layout()
53 plt.savefig("PICS/GraphsToUse/Welch_PowerSpektrum_SymPlane_PIV.pdf")
54 plt.show()

```

```

1  "Written by Hasan Besriovic - Spring 2020"
2  "Script which extracts data from PIV data plots and plots it"
3
4  import matplotlib.pyplot as plt
5  import Simple_Functions as SF
6  import os
7
8  "Specify which data to extract and calculate the average velocity from velocity plot in symmetry plane"
9  Str_1 = "PIV/AvgV/"
10 Str_2 = ["ms_AvgV_SWP_70mm/B00002.dat"]#,"ms_AvgV_SWP_70mm/B00002.dat"]
11 Str_3 = ["9_1","10_1","13_1"]
12 Standarddeviation = ["ms_AvgV_SWP_70mm/B00002.dat"]#,"ms_AvgV_SWP_70mm/B00002.dat"]
13 AbsVelo = ["ms_AvgV_SWP_70mm/B00003.dat"]#,"ms_AvgV_SWP_70mm/B00003.dat"]
14 Uncertainty_loc = "PIV/Uncertainty/xy-plot/SYM"
15 Uncertainty_Str = ["ms_Uncertainty_V_40mm/B00001.dat"]
16
17 Files = []
18 ErrorFiles = []
19 AvgVeloFiles = []
20 for i in range(len(Str_2)):
21     for Str in Str_3:
22         Files.append(Str_1+Str+Str_2[i])
23         ErrorFiles.append((Uncertainty_loc+Str+Uncertainty_Str[i]))
24         AvgVeloFiles.append(Str_1+Str+AbsVelo[i])
25
26 "Plotting"
27 fig,ax = plt.subplots(1,len(Str_2), figsize = (10,6))
28
29 "For the legend"
30 k=0
31 Ref_Velo = [9,10,13,1]
32 for i in range(len(Ref_Velo)):
33     Ref_Velo[i] = "$U_{ref}$S = "+str(Ref_Velo[i])+"m/s"
34
35 D = 4.8
36 for i in range(len(Str_2)):
37     for j in range(len(Str_3)):
38         xy = SF.xy_plotting(Files[j+k])
39         Avg = SF.xy_plotting(AvgVeloFiles[j+k])
40         y = [Value/D for Value in xy[0]]
41         x = [(Value-(sum(Avg[1])/len(Avg[1])))/(sum(Avg[1])/len(Avg[1])) for Value in xy[1]]
42
43 "Calculating the error and add for errorbars"
44 if os.path.isfile(ErrorFiles[j+k]):
45     Velo_error = [(Value)/(15*D*sum(Avg[1])/len(Avg[1]))
46                 for Value in SF.xy_plotting(ErrorFiles[j+k])[1]]
47     while len(Velo_error)<len(x):
48         Velo_error.append(Velo_error[-1])
49
50 "Choose which data has errorbars"
51 if len(Str_2)<2:
52     if Str_3[j] == "10_1":
53         plt.errorbar(x,y,xerr=Velo_error,capsize=2,label = Ref_Velo[j],marker='o',markerfacecolor = 'None')
54     else:
55         plt.plot(x,y,label=Ref_Velo[j])
56         plt.xlim(-1.020, -0.99)
57         plt.grid()
58 "For several plots in the same figure"
59 else:
60     if Str_3[j] == "10_1":
61         ax[i].errorbar(x,y,xerr=Velo_error,capsize=2,label = Ref_Velo[j],marker='o',markerfacecolor = 'None')
62     else:
63         ax[i].plot(x,y,label=Ref_Velo[j])
64         ax[i].set_xlim(-1.020, -0.99)
65         ax[i].grid()
66         ax[i].set_title(Str_2[i].split('ms_AvgV_')[1].split('/')[0])
67
68     k = k + len(Str_3)
69
70 "To organise the legend such that it is alphabetical"
71 handles, labels = ax.get_legend_handles_labels()
72 handles_sort = []
73 for i in range(len(labels)):
74     handles_sort.append(handles[labels.index(Ref_Velo[i])])
75
76 plt.legend(handles_sort,Ref_Velo,fontsize = 14,loc='center right')
77
78 "To add common y and x labels"
79 fig.add_subplot(111, frameon=False)

```

```
80 plt.tick_params(labelcolor='none', top=False, bottom=False, left=False, right=False)
81 plt.ylabel("y/D", fontsize = 20)
82 plt.xlabel(r"$\frac{U_y - U_{ref}}{U_{ref}}$", fontsize=20)
83
84 fig.tight_layout()
85 plt.savefig("PICS/GraphsToUse/AverageVelocity_Vy_SWP_70mm.pdf")
86 plt.show()
87
```

```

1  "Written by Hasan Besriovic - Spring 2020"
2  "Script which extracts data from PIV data plots and plots it"
3
4  import matplotlib.pyplot as plt
5  import Simple_Functions as SF
6  import os
7
8  "Specify which data to extract"
9  Str_1 = "PIV/AvgV/"
10 Str_2 = ["ms_AvgV_40mm/B00001.dat"]#,"ms_AvgV_60mm/B00001.dat"]
11 Str_3 = ["8","9_1","9_6","10_1","10_6","11_1","13_1"]
12 Standarddeviation = ["ms_AvgV_40mm/B00002.dat"]#,"ms_AvgV_60mm/B00002.dat"]
13 Uncertainty_loc = "PIV/Uncertainty/xy-plot/SYM"
14 Uncertainty_Str = ["ms_Uncertainty_V_40mm/B00001.dat"]
15
16 Files = []
17 ErrorFiles = []
18 for i in range(len(Str_2)):
19     for Str in Str_3:
20         Files.append(Str_1+Str+Str_2[i])
21         ErrorFiles.append(Uncertainty_loc+Str+Uncertainty_Str[i])
22
23 "plotting"
24 fig,ax = plt.subplots(1,len(Str_2), figsize = (10,6))
25
26 "For the legend"
27 k=0
28 Ref_Velo = [8,9,1,9,6,10,1,10,6,11,1,13,1]
29 for i in range(len(Ref_Velo)):
30     Ref_Velo[i] = "SU_{ref}S = "+str(Ref_Velo[i])+"m/s"
31
32 D = 4.8
33 for i in range(len(Str_2)):
34     for j in range(len(Str_3)):
35         xy = SF.xy_plotting(Files[j+k])
36         y = [Value/D for Value in xy[0]]
37         x = [(Value-(sum(xy[1])/len(xy[1])))/(sum(xy[1])/len(xy[1]))for Value in xy[1]]
38
39 "Calculating the error and add for errorbars"
40 if os.path.isfile(ErrorFiles[j+k]):
41     Velo_error = [Value/(2*D*sum(xy[1])/len(xy[1]))
42                 for Value in SF.xy_plotting(ErrorFiles[j+k])[1]]
43
44 PosMinVelo = y[x.index(min(x))]
45 yplot = []
46 xplot = []
47 Velo_errorplot = []
48 for y_val in y:
49     Range = 4
50     if y_val >= PosMinVelo-Range and PosMinVelo+Range >= y_val:
51         yplot.append(y_val)
52         xplot.append(x[y.index(y_val)])
53         if os.path.isfile(ErrorFiles[j+k]):
54             if len(Velo_error)>y.index(y_val):
55                 Velo_errorplot.append(Velo_error[y.index(y_val)])
56             else:
57                 Velo_errorplot.append(Velo_error[len(Velo_error)-1])
58
59 "Choose which data has errorbars"
60 if len(Str_2)<2:
61     if Str_3[j+k] == "9_1" or Str_3[j+k]=="13_1":
62         plt.errorbar(xplot,yplot,xerr=Velo_errorplot,capsize=3,label = Ref_Velo[j],marker='o',
63                     markerfacecolor='None')
64     else:
65         plt.plot(xplot,yplot,label = Ref_Velo[j])
66
67 plt.xlim(-0.20, 0.05)
68 plt.ylim(13.5,17)
69 plt.grid()
70 "For several plots in one figure"
71 else:
72     if Str_3[j+k] == "9_1" or Str_3[j+k]=="13_1":
73         ax[i].errorbar(xplot,yplot,xerr=Velo_errorplot,capsize=3,label = Ref_Velo[j],marker="x")
74     else:
75         ax[i].plot(xplot,yplot,label = "SU_{ref}S = "+str(Ref_Velo[j+k])+"m/s")
76
77 ax[i].set_xlim(-0.20, 0.05)
78 ax[i].set_ylim(13.5,17)
79 ax[i].grid()

```

```

80     ax[i].set_title(Str_2[i].split('ms_AvgV_')[1].split('/')[0])
81
82     k = k + len(Str_3)
83
84     "To organise the legend such that it is alphabetical"
85     handles, labels = ax.get_legend_handles_labels()
86     handles_sort = []
87     for i in range(len(labels)):
88         handles_sort.append(handles[labels.index(Ref_Velo[i])])
89
90     plt.legend(handles_sort,Ref_Velo,fontsize = 14,loc='center right')
91
92     "To add common y and x labels"
93     fig.add_subplot(111, frameon=False)
94     plt.tick_params(labelcolor='none', top=False, bottom=False, left=False, right=False)
95     plt.ylabel("y/D", fontsize=20)
96     plt.xlabel(r"$\frac{U-U_{ref}}{U_{ref}}$", fontsize=20)
97
98     plt.tight_layout()
99     plt.savefig("PICS/GraphsToUse/AverageVelocity_40mm.pdf")
100    plt.show()
101
102

```

```

1  "Written by Hasan Besriovic - Spring 2020"
2  "Script which extracts data from PIV data plots and plots it"
3
4  import matplotlib.pyplot as plt
5  import Simple_Functions as SF
6
7  "Specify which data to extract"
8  Str_1 = "PIV/Vorticity/"
9  Str_2 = ["ms_Vorticity_SWP_70mm/B00001.dat"]#, "ms_Vorticity_SWP_70mm/B00001.dat"]
10 Str_3 = ["9_1", "10_1", "13_1"]
11 Standarddeviation = ["ms_Vorticity_SWP_70mm/B00002.dat"]#, "ms_AvgV_60mm/B00002.dat"]
12 Files = []
13 ErrorFiles = []
14 for i in range(len(Str_2)):
15     for Str in Str_3:
16         Files.append(Str_1+Str+Str_2[i])
17         ErrorFiles.append((Str_1+Str+Standarddeviation[i]))
18
19 "Plotting"
20 fig,ax = plt.subplots(1,len(Str_2), figsize = (9,7.5))
21
22 "For the legend"
23 k=0
24 Ref_Velo_1 = [9.1,10.1,13.1]
25 Ref_Velo = [9.1,10.1,13.1]
26 for i in range(len(Ref_Velo)):
27     Ref_Velo[i] = "SU_{ref}$" +str(Ref_Velo[i])+"m/s"
28
29 D = 4.8
30 for i in range(len(Str_2)):
31     for j in range(len(Str_3)):
32         xy = SF.xy_plotting(Files[j+k])
33         y = [Value/D for Value in xy[0]]
34         x = [Value*D/(1000*Ref_Velo_1[j]) for Value in xy[1]]
35
36 "Calculating the error and add for errorbars"
37 Vorticity_error = [Value*0.0000003 for Value in SF.xy_plotting(ErrorFiles[j + k])[1]]
38
39 "Choose which data has errorbars"
40 if len(Str_2)-2:
41     if Str_3[j] == "10_1_":
42         plt.errorbar(x,y,xerr=Vorticity_error,capsize=2,label = Ref_Velo[j])
43     else:
44         plt.plot(x,y,label=Ref_Velo[j])
45         plt.xlim(-0.20, 0.20)
46         plt.grid()
47 "For several plots in the same figure"
48 else:
49     if Str_3[j] == "10_1_":
50         ax[i].errorbar(x,y,xerr=Vorticity_error,capsize=2,label = Ref_Velo[j])
51     else:
52         ax[i].plot(x,y,label=Ref_Velo[j])
53         ax[i].set_xlim(-0.16, 0.16)
54         ax[i].grid()
55         ax[i].set_title(Str_2[i].split('ms_Vorticity_SWP_')[1].split('/')[0] + "Downstream")
56
57     k = k + len(Str_3)
58
59 "To organise the legend such that it is alphabetical"
60 handles, labels = ax.get_legend_handles_labels()
61 handles_sort = []
62 for i in range(len(labels)):
63     handles_sort.append(handles[labels.index(Ref_Velo[i])])
64
65 plt.legend(handles_sort,Ref_Velo,fontsize = 14,loc='upper left')
66
67 "To add common y and x labels"
68 fig.add_subplot(111, frameon=False)
69 plt.tick_params(labelcolor='none', top=False, bottom=False, left=False, right=False)
70 plt.ylabel("$z/D", fontsize=20)
71 plt.xlabel(r'$S\frac{Vorticity}{D}\{U_{ref}\}$', fontsize=20)
72
73 fig.tight_layout()
74 plt.savefig("PICS/GraphsToUse/VorticitySWP_70mm.pdf")
75 plt.show()
76
77
78

```

```

1  "Written by Hasan Besriovic - Spring 2020"
2  "Script which extracts data from PIV data plots and plots it"
3
4  import matplotlib.pyplot as plt
5  import Simple_Functions as SF
6
7  "Specify which data to extract"
8  Str_1 = "PIV/Vorticity/"
9  Str_2 = ["ms_Vorticity_40mm/B00001.dat"]#, "ms_Vorticity_40mm/B00001.dat"
10 Str_3 = ["8", "9_1", "9_6", "10_1", "10_6", "11_1", "13_1"]
11 Standarddeviation = ["ms_Vorticity_40mm/B00002.dat"]#, "ms_AvgV_60mm/B00002.dat"
12 Files = []
13 ErrorFiles = []
14 for i in range(len(Str_2)):
15     for Str in Str_3:
16         Files.append(Str_1+Str+Str_2[i])
17         ErrorFiles.append((Str_1+Str+Standarddeviation[i]))
18
19 "plotting"
20 fig,ax = plt.subplots(1,len(Str_2),figsize=(6.2,5.2))
21
22 "For the legend"
23 Ref_Velo_1 = [8,9,1,9,6,10,1,10,6,11,1,13,1]
24 k=0
25 Ref_Velo = [8,9,1,9,6,10,1,10,6,11,1,13,1]
26 for i in range(len(Ref_Velo)):
27     Ref_Velo[i] = "SU_{ref}$ = "+str(Ref_Velo[i])+"m/s"
28
29
30 D=4.8
31 for i in range(len(Str_2)):
32     for j in range(len(Str_3)):
33         xy = SF.xy_plotting(Files[j+k])
34         y = [Value/D for Value in xy[0]]
35         x = [Value*D/(1000*Ref_Velo_1[j]) for Value in xy[1]]
36
37 "Calculating the error and add for errorbars"
38 Vorticity_error = [Value for Value in SF.xy_plotting(ErrorFiles[j + k])[1]]
39
40 PosinfVort = y[(x.index(min(x))+x.index(max(x)))/2]
41 yplot = []
42 xplot = []
43 Vorticity_errorplot = []
44 for y_val in y:
45     Range = 5
46     if y_val >= PosinfVort-Range and PosinfVort+Range >= y_val:
47         yplot.append(y_val)
48         xplot.append(x[y.index(y_val)])
49         Vorticity_errorplot.append(Vorticity_error[y.index(y_val)])
50
51 "Choose which data has errorbars"
52 if len(Str_2)<2:
53     if Str_3[j+k] == "9_1_" or Str_3[j+k] == "13_1_":
54         plt.errorbar(xplot,yplot,xerr=Vorticity_errorplot,
55                     capsizes=2,label = Ref_Velo[j],marker='o',markerfacecolor = 'None')
56     else:
57         plt.plot(xplot,yplot,label = Ref_Velo[j])
58     plt.xlim(-0.3, 0.3)
59     plt.ylim(13,17.5)
60     plt.grid()
61 "For several plots within the same figure"
62 else:
63     if Str_3[j+k] == "9_1_" or Str_3[j+k] == "13_1_":
64         ax[i].errorbar(xplot,yplot,xerr=Vorticity_errorplot,
65                       capsizes=2,label = Ref_Velo[j],marker='o',markerfacecolor = 'None')
66     else:
67         ax[i].plot(xplot,yplot,label = Ref_Velo[j])
68     ax[i].grid()
69     plt.xlim(-0.3, 0.3)
70     ax[i].set_ylim(13,17.5)
71     ax[i].set_title(Str_2[i].split('ms_Vorticity_')[1].split('/')[0])
72
73     k = k + len(Str_3)
74
75 "To organise the legend such that it is alphabetical"
76 handles, labels = ax.get_legend_handles_labels()
77 handles_sort = []
78 for i in range(len(labels)):
79     handles_sort.append(handles[labels.index(Ref_Velo[i])])

```

```
80
81 plt.legend(handles_sort,Ref_Velo,fontsize = 12,loc='upper left')
82
83 "To add common y and x labels"
84 fig.add_subplot(111, frameon=False)
85 plt.tick_params(labelcolor='none', top=False, bottom=False, left=False, right=False)
86 plt.ylabel("y/D",fontsize = 14)
87 plt.xlabel(r'$S\frac{\text{Vorticity} \cdot D}{U_{ref}}S$',fontsize = 14)
88
89 fig.tight_layout()
90 plt.savefig("PICS/GraphsToUse/VorticitySYM_40mm.pdf")
91 plt.show()
```

```

1  "Created by Hasan Besirovic"
2  "Script which calculates the diffusion rate of the vorticity for the VGs"
3
4  import Simple_Functions as SF
5  import matplotlib.pyplot as plt
6  import numpy as np
7  import scipy.signal as sps
8  from sklearn.linear_model import LinearRegression
9  from sklearn.preprocessing import PolynomialFeatures
10 from scipy.optimize import curve_fit
11
12 "Choosing the velocity and files"
13 U_ref = [9.1,10.1,13.1]
14 x = [45,50,55,60,65,70,75]
15 Str = ["PIV/Vorticity/9_1ms_Vorticity_SWP_", "PIV/Vorticity/10_1ms_Vorticity_SWP_", "PIV/Vorticity/
16 13_1ms_Vorticity_SWP_"]
17
18 "Getting the files in a specific order"
19 files = []
20 MaxAmountPeaks = []
21 for i in x:
22     for n in range(len(Str)):
23         files.append(Str[n]+str(i)+"mm/B00001.dat")
24
25 "Finding the main peak values for the vorticity plots for the use of checking decay"
26 for n in range(len(Str)):
27     for i in x:
28         file = Str[n]+str(i)+"mm/B00001.dat"
29         peaks_ = sps.find_peaks(SF.xy_plotting(file)[1],distance=1280/4)
30         valleys_ = sps.find_peaks([i*-1 for i in SF.xy_plotting(file)[1]],distance=1280/4)
31         Extremal = peaks.tolist()
32         Extremal.extend(valleys.tolist())
33         if len(MaxAmountPeaks) <= n:
34             MaxAmountPeaks.append(Extremal)
35         elif len(Extremal) > len(MaxAmountPeaks[n]):
36             MaxAmountPeaks[n] = Extremal
37         files.append(file)
38
39 "Appends the value of each peak and valley to a list and normalises it"
40 k = 0
41 x_value = []
42 y_value = []
43 D = 4.8#mm
44 for i in range(len(x)):
45     for j in range(len(Str)):
46         xy = SF.xy_plotting(files[j+k])
47         for a in MaxAmountPeaks[j]:
48             x_value.append(x[i]/D)
49             if xy[1][a]<=0:
50                 y_value.append(xy[1][a]*-1*D/(1000*U_ref[j]))
51             else:
52                 y_value.append(xy[1][a]*D/(1000*U_ref[j]))
53
54     k = k+len(Str)
55
56 """"""
57 #Just a test to illustrate the peaks and valleys found
58 plt.plot(xy[0],xy[1])
59 Test_x = []
60 Test_y = []
61 for a in MaxAmountPeaks[0]:
62     Test_x.append(xy[0][a])
63     Test_y.append(xy[1][a])
64 plt.plot(Test_x,Test_y,'*')
65 """"""
66 def linear(x,a,b):
67     return a*(x+b/a)
68
69 def exponential(x,a,b):
70     return a*np.exp(x)**(b)
71
72 fig_ = plt.subplots(figsize=(8,8.5))
73
74 plt.plot(x_value,y_value,'ko',markerfacecolor='None')
75
76 popt, pcov = curve_fit(exponential,x_value,y_value)
77 plt.plot(x_value,exponential(x_value,*popt),label="Exponential. Decay exponent = "+str(round(popt[1],4)))
78 print popt

```

```

79 popt, pcov = curve_fit(linear,x_value,y_value)
80 plt.plot(x_value,linear(x_value,*popt),label="Linear. Decay gradient = "+str(round(popt[0],4)))
81 print popt
82
83
84 """
85 "Linear regression for all the points and also across each velocity"
86 x_linReg = np.array(x_value).reshape((-1,1))
87 y_linReg = np.array(y_value)
88 model = LinearRegression().fit(x_linReg,y_linReg)
89
90 x_linReg_1 = np.array(x_value[:len(MaxAmountPeaks[0])*len(x)]).reshape((-1,1))
91 y_linReg_1 = np.array(y_value[:len(MaxAmountPeaks[0])*len(x)])
92 model_1 = LinearRegression().fit(x_linReg_1,y_linReg_1)
93
94
95 x_linReg_2 = np.array(x_value[len(MaxAmountPeaks[0])*len(x):len(MaxAmountPeaks[1])*len(x)+
96 len(MaxAmountPeaks[0])*len(x)]).reshape((-1,1))
97 y_linReg_2 = np.array(y_value[len(MaxAmountPeaks[0])*len(x):len(MaxAmountPeaks[1])*len(x)+
98 len(MaxAmountPeaks[0])*len(x)])
99 model_2 = LinearRegression().fit(x_linReg_2,y_linReg_2)
100
101
102 x_linReg_3 = np.array(x_value[len(MaxAmountPeaks[1])*len(x)+len(MaxAmountPeaks[0])*len(x):
103 len(MaxAmountPeaks[1])*len(x)+len(MaxAmountPeaks[0])*len(x)+len(MaxAmountPeaks[2])*len(x)]).reshape((-1,1)
104 ))
105 y_linReg_3 = np.array(y_value[len(MaxAmountPeaks[1])*len(x)+len(MaxAmountPeaks[0])*len(x):
106 len(MaxAmountPeaks[1])*len(x)+len(MaxAmountPeaks[0])*len(x)+len(MaxAmountPeaks[2])*len(x)])
107 model_3 = LinearRegression().fit(x_linReg_3,y_linReg_3)
108
109 "plotting both the points and corresponding linear regression lines"
110 fig_ = plt.subplots(figsize=(8,8.5))
111 plt.plot(x_value,model.predict(x_linReg),'r-',label="Total Average, Decay gradient = "+str(round(model.coef_4)))
112
113 plt.plot(x_value[:len(MaxAmountPeaks[0])*len(x)],model_1.predict(x_linReg_1),'k-',marker=" ",
114 label="Average 9.1m/s, Decay gradient = "+str(round(model_1.coef_4)))
115 plt.plot(x_value[:len(MaxAmountPeaks[0])*len(x)],y_value[:len(MaxAmountPeaks[0])*len(x)],'k*')
116
117 plt.plot(x_value[len(MaxAmountPeaks[0])*len(x):len(MaxAmountPeaks[1])*len(x)+len(MaxAmountPeaks[0])*len(x)],
118 model_2.predict(x_linReg_2),'k',marker='o',markerfacecolor = 'None',
119 label="Average 10.1m/s, Decay gradient = "+str(round(model_2.coef_4)))
120 plt.plot(x_value[len(MaxAmountPeaks[0])*len(x):len(MaxAmountPeaks[1])*len(x)+len(MaxAmountPeaks[0])*len(x)],
121 y_value[len(MaxAmountPeaks[0])*len(x):len(MaxAmountPeaks[1])*len(x)+len(MaxAmountPeaks[0])*len(x)],
122 'k',marker='o',linestyle='None',markerfacecolor = 'None')
123
124 plt.plot(x_value[len(MaxAmountPeaks[1])*len(x)+len(MaxAmountPeaks[0])*len(x):len(MaxAmountPeaks[1])*len(x)+
125 len(MaxAmountPeaks[0])*len(x)+len(MaxAmountPeaks[2])*len(x)],model_3.predict(x_linReg_3),
126 'k-',marker='s',markerfacecolor = 'None',label="Average 13.1m/s, Decay gradient = "+str(round(model_3.coef_4)))
127 plt.plot(x_value[len(MaxAmountPeaks[1])*len(x)+len(MaxAmountPeaks[0])*len(x):len(MaxAmountPeaks[1])*
128 len(x)+len(MaxAmountPeaks[0])*len(x)+len(MaxAmountPeaks[2])*len(x)],
129 y_value[len(MaxAmountPeaks[1])*len(x)+len(MaxAmountPeaks[0])*len(x):len(MaxAmountPeaks[1])*
130 len(x)+len(MaxAmountPeaks[0])*len(x)+len(MaxAmountPeaks[2])*len(x)],
131 'k',marker='s',linestyle='None',markerfacecolor = 'None')
132 """
133 plt.ylabel(r'$\frac{d}{dt} \{U_{ref}\}$',fontsize=14)
134 plt.xlabel('x/D',fontsize=14)
135 plt.legend(fontsize = 14)
136 plt.savefig("PICS/GraphsToUse/VortexDecay_SWP.pdf")
137 plt.show()
138
139
140

```

```

1  "Created by Hasan Besirovic"
2  "Script which calculates the diffusion rate of the vorticity for the von karman street"
3
4  import Simple_Functions as SF
5  import matplotlib.pyplot as plt
6  import numpy as np
7  import scipy.signal as sps
8  from sklearn.linear_model import LinearRegression
9  from sklearn.preprocessing import PolynomialFeatures
10 from scipy.optimize import curve_fit
11
12 "Specifying which files to get"
13 U_ref = [8,9,1,9,6,10,1,10,6,11,1,13,1]
14 x = [30,35,40,45,50,55,60,65,70]
15 Str = ["PIV/Vorticity/8ms_Vorticity_", "PIV/Vorticity/9_1ms_Vorticity_", "PIV/Vorticity/9_6ms_Vorticity_",
16        "PIV/Vorticity/10_1ms_Vorticity_", "PIV/Vorticity/10_6ms_Vorticity_", "PIV/Vorticity/11_1ms_Vorticity_",
17        "PIV/Vorticity/13_1ms_Vorticity_"]
18
19 "Getting the files in a specific order"
20 files = []
21 MaxAmountPeaks = []
22 for i in x:
23     for n in range(len(Str)):
24         files.append(Str[n]+str(i)+"mm/B00001.dat")
25
26 "Finding the peak and valley for the data"
27 for n in range(len(Str)):
28     for i in x:
29         file = Str[n]+str(i)+"mm/B00001.dat"
30         peaks_ = sps.find_peaks(SF.xy_plotting(file)[1],distance=1280)
31         valleys_ = sps.find_peaks([i*-1 for i in SF.xy_plotting(file)[1]],distance=1280)
32         Extremal = peaks.tolist()
33         Extremal.extend(valleys.tolist())
34         if len(MaxAmountPeaks) <= n:
35             MaxAmountPeaks.append(Extremal)
36         elif len(Extremal) > len(MaxAmountPeaks[n]):
37             MaxAmountPeaks[n] = Extremal
38
39 "Appending the values which are needed for plotting and linear regression and which are normalised "
40 k = 0
41 x_value = []
42 y_value = []
43 D = 4.8
44 for i in range(len(x)):
45     for j in range(len(Str)):
46         xy = SF.xy_plotting(files[j+k])
47         for a in MaxAmountPeaks[j]:
48             x_value.append(x[i]/D)
49             if xy[1][a]<=0:
50                 y_value.append(xy[1][a]*-1*D/(1000*U_ref[j]))
51             else:
52                 y_value.append(xy[1][a]*D/(1000*U_ref[j]))
53     k = k+len(Str)
54
55 """"""
56 Just a test to illustrate the peaks and valleys found
57
58 plt.plot(xy[0],xy[1])
59 Test_x = []
60 Test_y = []
61 for a in MaxAmountPeaks[0]:
62     Test_x.append(xy[0][a])
63     Test_y.append(xy[1][a])
64 plt.plot(Test_x,Test_y,'*')
65 """"""
66
67 "For the curvefit of a specific function"
68 def hypFunc(x,a,b):
69     return a/(b+x)
70
71 def exponential(x,a,b):
72     return a*np.exp(x)**(b)
73
74 fig_ = plt.subplots(figsize=(8,6))
75
76 popt, pcov = curve_fit(hypFunc,x_value,y_value)
77 plt.plot(x_value,hypFunc(x_value,*popt),label="Curvefit, hyperbolic")
78 residuals = y_value-hypFunc(x_value,*popt)
79 ss_res = np.sum(residuals**2)

```

```

80 ss_tot = np.sum((y_value-np.mean(y_value))**2)
81 R = 1-ss_res/ss_tot
82 print popt, np.sqrt(R)
83 popt, pcov = curve_fit(exponential,x_value,y_value)
84 plt.plot(x_value,exponential(x_value,*popt),label="Exponential")
85 residuals = y_value-exponential(x_value,*popt)
86 ss_res = np.sum(residuals**2)
87 ss_tot = np.sum((y_value-np.mean(y_value))**2)
88 R = 1-ss_res/ss_tot
89 print popt, np.sqrt(R)
90
91 "For the polynomial regression"
92 x_linReg = np.array(x_value).reshape((-1,1))
93 y_linReg = np.array(y_value)
94
95 Transform = PolynomialFeatures(degree=2,include_bias=False).fit_transform(x_linReg)
96 model = LinearRegression().fit(Transform,y_linReg)
97 intercept, coefficients = model.intercept_, model.coef_
98 #print intercept, coefficients
99
100 #plt.plot(x_value,model.predict(Transform),'r-',label="Total Average, dw/dx = ")
101 plt.plot(x_value,y_value,'ks', markerfacecolor='None')
102
103
104 plt.ylabel(r'$\frac{Vorticity \cdot D}{U_{ref}}S$', fontsize=14)
105 plt.xlabel('x/D',fontsize=14)
106 plt.legend()
107
108 plt.savefig("PICS/GraphsToUse/VortexDecay_SYM.pdf")
109 plt.show()

```

Risk Assessment



Risk Assessment Report

HiFrancis Blade Cascade

Project name	PIV measurements on blade cascade for HiFrancis project
Apparatus	Double-Cavity High speed laser, 2*10mJ, 1000Hz, 527nm
Unit	EPT
Equipment manager	Bård Brandåstrø
Project leader	Pål Tore Storli
HSE coordinator	Morten Grønli
HSE responsible (linjeleder)	Therese Løvås
Location	Waterpower Laboratory
Room number	11
Risk assessment performed by	Magne Tveit Bolstad

Approval:

Apparatur kort (UNIT CARD) valid for:	12 months
Forsøk pågår kort (EXPERIMENT IN PROGRESS) valid for:	12 months

Rolle	Navn	Dato	Signatur
Project leader	Pål-Tore Storli	24/8 2017	
HSE coordinator	Morten Grønli		
HMS responsible (linjeleder)	Therese Løvås		

TABLE OF CONTENTS

1	INTRODUCTION	1
2	CONCLUSION	ERROR! BOOKMARK NOT DEFINED.
3	ORGANISATION	1
4	RISK MANAGEMENT IN THE PROJECT	1
5	DESCRIPTIONS OF EXPERIMENTAL SETUP	2
6	EVACUATION FROM THE EXPERIMENTAL AREA.....	2
7	WARNING	2
7.1	Before experiments.....	2
7.2	Non-conformance	2
8	ASSESSMENT OF TECHNICAL SAFETY	3
8.1	HAZOP	3
8.2	Flammable, reactive and pressurized substances and gas.....	3
8.3	Pressurized equipment.....	4
8.4	Effects on the environment (emissions, noise, temperature, vibration, smell).....	4
8.5	Radiation	4
8.6	Chemicals	4
8.7	Electricity safety (deviations from the norms/standards).....	4
9	ASSESSMENT OF OPERATIONAL SAFETY	4
9.1	Procedure HAZOP.....	4
9.2	Operation and emergency shutdown procedure.....	4
9.3	Training of operators.....	5
9.4	Technical modifications.....	5
9.5	Personal protective equipment.....	5
9.5.1	General Safety	5
9.6	Safety equipment	5
9.7	Special predations	5
10	QUANTIFYING OF RISK - RISK MATRIX.....	5
11	REGULATIONS AND GUIDELINES	6
12	DOCUMENTATION.....	6
13	GUIDANCE TO RISK ASSESSMENT TEMPLATE.....	7

1 INTRODUCTION

PIV measurements will be performed on a Site Acceptance Test-rig in accordance with the new PIV equipment at the waterpower laboratory. Measurements will be performed in May-June 2017.

2 ORGANISATION

Role	
Project leader	Pål Tore Storli
Equipment manager	Bård Brandåstrø
Room manager	Bård Brandåstrø
HSE coordinator	Morten Grønli
HSE responsible (linjeleder):	Therese Løvås

3 RISK MANAGEMENT IN THE PROJECT

Hovedaktiviteter risikostyring	Nødvendige tiltak, dokumentasjon	DATE
Prosjekt initiering Project initiation	Prosjekt initiering mal	X
Veiledningsmøte Guidance Meeting	Skjema for Veiledningsmøte med pre-risikovurdering	X
Innledende risikovurdering Initial Assessment	Fareidentifikasjon – HAZID Skjema grovanalyse	X
Vurdering av teknisk sikkerhet Evaluation of technical security	Prosess-HAZOP Tekniske dokumentasjoner	X
Vurdering av operasjonell sikkerhet Evaluation of operational safety	Prosedyre-HAZOP Opplæringsplan for operatører	X
Sluttvurdering, kvalitetssikring Final assessment, quality assurance	Uavhengig kontroll Utstedelse av apparaturkort Utstedelse av forsøk pågår kort	X

4 DESCRIPTIONS OF EXPERIMENTAL SETUP

- Drawings and photos describing the setup.
- Process and Instrumentation Diagram (PID) with list of components
- Location of the operator, gas bottles, shutdown valves for water / air.

5 EVACUATION FROM THE EXPERIMENTAL AREA

Evacuate at signal from the alarm system or local gas alarms with its own local alert with sound and light outside the room in question, see 6.2

Evacuation from the rigging area takes place through the marked emergency exits to the assembly point, (corner of Old Chemistry Kjelhuset or parking 1a-b.)

Action on rig before evacuation:

Describe in which condition the rig should be left in case of evacuation (emergency shutdown procedure, water, gas, electric supply, etc.)

6 WARNING

6.1 Before experiments

Send an e-mail with information about the planned experiment to:

iept-experiments@ivt.ntnu.no

The e-mail must include the following information:

- Name of responsible person:
- Experimental setup/rig:
- Start Experiments: (date and time)
- Stop Experiments: (date and time)

You must get the approval back from the laboratory management before start up. All running experiments are notified in the activity calendar for the lab to be sure they are coordinated with other activity.

6.2 Non-conformance

FIRE

If you are NOT able to extinguish the fire, activate the nearest fire alarm and evacuate area.

Be then available for fire brigade and building caretaker to detect fire place.

If possible, notify:

NTNU	SINTEF
Morten Grønli, Mob: 918 97 515	Harald Mæhlum, Mob: 930 14 986
Therese Løvås, Mob: 91897007	Anne Karin T. Hemmingsen Mob: 930 19 669
NTNU – SINTEF Beredskapstelefon	800 80 388

GAS ALARM

If a gas alarm occurs, close gas bottles immediately and ventilate the area. If the level of the gas concentration does not decrease within a reasonable time, activate the fire alarm and evacuate the lab. Designated personnel or fire department checks the leak to determine whether it is possible to seal the leak and ventilate the area in a responsible manner.

PERSONAL INJURY

- First aid kit in the fire / first aid stations
- Shout for help
- Start life-saving first aid
- CALL 113 if there is any doubt whether there is a serious injury

OTHER NON-CONFORMANCE (AVVIK)

NTNU:

You will find the reporting form for non-conformance on:
<https://innsida.ntnu.no/wiki/-/wiki/Norsk/Melde+avvik>

SINTEF:

Synergi

7 ASSESSMENT OF TECHNICAL SAFETY

7.1 HAZOP

See Chapter 13 "Guide to the report template".

The experiment set up is divided into the following nodes:

Node 1	Blade cascade
Node 2	Laser class IV
Node 3	Tent/enclosure

Attachments, Form: Hazop_mal

Conclusion

Node 1:

- Pressure is supervised during operation

Node 2:

- Radiation area shielded
- Appropriate signalling and lights in place, light active during operation

Node 3:

- Appropriate signalling and lights in place, light active during operation

7.2 Flammable, reactive and pressurized substances and gas

See Chapter 13 "Guide to the report template".

NO	
----	--

7.3 Pressurized equipment

See Chapter 13 "Guide to the report template".

YES	
-----	--

7.4 Effects on the environment (emissions, noise, temperature, vibration, smell)

See Chapter 13 "Guide to the report template".

NO	
----	--

7.5 Radiation

See Chapter 13 "Guide to the report template".

YES	Radiation Sources need to have an own risk assessment
-----	---

Attachments: Radiation risk assessment

Conclusion:

7.6 Chemicals

See Chapter 13 "Guide to the report template".

NO	
----	--

7.7 Electricity safety (deviations from the norms/standards)

See Chapter 13 "Guide to the report template".

NO	
----	--

8 ASSESSMENT OF OPERATIONAL SAFETY

Ensure that the procedures cover all identified risk factors that must be taken care of. Ensure that the operators and technical performance have sufficient expertise.

8.1 Procedure HAZOP

See Chapter 13 "Guide to the report template".

The method is a procedure to identify causes and sources of danger to operational problems.

Attachments:: HAZOP_MAL_Prosegyre

8.2 Operation procedure and emergency shutdown procedure

See Chapter 13 "Guide to the report template".

The operating procedure is a checklist that must be filled out for each experiment.

Emergency procedure should attempt to set the experiment set up in a harmless state by unforeseen events.

Attachments: Procedure for running experiments

Emergency shutdown procedure:

8.3 Training of operators

8.4 Technical modifications

8.5 Personal protective equipment

- *It is mandatory use of appropriate eye protection in the rig zone*

8.6 General Safety

- *The area around the staging attempts shielded.*
- *Operator has to be present during experiments.*

8.7 Safety equipment

- *Warning signs and warning light, see the Regulations on Safety signs and signalling in the workplace*

8.8 Special predations

9 QUANTIFYING OF RISK - RISK MATRIX

See Chapter 13 "Guide to the report template".

The risk matrix will provide visualization and an overview of activity risks so that management and users get the most complete picture of risk factors.

IDnr	Aktivitet-hendelse	Frekv-Sans	Kons	RV
1	Unintentional rarefaction/reflection of laser beam	1	A	1A
2	People without protective goggles entering radiation area	1	C	1C
3	Damaging lab equipment	2	B	2B
4	Water-damage on lab equipment	3	B	3C
5	Structural failure due to high pressure	1	C	1C

Conclusion: There is little remaining risk. The most prominent risk is that people unintentionally wander into the radiation area without protective goggles, but proper signalling and blocking should prevent this. The risk is therefore acceptable.

10 REGULATIONS AND GUIDELINES

Se <http://www.arbeidstilsynet.no/regelverk/index.html>

- Lov om tilsyn med elektriske anlegg og elektrisk utstyr (1929)
- Arbeidsmiljøloven
- Forskrift om systematisk helse-, miljø- og sikkerhetsarbeid (HMS Internkontrollforskrift)
- Forskrift om sikkerhet ved arbeid og drift av elektriske anlegg (FSE 2006)
- Forskrift om elektriske forsyningsanlegg (FEF 2006)
- Forskrift om utstyr og sikkerhetssystem til bruk i eksplosjonsfarlig område NEK 420
- Forskrift om håndtering av brannfarlig, reaksjonsfarlig og trykksatt stoff samt utstyr og anlegg som benyttes ved håndteringen
- Forskrift om Håndtering av eksplosjonsfarlig stoff
- Forskrift om bruk av arbeidsutstyr.
- Forskrift om Arbeidsplasser og arbeidslokaler
- Forskrift om Bruk av personlig verneutstyr på arbeidsplassen
- Forskrift om Helse og sikkerhet i eksplosjonsfarlige atmosfærer
- Forskrift om Høytrykksspyling
- Forskrift om Maskiner
- Forskrift om Sikkerhetsskiltning og signalgivning på arbeidsplassen
- Forskrift om Stillaser, stiger og arbeid på tak m.m.
- Forskrift om Sveising, termisk skjæring, termisk sprøyting, kullbuemeisling, lodding og sliping (varmt arbeid)
- Forskrift om Tekniske innretninger
- Forskrift om Tungt og ensformig arbeid
- Forskrift om Vern mot eksponering for kjemikalier på arbeidsplassen (Kjemikalieforskriften)
- Forskrift om Vern mot kunstig optisk stråling på arbeidsplassen
- Forskrift om Vern mot mekaniske vibrasjoner
- Forskrift om Vern mot støy på arbeidsplassen

Veiledninger fra arbeidstilsynet

se: <http://www.arbeidstilsynet.no/regelverk/veiledninger.html>

11 DOCUMENTATION

- Tegninger, foto, beskrivelser av forsøksoppsetningen
- Hazop_mal
- Sikker bruk av LASERE, retningslinje
- HAZOP_MAL_Proseidyre
- Forsøksproseidyre
- Opplæringsplan for operatører
- Skjema for sikker jobb analyse, (SJA)
- Apparatorkortet
- Forsøk pågå kort

12 GUIDANCE TO RISK ASSESSMENT TEMPLATE

Chapter 7 Assessment of technical safety.

Ensure that the design of the experiment set up is optimized in terms of technical safety.

Identifying risk factors related to the selected design, and possibly to initiate re-design to ensure that risk is eliminated as much as possible through technical security.

This should describe what the experimental setup actually are able to manage and acceptance for emission.

7.1 HAZOP

The experimental set up is divided into nodes (eg motor unit, pump unit, cooling unit.). By using guidewords to identify causes, consequences and safeguards, recommendations and conclusions are made according to if necessary safety is obtained. When actions are performed the HAZOP is completed.

(e.g. "No flow", cause: the pipe is deformed, consequence: pump runs hot, precaution: measurement of flow with a link to the emergency or if the consequence is not critical used manual monitoring and are written into the operational procedure.)

7.2 Flammable, reactive and pressurized substances and gas.

According to the Regulations for handling of flammable, reactive and pressurized substances and equipment and facilities used for this:

Flammable material: Solid, liquid or gaseous substance, preparation, and substance with occurrence or combination of these conditions, by its flash point, contact with other substances, pressure, temperature or other chemical properties represent a danger of fire.

Reactive substances: Solid, liquid, or gaseous substances, preparations and substances that occur in combinations of these conditions, which on contact with water, by its pressure, temperature or chemical conditions, represents a potentially dangerous reaction, explosion or release of hazardous gas, steam, dust or fog.

Pressurized : Other solid, liquid or gaseous substance or mixes having fire or hazardous material response, when under pressure, and thus may represent a risk of uncontrolled emissions

Further criteria for the classification of flammable, reactive and pressurized substances are set out in Annex 1 of the Guide to the Regulations "Flammable, reactive and pressurized substances"

<http://www.dsb.no/Global/Publikasjoner/2009/Veiledning/Generell%20veiledning.pdf>

http://www.dsb.no/Global/Publikasjoner/2010/Tema/Temaveiledning_bruk_av_farlig_stoff_Del_1.pdf

Experiment setup area should be reviewed with respect to the assessment of Ex zone

- Zone 0: Always explosive atmosphere, such as inside the tank with gas, flammable liquid.
- Zone 1: Primary zone, sometimes explosive atmosphere such as a complete drain point
- Zone 2: secondary discharge could cause an explosive atmosphere by accident, such as flanges, valves and connection points

7.4 Effects on the environment

With pollution means: bringing solids, liquid or gas to air, water or ground, noise and vibrations, influence of temperature that may cause damage or inconvenience effect to the environment.

Regulations: <http://www.lovddata.no/all/hl-19810313-006.html#6>

NTNU guidance to handling of waste:<http://www.ntnu.no/hms/retningslinjer/HMSR18B.pdf>

7.5 Radiation

Definition of radiation

Ionizing radiation: Electromagnetic radiation (in radiation issues with wavelength <100 nm) or rapid atomic particles (e.g. alpha and beta particles) with the ability to stream ionized atoms or molecules.

Non ionizing radiation: Electromagnetic radiation (wavelength >100 nm), og ultrasound₁ with small or no capability to ionize.

Radiation sources: All ionizing and powerful non-ionizing radiation sources.

Ionizing radiation sources: Sources giving ionizing radiation e.g. all types of radiation sources, x-ray, and electron microscopes.

Powerful non ionizing radiation sources: Sources giving powerful non ionizing radiation which can harm health and/or environment, e.g. class 3B and 4. MR₂ systems, UVC₃ sources, powerful IR sources₄.

₁Ultrasound is an acoustic radiation ("sound") over the audible frequency range (> 20 kHz). In radiation protection regulations are referred to ultrasound with electromagnetic non-ionizing radiation.

₂MR (e.g. NMR) - nuclear magnetic resonance method that is used to "depict" inner structures of different materials.

₃UVC is electromagnetic radiation in the wavelength range 100-280 nm.

₄IR is electromagnetic radiation in the wavelength range 700 nm - 1 mm.

For each laser there should be an information binder (HMSRV3404B) which shall include:

- General information
- Name of the instrument manager, deputy, and local radiation protection coordinator
- Key data on the apparatus
- Instrument-specific documentation
- References to (or copies of) data sheets, radiation protection regulations, etc.
- Assessments of risk factors
- Instructions for users
- Instructions for practical use, startup, operation, shutdown, safety precautions, logging, locking, or use of radiation sensor, etc.
- Emergency procedures
- See NTNU for laser: <http://www.ntnu.no/hms/retningslinjer/HMSR34B.pdf>

7.6 The use and handling of chemicals.

In the meaning chemicals, a element that can pose a danger to employee safety and health

See: <http://www.lovddata.no/cgi-wift/ldles?doc=/sf/sf/sf-20010430-0443.html>

Safety datasheet is to be kept in the HSE binder for the experiment set up and registered in the database for chemicals.

Chapter 8 Assessment of operational procedures.

Ensures that established procedures meet all identified risk factors that must be taken care of through operational barriers and that the operators and technical performance have sufficient expertise.

8.1 Procedure Hazop

Procedural HAZOP is a systematic review of the current procedure, using the fixed HAZOP methodology and defined guidewords. The procedure is broken into individual operations (nodes) and analyzed using guidewords to identify possible nonconformity, confusion or sources of inadequate performance and failure.

8.2 Procedure for running experiments and emergency shutdown.

Have to be prepared for all experiment setups.

The operating procedure has to describe stepwise preparation, startup, during and ending conditions of an experiment. The procedure should describe the assumptions and conditions for starting, operating parameters with the deviation allowed before aborting the experiment and the condition of the rig to be abandoned.

Emergency procedure describes how an emergency shutdown have to be done, (conducted by the uninitiated),

what happens when emergency shutdown, is activated. (electricity / gas supply) and which events will activate the emergency shutdown (fire, leakage).

Chapter 9 Quantifying of RISK

Quantifying of the residue hazards, Risk matrix

To illustrate the overall risk, compared to the risk assessment, each activity is plotted with values for the probability and consequence into the matrix. Use task IDnr.

Example: If activity IDnr. 1 has been given a probability 3 and D for consequence the risk value become D3, red. This is done for all activities giving them risk values.

In the matrix are different degrees of risk highlighted in red, yellow or green. When an activity ends up on a red risk (= unacceptable risk), risk reducing action has to be taken

CONSEQUENCES	Catastrophic	E1	E2	E3	E4	E5
	Major	D1	D2	D3	D4	D5
	Moderate	C1	C2	C3	C4	C5
	Minor	B1	B2	B3	B4	B5
	Insignificant	A1	A2	A3	A4	A5
		Rare	Unlikely	Possible	Likely	Almost
		PROBABILITY				

Table 8. Risk's Matrix

Table 9. The principle of the acceptance criterion. Explanation of the colors used in the matrix

COLOUR	DESCRIPTION
Red	Unacceptable risk Action has to be taken to reduce risk
Yellow	Assessment area. Actions has to be considered
Green	Acceptable risk. Action can be taken based on other criteria